ΣΕΙΣΜΟΛΟΓΙΑ. — **Geoelectric Structure of the VAN-Station at Ioannina Sensitive to the Detection of Seismic Electric Signals (SES),** by *J. Makris, N. Bogris* and *K. Eftaxias**, διὰ τοῦ ἀκαδημαϊκοῦ κ. Καίσαρος Ἀλεξοπούλου.


ABSTRACT

Magnetotelluric and magnetic prospections of the area around the VAN-station of Ioannina region, indicate that the geoelectric structure is compatible with the following model: the regional conductivity structure is two-dimensional (2D) with strike-direction ~N40°W, while small-scale near-surface 3D-inhomogeneities are also present. These near-surface semi-static scatterers reflect strong local channelling with (linear) polarization directions of the electric field which vary drastically with the measuring site (e.g., even at distances of the order of 100m). The combination of the impedance tensor decomposition analysis with the magnetotelluric study of Mohr circles and the magnetic prospection analysis successfully resolves the characteristics of the near-surface 3D-distorting bodies and the principal axis system (together with strike and dip-directions) of the underlying regional 2D-structure. Furthermore, the magnetic prospection as well as the 1D-Occam inversion indicate the probable existence of a very conductive body (of the order of a few Ωm) at a depth of the order of a few Km, embedded in a more resistive medium with resistivity of the order of a few thousands Ωm.


## INTRODUCTION

Since 1981, Varotsos et al *[Varotsos et al., 1996]* are studying experimentally and theoretically the transient variations of the electric field of the earth hereafter called Seismic Electric Signals (SES) in a research effort aiming in predicting earthquakes. The SES-study revealed two basic properties:

(i) SES are detectable only at certain sites of the earth's surface, which are called «*sensitive sites*».

(ii) Each of these sites is sensitive only to SES from certain focal area(s) that are not always close to them.

These two properties conform what Varotsos et al. call «*selectivity effect*». The peculiarity of a «*sensitive site*» is probably correlated with the

---

* Ι. ΜΑΚΡΗΣ - Ν. ΜΠΟΓΡΗΣ - Κ. ΕΥΤΑΞΙΑΣ. **Γεωηλεκτρικὴ δομὴ τοῦ εὐαίσθητου στὰ προσεισμικὰ ἠλεκτρικὰ σήματα (SES) σταθμοῦ ΒΑΝ Ἰωαννίνων.**

geoelectric structure of the crust just beneath this site and/or of the crust of the vast region between the focal area and the «*sensitive site*».

The main objective of this paper is to present an extensive magnetotelluric (MT) study of an area sensitive to the detection of SES. As a first step we selected the region around Ioannina-city, at north-western Greece where the VAN-station (IOA) is operated since 1981 (see Fig. 1). The MT-measurements

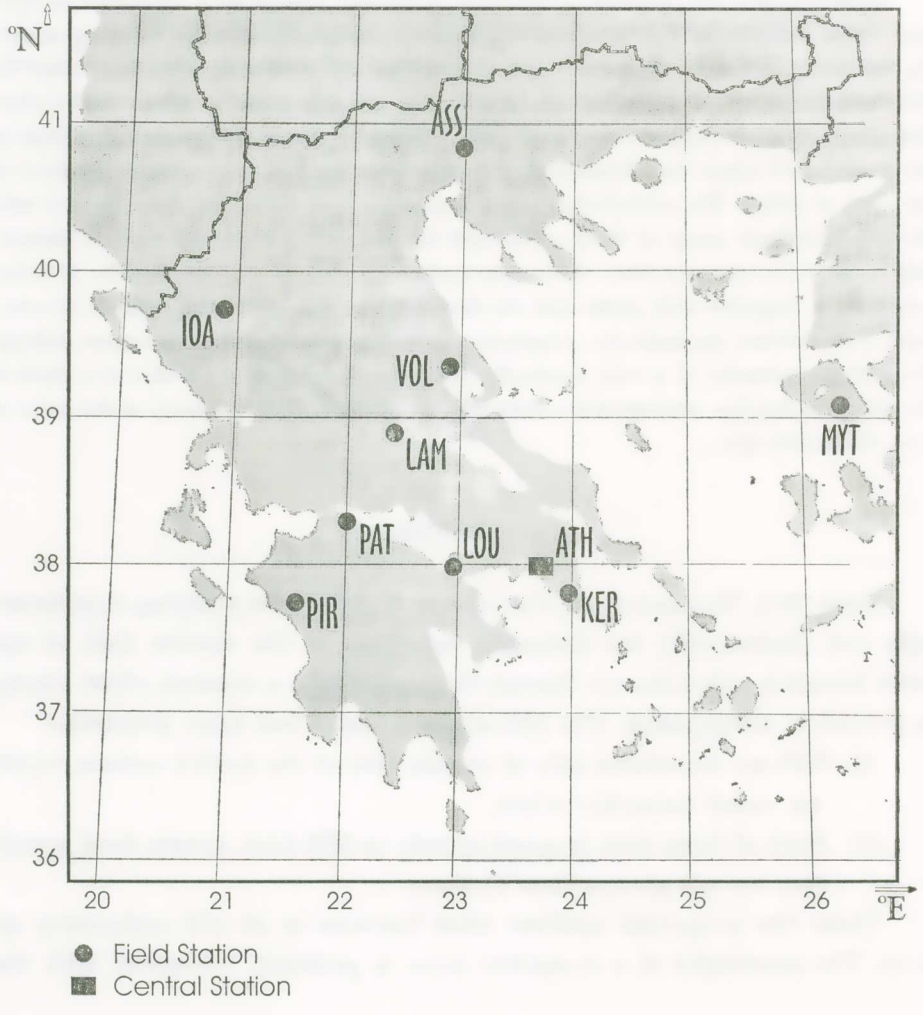


Fig. 1. Map of Greece showing the basic configuration of the VAN-telemetric network. The Ioannina (IOA) station, sensitive to the detection of SES, is the subject of an extensive MT-prospection.

were conducted at three neighbouring areas (hereafter cited as A, B and C respectively) and a site between areas B and C, cited (B-C), where the short dipoles of IOA-station are installed (see Fig. 2). The MT-study was extended to two additional locations: Lykotrichi area, ~4 Km north-west from IOA - station (see Fig. 2) and Protopappas area, ~15 Km north-west from IOA - station.

The magnetotelluric (MT) method was proposed as an efficient technique for mapping the subsurface electrical conductivity structure. The method assumes a linear relationship between the horizontal natural magnetic and electric fields at the earth's surface, over a broad frequency range and independent of source polarization and position. The field transfer function, termed the impedance tensor, is estimated in the frequency domain from the experimental MT-data. The extraction from the data of scalar parameters that will have interpretable physical meaning, in terms of the actual conductivity structure within the earth, is the aim of the impedance tensor analysis. The interpretation is easiest in those cases where the surveyed structure is either one - dimensional (1D) i.e., homogeneous or horizontally layered, or two-dimensional (2D) i.e., uniform along a horizontal axis (strike-direction). However, the experimentally determined MT-impedance tensor very rarely conform to the ideal 1D or 2D-form. Therefore, a 3D-modeling is necessary in order to analyze the responses of arbitrary (3D) geoelectric structures.

In the MT-study we proceed in two consecutive stages; the first is the conventional MT-analysis where the electromagnetic response of the subsurface hemispace is considered as unified (see chapter I), while in the subsequent MT-tensor decomposition analysis (discussed in chapter II), the impedance tensor is decomposed in more than one tensors.

## I. CONVENTIONAL MAGNETOTELLURIC ANALYSIS

A linear relationship between the horizontal electric and magnetic field at the earth's surface is assumed and hence, in the frequency domain, the transfer function, between the electric and magnetic field, i.e., the *impedance tensor*, is given by the pair of the following linear equations *[Kaufman et al., 1981], [Keller et al., 1986]*:

$$E_x(r,\omega) = Z_{xx}(r,\omega)H_x + Z_{xy}(r,\omega)H_y \qquad [I.1a]$$

$$E_y(r,\omega) = Z_{yx}(r,\omega)H_x + Z_{yy}(r,\omega)H_y \qquad [I.1.b]$$

or, in matrix notation:

$$E = \mathbf{Z} \cdot H \qquad [I.2]$$

where:

$$\mathbf{Z}(r,\omega) = \begin{pmatrix} Z_{xx}(r,\omega) & Z_{xy}(r,\omega) \\ Z_{yx}(r,\omega) & Z_{yy}(r,\omega) \end{pmatrix} \qquad [I.3]$$

The conventional interpretation of MT-data requires the extraction of scalar parameters from the impedance tensor **Z** which depends on the frequency and the selected measuring coordinate system. The latter dependence imposes the extraction of scalar parameters not only from the measured impedance tensor corresponding to the selected coordinate system, but from the principal impedance tensor corresponding to the intrinsic of the structure coordinate system as well. An important special case arises when the subsurface is assumed as uniform along one horizontal axis of the coordinate system (2D-symmetry).

From the rotation of the impedance tensor:

$$\mathbf{Z}'(\theta) = R\mathbf{Z}_m R^t \qquad [I.4]$$

where:

$$R = \begin{pmatrix} \cos\theta & \sin\theta \\ -\sin\theta & \cos\theta \end{pmatrix} \qquad [I.5]$$

is the rotation operator, a new rotated impedance tensor $\mathbf{Z}'(\theta)$ is defined in another coordinate system which results from the rotation of the measuring coordinate system $\theta$ degrees clockwise. If there is an angle $\theta_0$ in which the tensor $\mathbf{Z}'(\theta_0)$ can be considered as approaching the ideal form of the impedance tensor for a 2D-structure, then the $\mathbf{Z}'(\theta_0)$ is termed the *principal impedance tensor*. Therefore, it is evident that a procedure for the analytic calculation of

the *strike angle* $\theta_0$ should be specified. Furthermore, scalar parameters that will indicate the deviation of the actual structure from the ideal 2D-structure should be defined; these parameters will represent the reliability of the strike angle $\theta_0$ and of other scalar parameters e.g., the principal apparent resistivities and their corresponding phases.

*Tensor rotation on the complex plane*

The clockwise rotated impedance tensor elements are given by the equations *[Swift, 1967], [Eggers, 1982]*:

$$Z'_{xx} = Z_2 + Z_3 \sin(2\theta) + Z_4 \cos(2\theta) \qquad [I.6.a]$$

$$Z'_{xy} = Z_1 + Z_3 \cos(2\theta) - Z_4 \sin(2\theta) \qquad [I.6.b]$$

$$Z'_{yx} = -Z_1 + Z_3 \cos(2\theta) - Z_4 \sin(2\theta) = -Z'_{xy}\left(\theta + \frac{\pi}{2}\right) \qquad [I.6.c]$$

$$Z'_{yy} = Z_2 - Z_3 \sin(2\theta) - Z_4 \cos(2\theta) = Z'_{xx}\left(\theta + \frac{\pi}{2}\right) \qquad [I.6.d]$$

where:

$$Z_1 = \frac{(Z_{xy} - Z_{yx})}{2},\ Z_2 = \frac{(Z_{xx} + Z_{yy})}{2},\ Z_3 = \frac{(Z_{xy} + Z_{yx})}{2},\ Z_4 = \frac{(Z_{xx} - Z_{yy})}{2}.$$

All the elements $Z'_{ij}(\theta)$ trace out ellipses in the complex plane under a rotation through $\pi$ radians (see Fig. I.1). A study of eqs [I.6.a-d] leads to the following properties:

- $Z_1$, $Z_2$ are rotationally invariant.
- The diagonal elements of the impedance tensor trace out the same ellipse with centroid $Z_2$.
- The off-diagonal elements of the impedence tensor trace out ellipses with centroids $\pm Z_1$.

- The ellipses of all the elements of the impedance tensor have the same size and shape and are defined by the conjugate radii $Z_3$ and $Z_4$.
- The following relations hold:

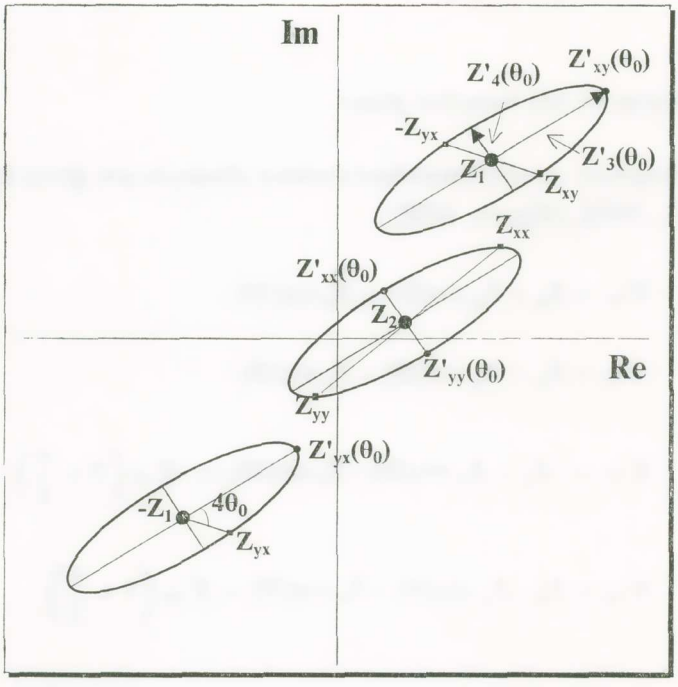


Fig. I.1. Rotational diagrams, at the complex plane, of the impedance tensor elements for the case of a 3D-structure.

$$Z'_{yx}(\theta) = -Z'_{xy}\left(\theta \pm \frac{\pi}{2}\right)$$

$$Z'_{yy}(\theta) = Z'_{xx}\left(\theta \pm \frac{\pi}{2}\right)$$

which explain the relative position of the elements ($Z_{xy}$, $Z_{yx}$) and ($Z_{xx}$, $Z_{yy}$) in the corresponding ellipses.

- When the off-diagonal elements are on the main axis of the ellipse, the

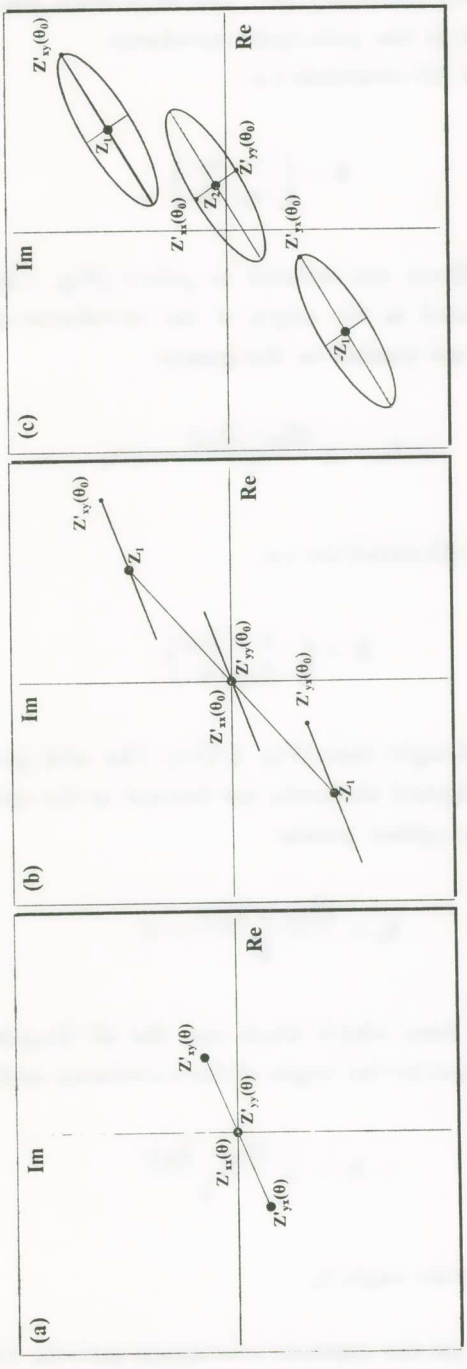


Fig. I.2. Rotational diagrams, at the complex plane, of the impedance tensor elements: **(a)** 1D-symmetry, **(b)** 2D-symmetry **(c)** 3D-symmetry.

diagonal are on the secondary one. The impedance which corresponds to this configuration is the *principal impedance.*

In the case of the 1D-structure i.e.,

$$\mathbf{Z} = \begin{pmatrix} 0 & z_0 \\ -z_0 & 0 \end{pmatrix} \qquad [I.7]$$

the aforementioned ellipses are reduced to points [Fig. I.2(a)]; the diagonal elements are then located in the origin of the coordinate system, while the off-diagonal elements are located in the points:

$$\pm Z_1 = \pm \frac{(Z_{xy} - Z_{yx})}{2} = \pm z_0$$

In the case of the 2D-structure i.e.,

$$\mathbf{Z} = \begin{pmatrix} 0 & Z_{xy} \\ -Z_{yx} & 0 \end{pmatrix} \qquad [I.8]$$

the ellipses reduce to straight lines [Fig. I.2(b)]. The mid points of the lines which trace out the diagonal elements, are located in the symmetrical to the origin of the coordinate system points:

$$Z_2 = \frac{(Z_{xx} + Z_{yy})}{2} = 0$$

The mid points of the lines which trace out the off-diagonal elements, are located in the symmetrical to the origin of the coordinate system points:

$$\pm Z_1 = \pm \frac{(Z_{xy} - Z_{yx})}{2}$$

*Determination of the strike angle* $\theta_0$

The principal axes (of the intrinsic coordinate system) arise from the rotation of the measuring coordinate system through an angle $\theta_0$ (termed as

the *strike angle*), at which $Z_3$ and $Z_4$ reach their largest and smallest values respectively *[Swift, 1967], [Sims and Bostick, 1969]*, i.e.,

$$|Z_3| = |Z'_{xy}(\theta) + Z'_{yx}(\theta)| = \max$$
$$|Z_4| = |Z'_{xx}(\theta) - Z'_{yy}(\theta)| = \min$$

Such a scheme finds the *true* principal axis coordinate system only in the case of a 2D-structure. The above conditions give the following relation for the angle $\theta_0$:

$$\tan 4\theta_0 = \frac{2\mathrm{Re}(Z_3 Z_4^*)}{|Z_4|^2 - |Z_3|^2} \qquad [I.9.a]$$

or

$$\theta_0 = \frac{1}{4} \tan^{-1}\left(\frac{2(R_1R_2 + I_1I_2)}{(R_1^2 - R_2^2) + (I_1^2 - I_2^2)}\right) \qquad [I.9.b]$$

where $R_1$, $R_2$ and $I_1$, $I_2$ denote the real and imaginary parts of the complex quantities $Z_{xx} - Z_{yy}$ and $Z_{xy} + Z_{yx}$ respectively.

The same angle arises from the maximization and minimization of the following functions *[Swift, 1967]* respectively:

$$|Z'_{xy}(\theta)|^2 + |Z'_{yx}(\theta)|^2 = \max$$

$$|Z'_{xx}(\theta)|^2 + |Z'_{yy}(\theta)|^2 = \min$$

The strike angle defines the intrinsic coordinate system, but it does not distinguish between the strike and dip-directions of the 2D-geoelectric structure. This can be achieved with additional information derived either from the vertical component of the magnetic field (see chapter IV), or from geological insights.

*Determination of skew and ellipticity*

*Skew* and *ellipticity* are two additional parameters which are extracted

from the rotated impedance tensor $\mathbf{Z}'$ and indicate the extend to which the rotated impedance tensor deviates from that of an ideal 1D or 2D-structure.

The *skew* measures the distance from the origin of the diagonal element rotation ellipse, normalized by the distance from the origin of the off-diagonal rotation ellipses:

$$s = \frac{|Z_2|}{|Z_1|} = \frac{|Z_{xx} + Z_{yy}|}{|Z_{xy} - Z_{yx}|} \qquad [I.10]$$

The *ellipticity* of the rotation ellipse is defined as:

$$\beta = \frac{|Z'_4(\theta_0)|}{|Z'_3(\theta_0)|} = \frac{|Z'_{xx}(\theta_0) - Z'_{yy}(\theta_0)|}{|Z'_{xy}(\theta_0) + Z'_{yx}(\theta_0)|} \qquad [I.11]$$

Note that the skew s is a rotationally invariant parameter, while the ellipticity is not. Furthermore, the skew is more sensitive to the departure from an ideal 1D or 2D-structure for higher frequencies, while the ellipticity for lower frequencies; hence, the two indices are complimentary.

*Determination of apparent resistivities and phases from the impedance tensor*

The apparent resistivities and their corresponding phases are estimated using the relations:

$$\rho_{ij}(\theta,\omega) = \frac{|Z'_{ij}(\theta,\omega)|^2}{\omega\mu_0} \qquad [I.12]$$

$$\varphi_{ij}(\theta,\omega) = \tan^{-1}\left(\frac{\mathrm{Im}[Z'_{ij}(\theta,\omega)]}{\mathrm{Re}[Z'_{ij}(\theta,\omega)]}\right) \qquad [I.13]$$

The necessity of defining the apparent resistivities arises from the fact that, in the frequency domain, the impedance tensor elements do not have any direct physical meaning. For the MT-interpretation we look for scalar parameters which are more amenable to physical intuition with regard to the unknown subsurface conductivity distribution. The principal apparent resistivities and phases correspond to the off-diagonal elements of the rotated (through the strike angle $\theta_0$), impedance tensor.

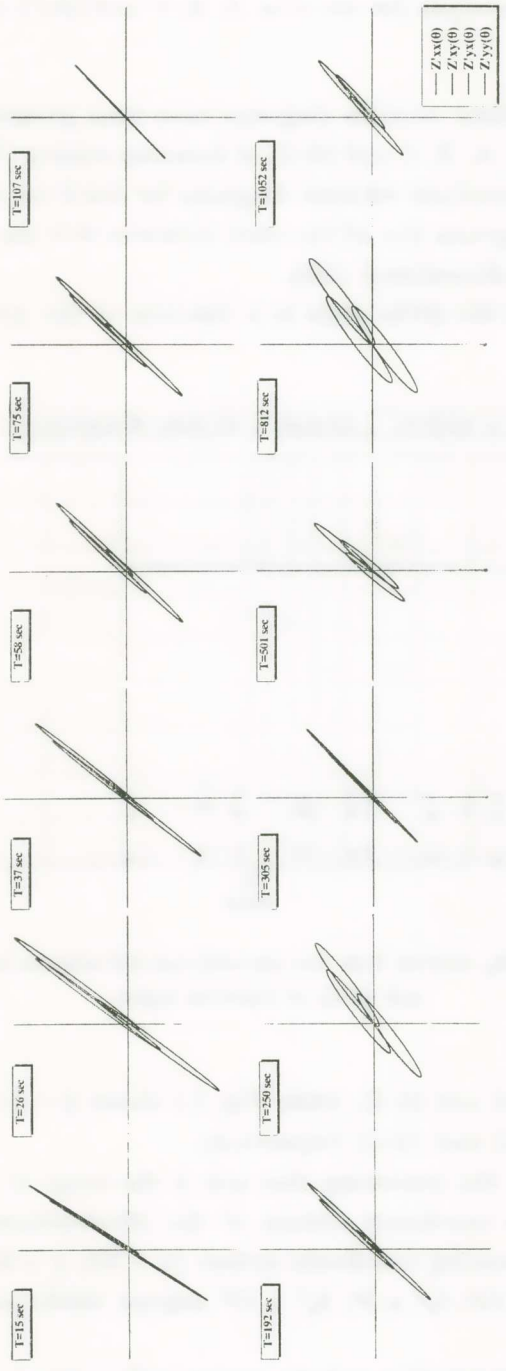


Fig. I.3. Rotational diagrams of the elements of the MT-impedance tensor for site B of Ioannina region.

*I.1. Experimental analysis for the sites A, B, C and (B-C) at Ioannina VAN station*

The magnetotelluric rotation diagrams have been plotted for each one of the four sites called A, B, C and (B-C) of Ioannina station *[Makris, 1997]*. In Fig. I.3 the magnetotelluric rotation diagrams for site B are depicted. An inspection of these diagrams (for all the sites) indicates that the structure can be considered as two-dimensional (2D).

Fig. I.4 depicts the strike angle as a function of the period, $\theta_0 = \theta_0$ (T),

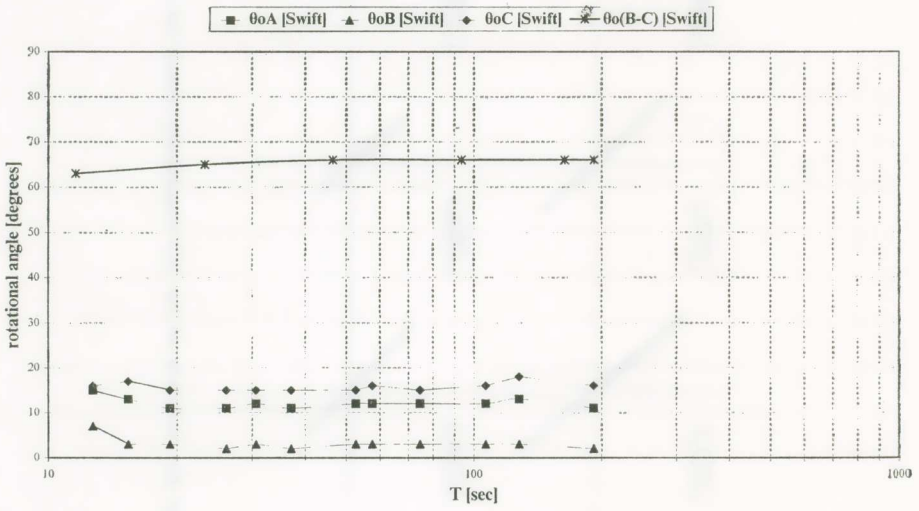


Fig. I.4. Strike angle, $\theta_0$, derived from the conventional MT-analysis for the sites A, B, C and (B-C) of Ioannina region.

for the sites A, B, C and (B-C), while Fig. I.5 shows $\beta = \beta$ (T) and $s = s$ (T) for the sites A, B, C and (B-C) respectively.

At each one of the measuring sites and in the range of periods T = 10 – 200sec, an intrinsic coordinate system of the 2D-structure arises from the rotation of the measuring coordinate system (x ≡ NS, y ≡ EW) through the strike angles $\theta_0^A \approx 12^o$, $\theta_0^B \approx 3^o$, $\theta_0^C \approx 15^o$ degrees clockwise and $\theta_0^{B-C} \approx 66^o$ counterclockwise.

The apparent resistivities and the corresponding phases of the measuring

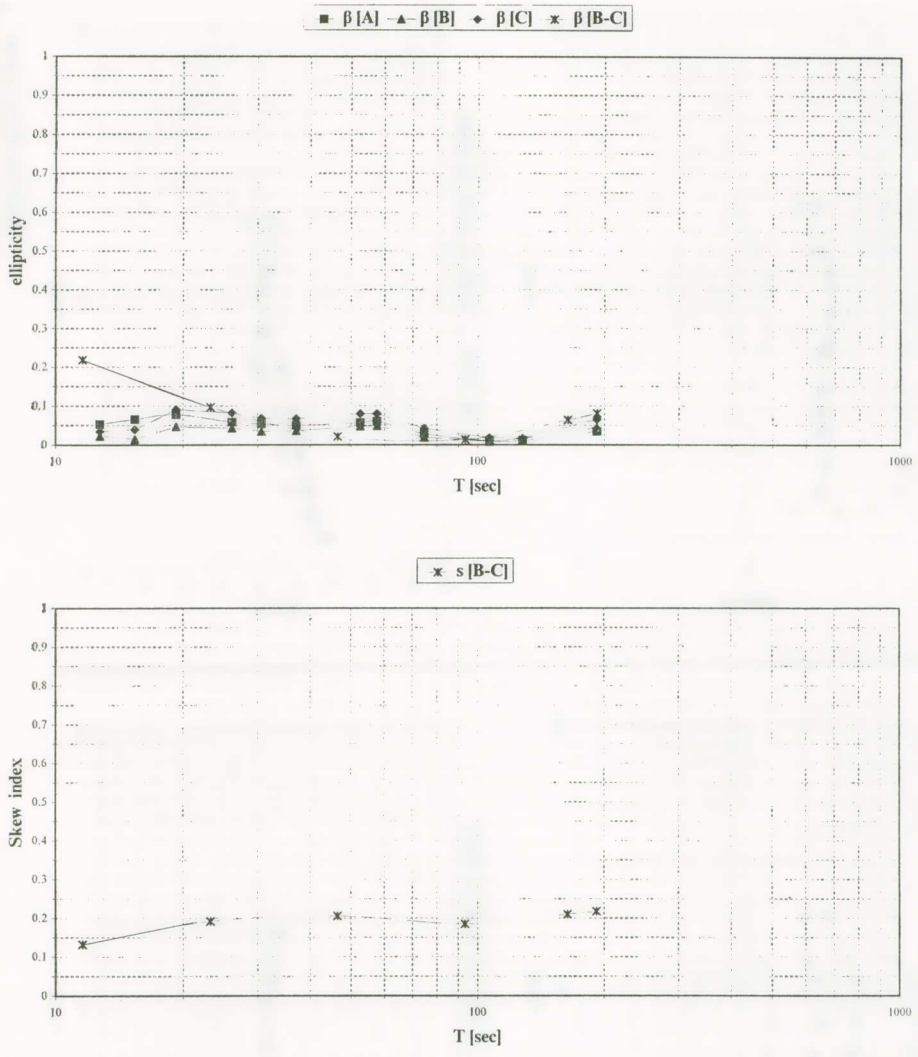


Fig. I.5. Ellipticity, β, derived from the conventional MT-analysis for the sites A, B, C and (B-C) of Ioannina region, and skew, s, for the site (B-C).

and the strike (intrinsic) coordinate system, for site B, are presented in Fig. I.6. Similar plots for the other sites can be found in *[Makris, 1997]*.

An inspection of the MT-rotation diagrams and a study of the plots $\theta_0 = \theta_0(T)$, $\beta = \beta(T)$, $s = s(T)$ and $\rho_{ij} = \rho_{ij}(T)$, $\varphi_{ij} = \varphi_{ij}(T)$ for all the sites indicate that, at each site, the subsurface geoelectric structure approximates that of a 2D-symmetry [because $s(T) < 0.3$ and $\beta(T) < 0.2$]; note however, that the

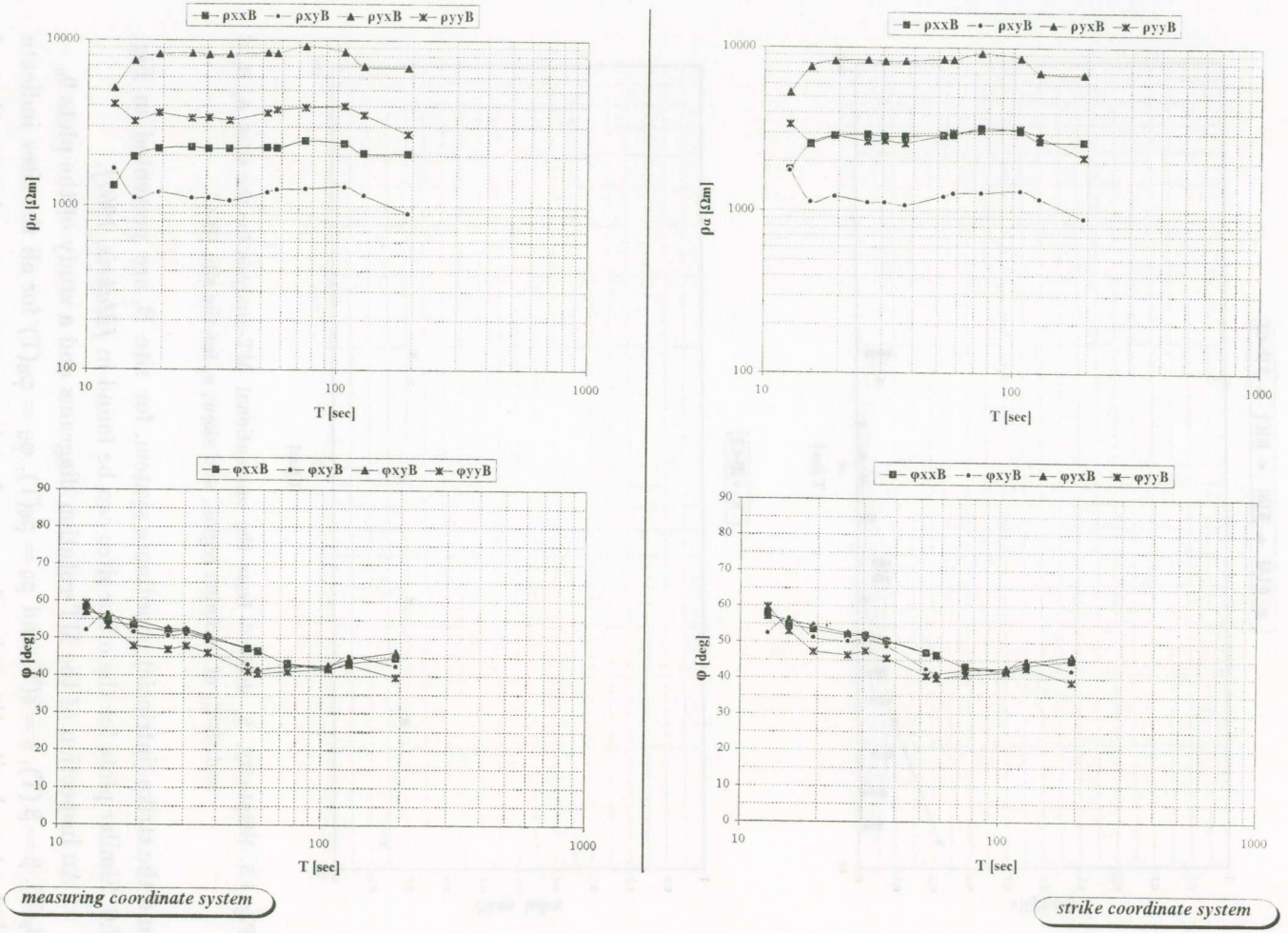


Fig. I.6. Apparent resistivities and the corresponding phases for the measuring and the strike coordinate system respectively.

strike angle varies from site to site, and that a significant difference exists when comparing $\rho_{xy}$ and $\rho_{yx}$.

*I.2. Eigenstate formulation of the magnetotelluric impedance tensor*

The following set of scalar parameters was introduced in the previous section:

$$\{\theta_0, s, \beta, \rho_{ij}(\theta_0, T), \varphi_{ij}(\theta_0, T)\}$$

However, there are two important problems in this approach. The apparent resistivities, as defined from the off-diagonal elements of the rotated (to the strike) impedance tensor, are independent of the trace of the impedance tensor. It is therefore problematic that the apparent resistivities, which should have physical analogues and are most heavily used in the interpretation, are insensitive to the addition of an arbitrary constant to the diagonal elements of the impedance tensor. Furthermore, the aforementioned parameter set is incomplete. There are two degrees of freedom in the impedance tensor which are transparent to all the parameters.

Eggers *[Eggers, 1982]*, tried to overcome these problems by considering the eigenstate formulation of the impedance tensor. The eigenstates are defined by the equation:

$$E^i = \Lambda^i \cdot H^i \qquad [I.14]$$

where $E^i \cdot H^i = 0$ in the frequency domain.
The necessary and sufficient condition for this to be true for non-trivial $H^i$, is that $\Lambda^i$ to be skew symmetric:

$$\Lambda^i = \begin{pmatrix} 0 & \lambda^i \\ -\lambda^i & 0 \end{pmatrix} \qquad [I.15]$$

and identical (in form) to the operator relating the electric and magnetic fields of an arbitrary polarization at the Transverse Electromagnetic Mode (TEM) of wave propagation in a homogeneous medium. The eigenvalues and the corresponding eigenvectors are given by:

$$\lambda^{\pm} = Z_1 \pm \sqrt{Z_1^2 - \det \mathbf{Z}_m} \qquad [I.16]$$

where $Z_1 = \frac{Z_{xy} - Z_{yx}}{2}$ and $\det \mathbf{Z}_m = Z_{xx}Z_{yy} - Z_{xy}Z_{yx}$,

$$H^+ = \begin{pmatrix} \lambda^{\pm} - Z_{xy} \\ Z_{xx} \end{pmatrix} \qquad [I.17.a]$$

$$E^+ = \begin{pmatrix} -Z_{yy} \\ Z_{yx} + \lambda^{\pm} \end{pmatrix} \qquad [I.17.b]$$

The properties of the eigenvalues and the eigenvectors can be summarized as follows:

- Since $Z_1$ and $\det \mathbf{Z}_m$ are rotationally invariant, the eigenvalues $\lambda^{\pm}$ are also rotationally invariant.
- For the 1D-case, the impedance tensor takes the anti-symmetric form:e

$$\mathbf{Z}_{1D} = \begin{pmatrix} 0 & z_0 \\ -z_0 & 0 \end{pmatrix}$$

and hence, $Z_1 = z_0$ and $\det \mathbf{Z}_{1D} = z_0^2$.

The eigenvalues degenerate ($\lambda^+ = z_0$), and are equal to the conventional principal components.

- For the 2D-case, in the intrinsic coordinate system, the impedance tensor takes the form:

$$\mathbf{Z}_{2D} = \begin{pmatrix} 0 & z_1 \\ -z_2 & 0 \end{pmatrix}$$

where $Z_1 = \frac{z_1 + z_2}{2}$ and $\det \mathbf{Z}_{2D} = z_1 z_2$.

There are two distinct eigenvalues which are identical to the principal impedances $z_1$ and $z_2$. As the eigenvalues are rotationally invariant, the generality is not lost when using the rotated form of the impedance tensor.

- For the general 3D-case:

$$Z_1 = \frac{Z_{xy} - Z_{yx}}{2} \quad \text{and} \quad \det \mathbf{Z}_{3D} = Z_{xx}Z_{yy} - Z_{xy}Z_{yx}$$

therefore, the eigenvalues are given by the equation:

$$\lambda^+ = Z_1 \pm \sqrt{Z_3^2 - Z_{xx}Z_{yy}} \qquad [I.18]$$

where $Z_3 = \frac{Z_{xy} + Z_{yx}}{2}$.

- The two pairs of eigenvectors ($E^+$, $H^+$) and ($E^-$,$H^-$) define the two polarization states of the electromagnetic field.

The orientation of the major axis of the polarization ellipse is given, in terms of elements of the eigenvectors, by the relation:

$$\tan 2\psi = \frac{2\mathrm{Re}\,(E_x E_y^*)}{|E_x|^2 - |E_y|^2} \qquad [I.19]$$

The ellipticity of the polarization ellipse is defined as follows:

$$\xi = \frac{1 - r}{1 + r} \qquad [I.20]$$

where $r = \frac{|E_x^2 + E_y^2|}{|E_x^2| + |E_y^2| - 2\mathrm{Im}\,(E_x E_y^*)}$

In the case of a 2D-structure the eigenvectors of the electric and magnetic field should be linearly polarized and perpendicular to each other ($\psi^+ - \psi^- = 90^o$, $\xi^+ = 0$). The depart from these conditions, indicates the presence of a 3D-structure.

*I.3. Experimental analysis using Eggers' procedure*

Following Eggers' analysis, the scalar parameters $\lambda^{\pm}$ (the eigenvalues), $\rho^+$ (the apparent resistivities), $\varphi^{\pm}$(the corresponding phases), $\psi^{\pm}$ (the orienta-

**Table I. Eggers' parameters determined from MT-data collected at site A of Ioannina region**

| T | $\|\lambda^+\|$ | $\rho^+$ | $\varphi^+$ | $\|\lambda^-\|$ | $\rho^-$ | $\varphi^-$ | $\psi^+[E^+]$ | $\psi^-[E^-]$ | $\psi^+[E^+]$-$\psi^-[E^-]$ | $\|\xi[E^+]\|$ | $\|\xi[E^-]\|$ |
|---|---|---|---|---|---|---|---|---|---|---|---|
| 12.742 | 4.083 | 42.485 | 83.17 | 40.754 | 4232.652 | -109.84 | 37.04 | 83.01 | -45.96 | 0.077 | 0.024 |
| 15.421 | 1.216 | 4.558 | 118.24 | 44.533 | 6116.635 | -117.58 | 34.53 | 81.62 | -47.09 | 0.074 | 0.008 |
| 19.275 | 0.904 | 3.154 | 88.63 | 42.443 | 6944.360 | -121.86 | 31.19 | 81.32 | -50.13 | 0.082 | 0.005 |
| 26.130 | 0.537 | 1.509 | 60.32 | 36.596 | 6999.092 | -124.63 | 31.07 | 81.24 | -50.17 | 0.057 | 0.001 |
| 30.654 | 0.475 | 1.385 | 70.16 | 33.470 | 6868.091 | -125.08 | 31.77 | 81.28 | -49.51 | 0.051 | 0.000 |
| 37.079 | 0.391 | 1.134 | 70.58 | 30.619 | 6952.618 | -127.05 | 31.27 | 81.15 | -49.87 | 0.050 | 0.001 |
| 52.622 | 0.297 | 0.931 | 60.06 | 25.615 | 6905.401 | -130.60 | 32.48 | 81.11 | -48.63 | 0.058 | 0.002 |
| 57.6 | 0.314 | 1.136 | 64.14 | 24.225 | 6760.429 | -131.08 | 33.26 | 81.15 | -47.90 | 0.062 | 0.003 |
| 74.667 | 0.331 | 1.639 | 73.23 | 22.716 | 7706.120 | -135.19 | 31.96 | 81.19 | -49.23 | 0.028 | 0.003 |
| 106.667 | 0.296 | 1.873 | 72.70 | 18.423 | 7240.516 | -136.95 | 33.28 | 81.15 | -47.88 | 0.011 | 0.004 |
| 128 | 0.306 | 2.397 | 95.04 | 15.347 | 6029.859 | -135.84 | 34.43 | 80.98 | -46.55 | 0.006 | 0.010 |
| 192 | 0.168 | 1.078 | 70.33 | 12.544 | 6042.214 | -134.20 | 31.32 | 80.85 | -49.53 | 0.039 | 0.004 |

**Table II.** Eggers' parameters determined from MT-data collected at site B of Ioannina region

| T | $\lvert\lambda^+\rvert$ | $\rho^+$ | $\varphi^+$ | $\lvert\lambda^-\rvert$ | $\rho^-$ | $\varphi^-$ | $\psi^+[E^+]$ | $\psi^-[E^-]$ | $\psi^+[E^+]-\psi^-[E^-]$ | $\lvert\xi[E^+]\rvert$ | $\lvert\xi[E^-]\rvert$ |
|---|---|---|---|---|---|---|---|---|---|---|---|
| 12.742 | 9.874 | 248.479 | 28.35 | 28.160 | 2020.848 | -128.09 | 36.74 | 67.14 | -30.40 | 0.061 | 0.039 |
| 15.421 | 4.098 | 51.799 | 83.19 | 34.120 | 3590.486 | -121.19 | 31.36 | 64.58 | -33.22 | 0.037 | 0.023 |
| 19.275 | 3.306 | 42.139 | 85.24 | 31.516 | 3828.911 | -120.59 | 31.92 | 63.99 | -32.07 | 0.069 | 0.022 |
| 26.130 | 2.480 | 32.143 | 82.30 | 27.637 | 3991.756 | -123.83 | 31.00 | 63.77 | -32.77 | 0.056 | 0.016 |
| 30.654 | 2.087 | 26.707 | 80.48 | 24.931 | 3810.673 | -124.85 | 31.54 | 63.67 | -32.13 | 0.045 | 0.014 |
| 37.079 | 1.895 | 26.625 | 78.49 | 22.985 | 3917.820 | -126.42 | 30.99 | 63.72 | -32.73 | 0.047 | 0.013 |
| 52.622 | 1.643 | 28.422 | 56.73 | 19.278 | 3911.353 | -129.49 | 31.81 | 63.96 | -32.15 | 0.052 | 0.005 |
| 57.6 | 1.553 | 27.770 | 49.87 | 18.113 | 3779.489 | -130.29 | 32.49 | 63.95 | -31.46 | 0.050 | 0.002 |
| 74.667 | 1.239 | 22.925 | 55.39 | 16.848 | 4238.695 | -135.30 | 31.88 | 63.72 | -31.84 | 0.022 | 0.005 |
| 106.667 | 0.946 | 19.102 | 62.69 | 13.078 | 3648.994 | -135.87 | 33.26 | 63.20 | -29.94 | 0.015 | 0.012 |
| 128 | 0.768 | 15.083 | 90.79 | 10.308 | 2719.881 | -133.01 | 34.63 | 62.19 | -27.55 | 0.027 | 0.021 |
| 192 | 0.635 | 15.467 | 95.71 | 8.958 | 3081.155 | -128.58 | 31.32 | 61.98 | -30.66 | 0.068 | 0.026 |

**Table III. Eggers' parameters determined from MT-data collected at site C of Ioannina region**

| T | $\|\lambda^+\|$ | $\rho^+$ | $\varphi^+$ | $\|\lambda^-\|$ | $\rho^-$ | $\varphi^-$ | $\psi^+[E^+]$ | $\psi^-[E^-]$ | $\psi^+[E^+]-\psi^-[E^-]$ | $\|\xi[E^+]\|$ | $\|\xi[E^-]\|$ |
|---|---|---|---|---|---|---|---|---|---|---|---|
| 12.742 | 5.049 | 64.965 | 88.46 | 28.829 | 2118.037 | -116.53 | 28.90 | 93.98 | -65.08 | 0.082 | 0.051 |
| 15.421 | 4.263 | 56.058 | 94.60 | 30.531 | 2874.855 | -119.53 | 29.89 | 93.59 | -63.70 | 0.074 | 0.036 |
| 19.275 | 3.322 | 42.542 | 85.83 | 28.766 | 3190.054 | -122.96 | 27.88 | 92.17 | -64.29 | 0.109 | 0.019 |
| 26.130 | 2.323 | 28.212 | 83.39 | 24.439 | 3121.377 | -125.26 | 28.72 | 91.44 | -62.72 | 0.094 | 0.013 |
| 30.654 | 2.010 | 24.764 | 80.51 | 22.335 | 3058.342 | -126.09 | 28.99 | 91.38 | -62.39 | 0.079 | 0.011 |
| 37.079 | 1.644 | 20.044 | 81.18 | 20.392 | 3083.752 | -127.94 | 28.58 | 91.29 | -62.71 | 0.081 | 0.014 |
| 52.622 | 1.300 | 17.777 | 78.66 | 17.197 | 3112.486 | -131.39 | 29.71 | 91.10 | -61.40 | 0.090 | 0.012 |
| 57.6 | 1.205 | 16.733 | 66.57 | 16.320 | 3068.172 | -132.20 | 30.45 | 91.01 | -60.57 | 0.083 | 0.004 |
| 74.667 | 1.277 | 24.337 | 58.34 | 15.303 | 3497.264 | -135.58 | 29.04 | 91.49 | -62.46 | 0.047 | 0.006 |
| 106.667 | 1.082 | 24.994 | 68.22 | 12.451 | 3307.155 | -136.48 | 30.72 | 91.90 | -61.18 | 0.035 | 0.021 |
| 128 | 0.943 | 22.749 | 69.70 | 10.222 | 2675.033 | -135.79 | 32.73 | 92.67 | -59.95 | 0.036 | 0.024 |
| 192 | 0.827 | 26.280 | 57.41 | 8.194 | 2578.259 | -134.65 | 29.54 | 93.16 | -63.62 | 0.069 | 0.005 |

tion of the major axis of each polarization ellipse) and $\xi$ (the corresponding ellipticity) are presented in Tables I, II and III for the sites A, B and C respectively. Indicatively, the polarization ellipses for the eigenvectors of the electric and magnetic field at site B are depicted in Fig. I.7.

From the inspection of Tables I-III and Fig. I.7 it is evident that there is a deviation from the ideal 2D-structure, because the two eigenvectors of the electric field (and correspondingly those of the magnetic field) are not perpendicular to each other.

## II. THE DECOMPOSITION OF THE MAGNETOTELLURIC IMPENDANCE TENSOR IN THE PRESENCE OF 3D-LOCAL GALVANIC DISTORTION

### *II.1. The physical background*

The aim of the magnetotelluric method is the mapping of the actual conductivity distribution in the subsurface under prospection. It is considered that the earth consists of a 1D or 2D-background termed as *regional structure* (i.e., the horizontal dimensions of which are comparable with the depth of penetration) coupled with local (compared to the penetration depth) three-dimensional (3D) zones of anomalous conductivity. These near surface anomalies act as *semi-static scatterers* (usually called *galvanic*) which mainly affect the observed electric field in direction and magnitude. Physically, 3D - galvanic distortion is caused by the presence of electric charges at discontinuities or gradients in electrical conductivity. The local 3D-surface structure causes the observed magnetotelluric impedance tensor to be a location dependent mixture of the local and regional responses; this can include distortion of both in magnitude and phase. The above phenomenon is usually termed as «*static shift*».

Thus, let us consider a model of the earth where the regional conductivity structure is disturbed from the existence of a local surface inhomogeneity. The regional electromagnetic field far from the inhomogeneity is denoted ($e^r$, $h^r$). The local surface scatterer distorts the electromagnetic field ($e^r$, $h^r$) and the distortion is described by the relations:

$$e = e^r + \mathbf{D}e^r \qquad [II.1.a]$$

$$h = h^r + \mathbf{F}e^r \qquad [II.1.b]$$

where the 3rd-order matrices **D** and **F** are real and frequency independent, under the assumption that the wave-lengths of the investigated band are appreciably larger than the scale-length of the local inhomogeneity *[Wannamaker et al., 1984a, 1984b], [Zhang, 1989].*

Generally, the electric and magnetic fields ($e^r$, $h^r$) exhibit horizontal and vertical components:

$$e^r = e^r_h + e^r_z \qquad [II.2.a]$$

$$h^r = h^r_h + h^r_z \qquad [II.2.b]$$

It is a fundamental hypothesis of the magnetotelluric study that the incident electromagnetic field to the surface of the earth has only horizontal components. Thus, eq. [II.1.a], due to eq. [II.2.a] can be written:

$$\begin{aligned} e = e^r + \mathbf{D}e^r = e^r_h + e^r_z + \mathbf{D}_h e^r_h + D_{xz} e^r_z \hat{u}_x + D_{yz} e^r_z \hat{u}_y + \\ + (D_{zx} e^r_x + D_{zy} e^r_y + D_{zz} e^r_z)\hat{u}_z \end{aligned} \qquad [II.3]$$

where $\hat{u}_x$, $\hat{u}_y$ and $\hat{u}_z$ denote the unit vectors. Introducing the transfer function $e^r_z = X^r e^r_x + Y^r e^r_y$ and the tensor $\mathbf{D}_z = \begin{pmatrix} X^r D_{xz} & Y^r D_{xz} \\ X^r D_{yz} & Y^r D_{yz} \end{pmatrix}$, eq. [II.3] provides the relation between the horizontal regional electric field, $e^r$, and the horizontal electric field at the measuring site, e:

$$e_h = (\mathbf{I} + \mathbf{D}_h + \mathbf{D}_z)e^r_h \qquad [II.4.a]$$

We define the effective distortion tensor: $\mathbf{P}_h = \mathbf{D}_h + \mathbf{D}_z$. Then, eq. [II.4.a] takes the form:

$$e_h = (\mathbf{I} + \mathbf{P}_h)e^r_h \qquad [II.4.b]$$

An analogous procedure leads to the relation between the horizontal components of the regional magnetic field, $h^r$, and the horizontal components of the magnetic field at the measuring site, h. Thus, the combination of eqs [II.1.b] and [II.2.b] gives:

$$h = h^r + \mathbf{F}e^r = h_h^r + h_z^r + \mathbf{F}_h e_h^r + F_{xz}e_z^r\hat{u}_x + F_{yz}e_z^r\hat{u}_y + (F_{zx}e_x^r + F_{zy}e_y^r + F_{zz}e_z^r)\hat{u}_z \quad [II.5]$$

Introducing now the transfer function $e_z^r = X^r e_x^r + Y^r e_y^r$ and defining the tensor $\mathbf{F}_z = \begin{pmatrix} X^rF_{xz} & Y^rF_{xz} \\ X^rF_{yz} & Y^rF_{yz} \end{pmatrix}$, eq. [II.5] takes the form:

$$h_h = h_h^r + (\mathbf{F}_h + \mathbf{F}_z)e_h^r \quad [II.6.a]$$

We define again the effective distortion tensor: $\mathbf{Q}_h = \mathbf{F}_h + \mathbf{F}_z$. Then, eq. [II.6.a] can be as:

$$h_h = h_h^r + \mathbf{Q}_h e_h^r = h_h^r + \mathbf{Q}_h\mathbf{Z}_r h_h^r = (\mathbf{I} + \mathbf{Q}_h\mathbf{Z}_r)h_h^r \quad [II.6.b]$$

where $\mathbf{Z}_r$ the impedance tensor that refers to the regional geoelectric structure.

Hereafter we refer only to the horizontal components of the electromagnetic fields, by using the notation ($e_r$, $h_r$) for the regionally induced electromagnetic field and (e, h) for the measured electromagnetic field respectively. The measured quantities are correlated through:

$$e = \mathbf{Z}_m h \quad [II.7]$$

where $\mathbf{Z}_m$ is the (measured) impedance tensor. The combination of eqs [II.4.b], [II.6.b] and [II.7] leads to the relation:

$$\mathbf{Z}_m = (\mathbf{I} + \mathbf{P})\mathbf{Z}_r(\mathbf{I} + \mathbf{Q}\mathbf{Z}_r)^{-1} \quad [II.8.a]$$

This relation correlates the impedance tensor $\mathbf{Z}_m$ at a measuring site (i.e., close to the surface scatterer) with the impedance tensor $\mathbf{Z}_r$ that would be measured if the inhomogeneity were not present.

In the low frequency range the variation of the quantity $|\mathbf{Z}_r|$ with the period T obeys the rule $\propto \frac{1}{\sqrt{T}}$; thus eq. [II.8.a] takes the approximate form:

$$\mathbf{Z}_m \approx (\mathbf{I} + \mathbf{P})\mathbf{Z}_r \quad [II.8.b]$$

where the elements of the tensor **P** are real numbers and frequency independent. Defining the distortion tensor **C** as:

$$\mathbf{C} = \mathbf{I} + \mathbf{P} = \begin{pmatrix} C_1 & C_2 \\ C_3 & C_4 \end{pmatrix} \qquad \text{(II.9]}$$

where $C_1 = 1 + P_1$, $C_2 = P_2$, $C_3 = P_3$ and $C_4 = 1 + P_4$, eq. [II.8.b] is transformed to the relation:

$$\mathbf{Z}_m \approx \mathbf{C}\mathbf{Z}_r = \begin{pmatrix} C_1 & C_2 \\ C_3 & C_4 \end{pmatrix} \mathbf{Z}_r \qquad \text{[II.10]}$$

and the quantities $C_1$, $C_2$, $C_3$ and $C_4$ are real numbers and frequency independent *[Wannamaker et al., 1984a], [Chave et al., 1994].*

Notice that the conventional magnetotelluric analysis is not sufficient when galvanic distortion exists, since the extracted scalar parameters are not adequate to describe the structure even if the regional structure has an ideal 1D or 2D-symmetry. Indeed, for a galvanicaly distorting body embedded in a 1D-geoelectric structure the measured impedance tensor is:

$$\mathbf{Z}_m = \mathbf{C}\mathbf{Z}_r = \begin{pmatrix} C_1 & C_2 \\ C_3 & C_4 \end{pmatrix} \begin{pmatrix} 0 & z_0 \\ -z_0 & 0 \end{pmatrix} = \begin{pmatrix} -C_2 z_0 & C_1 z_0 \\ -C_4 z_0 & C_3 z_0 \end{pmatrix} \qquad \text{[II.11]}$$

The following remarks are valid:

a) The observed apparent resistivities differ from the actual regional apparent resistivities and they are static shifted (i.e., their frequency dependence results in a parallel displacement when compared with those of the 1D - structure).

b) The phases remain unchanged and are identical to those of the 1D-impedance tensor.

c) In the conventional analysis the skew is defined as follows:

$$s \equiv \frac{|Z_{xx} + Z_{yy}|}{|Z_{xy} - Z_{yx}|} = \frac{|C_3 - C_2|}{|C_1 + C_4|}$$

The skew index depends only on the distortion tensor elements (which

are real numbers); it does not depend on the regional tensor elements hence, in other words, the skew index measures not the deviation of the geoelectric structure from the ideal 1D-symmetry, but the deviation of the distortion tensor from the form:

$$\mathbf{C} = \begin{pmatrix} C_1 & 0 \\ 0 & C_4 \end{pmatrix}$$

The latter form of the distortion tensor would give a zero skew value if were calculated within the conventional magnetotellyric analysis.

d) By using eqs [I.9.a] and [II.11] it is derived:

$$\tan 4\theta = \frac{2(C_{yy} - C_{xx})\,(C_{xy} + C_{yx})}{(C_{xx} - C_{yy})^2 - (C_{xy} + C_{yx})^2} \qquad [II.12]$$

It is evident that, even if there was not a strike angle (e.g., when 1D-regional structure is considered), the conventional analysis results to the determination of a strike angle which depends only on the elements of the distortion tensor.

*II.2. The Bahr's procedure for the decomposition of the impedance tensor*

An important aspect in the interpretation of the magnetotelluric data is the evaluation of the regional impedance tensor when local 3D-surface anomalies exist. Bahr *[Bahr, 1985], [Bahr, 1988], [Bahr, 1991]*, attempted to extract information about the regional impedance tensor from the measured one. He found that galvanic distortion or current channelling does not destroy most of the existing information about an underlying 2D-inductive process.

By considering a 2D-regional geoelectric structure, the impedance tensor in the intrinsic coordinate system is given as:

$$\mathbf{Z}_{2D} = \begin{pmatrix} 0 & \alpha \\ -b & 0 \end{pmatrix} \qquad [II.13]$$

The scattering of the electric field by the local inhomogeneity can be described by an impedance tensor of the following form [*superposition model 3D-(local)/ 2D-(regional)*]:

$$\mathbf{Z}_m = \begin{pmatrix} C_1 & C_2 \\ C_3 & C_4 \end{pmatrix} \begin{pmatrix} 0 & \alpha \\ -b & 0 \end{pmatrix} = \begin{pmatrix} -C_2 b & C_1 \alpha \\ -C_4 b & C_3 \alpha \end{pmatrix} \qquad [II.14]$$

Since the distortion tensor is real and frequency independent (at low frequencies), the elements at each column of the impedance tensor should have the same phase. This does not happen in an arbitrary measuring coordinate system, where the elements of the impedance tensor should be linear combinations of the principal impedances; it is therefore evident that a dimensionality parameter must be defined that could describe how much the particular data depart from the aforementioned model assumed. By using the condition that the elements at each column of the impedance tensor should have the same phase, a rotationally invariant scalar parameter is defined, termed as the *regional skew*:

$$\eta = \left( \frac{|[D_1,S_2] - [S_1,D_2]|^{1/2}}{|D_2|} \right) \qquad [II.15]$$

where:

$$S_1 = Z_{xx} + Z_{yy} \quad D_1 = Z_{xx} - Z_{yy}$$
$$S_2 = Z_{xy} + Z_{yx} \quad D_2 = Z_{xy} - Z_{yx}$$

and $[A,B] = Re(A)Im(B) - Re(B)Im(A)$ the vector product of the complex A and B.

When the regional structure is 2D, the elements at each column of the impedance tensor in eq. [II.14] have the same phase, thus the *regional skew* becomes zero. If the regional structure is 1D, the elements of the impedance tensor in eq. [II.13] have the same phase, resulting again in null value of the *regional skew*, $\eta = 0$. Thus, another rotationally invariant parameter, which is a measure of the phase difference is introduced:

$$\mu = \frac{|[D_1,S_2] + [S_1,D_2]|^{1/2}}{|D_2|} \qquad [II.16]$$

It should be noted that $\mu$ becomes unstable if the conventional skew s, defined in eq. [I.10], is very small. The same happens for the *regional skew* when the parameter $\mu$ is very small indicating a less complex model than that of eq. [II.14]. So, $\mu$ is referred as an indicator of a regional 1D-structure.

**Table IV.** Parameters determined by Bahr's analysis of the MT-data from each of the sites A, B, C and B-C of Ioannina region.

| T | $\mu^A$ | $\eta^A$ | $\mu^B$ | $\eta^B$ | $\mu^C$ | $\eta^C$ |
|---|---|---|---|---|---|---|
| 12.742 | 0.57410 | 0.17978 | 0.75063 | 0.75063 | 0.44008 | 0.23471 |
| 15.421 | 0.49173 | 0.12364 | 0.36121 | 0.11809 | 0.38350 | 0.04742 |
| 19.275 | 0.52418 | 0.07131 | 0.66396 | 0.17118 | 0.53996 | 0.19288 |
| 26.130 | 0.44510 | 0.09453 | 0.57552 | 0.21383 | 0.49735 | 0.19815 |
| 30.654 | 0.42203 | 0.09079 | 0.50372 | 0.20391 | 0.45020 | 0.18676 |
| 37.079 | 0.41370 | 0.07006 | 0.51457 | 0.20556 | 0.44958 | 0.14356 |
| 52.622 | 0.45671 | 0.01592 | 0.65834 | 0.17950 | 0.48441 | 0.16526 |
| 57.6 | 0.47582 | 0.02645 | 0.68556 | 0.15680 | 0.48742 | 0.19419 |
| 74.667 | 0.29545 | 0.04437 | 0.37945 | 0.14728 | 0.35430 | 0.13404 |
| 106.667 | 0.16139 | 0.03192 | 0.21478 | 0.12872 | 0.24873 | 0.10868 |
| 128 | 0.10354 | 0.10354 | 0.24858 | 0.09103 | 0.25164 | 0.12679 |
| 192 | 0.35811 | 0.06622 | 0.63121 | 0.13118 | 0.45177 | 0.18021 |

| T | $\mu^{B-C}$ | $\eta^{B-C}$ |
|---|---|---|
| 0.552 | 0.35495 | 0.23566 |
| 0.820 | 0.37800 | 0.17446 |
| 1.450 | 0.27369 | 0.18519 |
| 11.601 | 0.45745 | 0.33093 |
| 23.256 | 0.34901 | 0.20304 |
| 46.512 | 0.20168 | 0.09192 |
| 93.458 | 0.15784 | 0.06672 |
| 163.934 | 0.29756 | 0.15019 |
| 192.308 | 0.37687 | 0.08592 |
| 285.714 | 0.43338 | 0.13154 |
| 416.667 | 0.34302 | 0.19956 |
| 666.667 | 0.45972 | 0.05147 |

**Table V.** Skew angles determined by Bahr's analysis of the MT-data from each of the sites A, B, C and B-C of Ioannina region.

| T | $\beta_1^A$ | $\beta_2^A$ | $\beta_2^A-\beta_1^A$ | $\beta_1^B$ | $\beta_2^B$ | $\beta_2^B-\beta_1^B$ | $\beta_1^C$ | $\beta_2^C$ | $\beta_2^C-\beta_1^C$ |
|---|---|---|---|---|---|---|---|---|---|
| 12.742 | -43.40 | 46.70 | 90.10 | -52.33 | 20.72 | 73.06 | -27.48 | 66.23 | 93.70 |
| 15.421 | -41.03 | 54.52 | 95.56 | -50.95 | 38.19 | 89.14 | -25.01 | 72.39 | 97.40 |
| 19.275 | -41.68 | 48.83 | 90.51 | -51.05 | 39.24 | 90.30 | -25.08 | 64.08 | 89.16 |
| 26.130 | -41.58 | 41.44 | 83.02 | -50.81 | 38.62 | 89.43 | -25.21 | 62.15 | 87.36 |
| 30.654 | -41.51 | 44.28 | 85.80 | -50.81 | 38.23 | 89.04 | -25.21 | 60.15 | 85.37 |
| 37.079 | -41.68 | 43.58 | 85.25 | -50.75 | 37.95 | 88.69 | -25.37 | 60.89 | 86.26 |
| 52.622 | -41.79 | 44.47 | 86.25 | -50.79 | 35.52 | 86.31 | -25.36 | 60.71 | 86.07 |
| 57.6 | -41.78 | 45.50 | 87.28 | -50.83 | 35.13 | 85.96 | -25.32 | 56.37 | 81.68 |
| 74.667 | -41.70 | 39.16 | 80.87 | -50.78 | 35.25 | 86.03 | -25.31 | 46.99 | 72.30 |
| 106.667 | -41.78 | 40.70 | 82.48 | -51.37 | 35.99 | 87.36 | -25.37 | 53.07 | 78.45 |
| 128 | -42.08 | 50.02 | 92.10 | -51.94 | 38.42 | 90.35 | -24.78 | 56.31 | 81.09 |
| 192 | -42.12 | 38.55 | 80.67 | -52.29 | 39.30 | 91.58 | -23.80 | 48.71 | 72.51 |

| T | $\beta_1^{B-C}$ | $\beta_2^{B-C}$ | $\beta_2^{B-C}-\beta_1^{B-C}$ |
|---|---|---|---|
| 0.552 | -2.36 | 18.07 | 20.44 |
| 0.820 | 1.06 | 30.03 | 28.96 |
| 1.450 | -1.27 | 16.05 | 17.32 |
| 11.601 | -5.26 | 70.30 | 75.55 |
| 23.256 | 0.90 | 83.85 | 82.95 |
| 46.512 | 3.01 | 83.65 | 80.63 |
| 93.458 | 2.89 | 80.56 | 77.67 |
| 163.934 | 2.83 | 78.26 | 75.43 |
| 192.308 | 3.35 | 87.67 | 84.32 |
| 285.714 | 0.93 | 74.11 | 73.18 |
| 416.667 | 3.88 | 78.16 | 74.28 |
| 666.667 | 5.83 | 78.56 | 72.73 |

*II.3. Experimental results using Bahr's analysis*

In Table IV the calculated values of $\mu$ and $\eta$ for various periods T and for the four neighbouring sites A, B, C and (B-C) of Ioannina region are presented (the skew s has also been calculated according to the conventional analysis).

An inspection of these results, indicates that the MT-data are compatible with the 3D-(local)/2D-(regional) model. Furthermore, by applying the technique of the telluric vectors suggested by Bahr *[Bahr, 1991]*, and calculating the *skew angles* $\beta_1$ and $\beta_2$ and their difference $-\beta_1 + \beta_2$, (see Table V) we found that $-\beta_1 + \beta_2 \approx 90^0$ in a wide period range and for all the measuring sites. This means that the local scatterer acts in such a way, so that the linear polarization of the electric field does not at all depend on the magnetic field polarization (*local channelling*).

*II.4. The Groom & Bailey's procedure for the decomposition of the impedance tensor*

It is usually assumed *[Groom, 1988]* that the earth is essentially flat with a two-dimensional conductivity structure on a large regional scale; this assumption implies that any local three-dimensional structures are all inductively weak. In the principal axis system of this two-dimensional structure (i.e., the x-horizontal axis is along the strike of the 2D-structure and the vertical axis is normal to the earth's surface), the regional horizontal electric field components, $e_r$, and magnetic field components, $h_r$, are linearly related:

$$e_r = \begin{pmatrix} 0 & \alpha \\ -b & 0 \end{pmatrix} h_r = \mathbf{Z}_{2D} h_r \qquad [II.17]$$

where $\alpha$ denotes the quantity $Z_\perp$ which is the impedance associated with the 2D-mode containing current only perpendicular to the strike and b denotes the quantity $Z_{||}$ which is the impedance associated with the mode containing current only parallel to the strike. When the horizontal electric field, e, and the horizontal magnetic field, h, are measured at a point of the earth surface, they deviate from the regional values $e_r$ and $h_r$, due to local conductivity variations. The electric field can be strongly distorted by charges that are accu-

mulated at conductivity gradients or boundaries; on the other hand, the magnetic field is not so strongly disturbed since it is due to a weighted spatial average of the telluric current density over a much larger volume. Therefore, we are justified to adopt the approximation: $h \simeq h_r$, but the electric field, e, should be related to $e_r$ through a distortion or channelling tensor, **C** *[Bahr, 1985], [Berdichevsky & Dmitriev, 1976]*:

$$e = \mathbf{C} \cdot e_r = \begin{pmatrix} C_1 & C_2 \\ C_3 & C_4 \end{pmatrix} e_r \qquad [II.18]$$

When small-scale surface scatterers (which are assumed to be inductively weak) are present, their effects can be considered as frequency independent and the elements of the tensor **C** as real numbers. In the absence of distortions, **C** will reduce to the identity tensor **I**.

In the case of a galvanic distortion and in order to recover information concerning the two-dimensional impedances, it has been shown, *[Bahr, 1985], [Zhang et al. 1987]*, that the exact knowledge of the elements of **C** is not necessary. The decomposition of the measured impedance tensor, however, it is a requisite to be done uniquely.

In the intrinsic (or principal axis) system of the regional structure, the impedance tensor that refers to the 2D-structure obeys the relation:

$$e_r = \mathbf{Z}_{2D}\, h_r$$

which, using eq. [II.18], gives:

$$e = \mathbf{C}\mathbf{Z}_{2D}\, h_r \qquad [II.19.a]$$

or in the measuring coordinate system:

$$e = \hat{\mathrm{R}}\mathbf{C}\mathbf{Z}_{2D}\,\hat{\mathrm{R}}^t h = \mathbf{Z}_m h \qquad [II.19.b]$$

where $\mathbf{Z}_m$ is the measured impedance tensor, $\mathbf{Z}_{2D}$ is the regional 2D-tensor in the regional inductive principal axis system (i.e., it has the form of eq. [II.17]), **C** is the distortion tensor expressed also at the regional intrinsic system and $\hat{\mathrm{R}}$ is the rotation operator which performs the vector transformation from the principal axis system to the measurement axis system.

The incompleteness of the above decomposition, due to the non-uniqueness, is best illustrated by the following argument *[Groom, 1988], [Groom & Bailey, 1989]*. By considering the transformations:

$$\mathbf{Z}'_{2D} = \mathbf{W}\mathbf{Z}_{2D} = \begin{pmatrix} W_1 & 0 \\ 0 & W_2 \end{pmatrix}\mathbf{Z}_{2D} \quad \text{and} \quad \mathbf{C}' = \mathbf{C}\mathbf{W}^{-1}$$

where $W_1$ and $W_2$ are non-zero real numbers, the new decomposition:

$$Z_m = \hat{R}\mathbf{C}'\mathbf{Z}'_{2D}\hat{R}^t \qquad [II.20]$$

is also valid as that of eq. [II.19.b], since $\mathbf{C}'$ is still real and $\mathbf{Z}'_{2D}$ still has the ideal 2D-form. We therefore conclude that, although the decomposition of the impedance tensor expressed with eq. [II.19.b] is physically correct, it is not unique and hence not yet a useful one.

Groom and Bailey *[Groom & Bailey, 1989]* proceeded to a useful factorization of the distortion tensor using a modified form of the Pauli spin matrices *[Spitz, 1985]*:

$$\mathbf{I} = \begin{pmatrix} 1 & 0 \\ 0 & 1 \end{pmatrix},\ \mathbf{\Sigma}_1 = \begin{pmatrix} 0 & 1 \\ 1 & 0 \end{pmatrix},\ \mathbf{\Sigma}_2 = \begin{pmatrix} 0 & -1 \\ 1 & 0 \end{pmatrix},\ \mathbf{\Sigma}_3 = \begin{pmatrix} 1 & 0 \\ 0 & -1 \end{pmatrix}$$

and suggested the following representation for the distortion tensor:

$$\mathbf{C} = g\mathbf{TSA} \qquad [II.21]$$

where g is a real scalar, while the tensor factors are defined from the equations:

$$\mathbf{T} = N_2(\mathbf{I} + t\mathbf{\Sigma}_2) \qquad [II.22.a]$$

$$\mathbf{S} = N_1(\mathbf{I} + e\mathbf{\Sigma}_1) \qquad [II.22.b]$$

$$\mathbf{A} = N_3(\mathbf{I} + s\mathbf{\Sigma}_3) \qquad [II.22.c]$$

The normalizing factors $N_i$ are defined in such a way so that each one of these tensors to preserve the power (but not the isotropy) of an isotropically pola-

rized random electric field. The meaning of this is that the intensity of the electric field distorted from a scatterer (the effect of which is described by one of the tensors **T**, **S** or **A**) will be the same with that of the field in the case where the scatterer is not present, for a random but isotropic polarization. For example:

$$N_2^2 \langle \mathbf{E}^t\mathbf{T}^t, \mathbf{T}\mathbf{E}\rangle = \langle \mathbf{E}^t, \mathbf{E}\rangle \qquad [II.23]$$

where the mean value is obtained versus the random of the isotropic polarization of the electric field. Equation [II.23] provides for the tensor **T**:

$$N_2^2 \left\langle (E_x\ E_y)\begin{pmatrix} 1 & t \\ -t & 1 \end{pmatrix}, \begin{pmatrix} 1 & -t \\ t & 1 \end{pmatrix}\begin{pmatrix} E_x \\ E_y \end{pmatrix}\right\rangle = \left\langle (E_x\ E_y), \begin{pmatrix} E_x \\ E_y \end{pmatrix}\right\rangle \Rightarrow$$

$$\Rightarrow N_2^2(1 + t^2)\ [\langle E_x^2\rangle + \langle E_y^2\rangle] = \langle E_x^2\rangle + \langle E_y^2\rangle \Rightarrow N_2 = \frac{1}{\sqrt{1 + t^2}}$$

For tensor **S** it is derived:

$$N_1 = \frac{1}{\sqrt{1 + e^2}}$$

And finally for tensor **A**:

$$N_3 = \frac{1}{\sqrt{1 + s^2}}$$

It is underlined that the product **TSA**, however, does not necessarily preserve the power of the electric field.

A physical insight into the effect of each one of these distortion tensors on the regional electric field can be obtained by studying Figs II.1, II.2 and II.3 which depict the effects of the tensors **T**, **S** and **A**, on a family of unit vectors. The act of the splitting tensor, **A**:

$$\mathbf{A} = N_3(\mathbf{I} + s\boldsymbol{\Sigma}_3) = N_3\begin{pmatrix} 1 + s & 0 \\ 0 & 1 - s \end{pmatrix} \qquad [II.24.a]$$

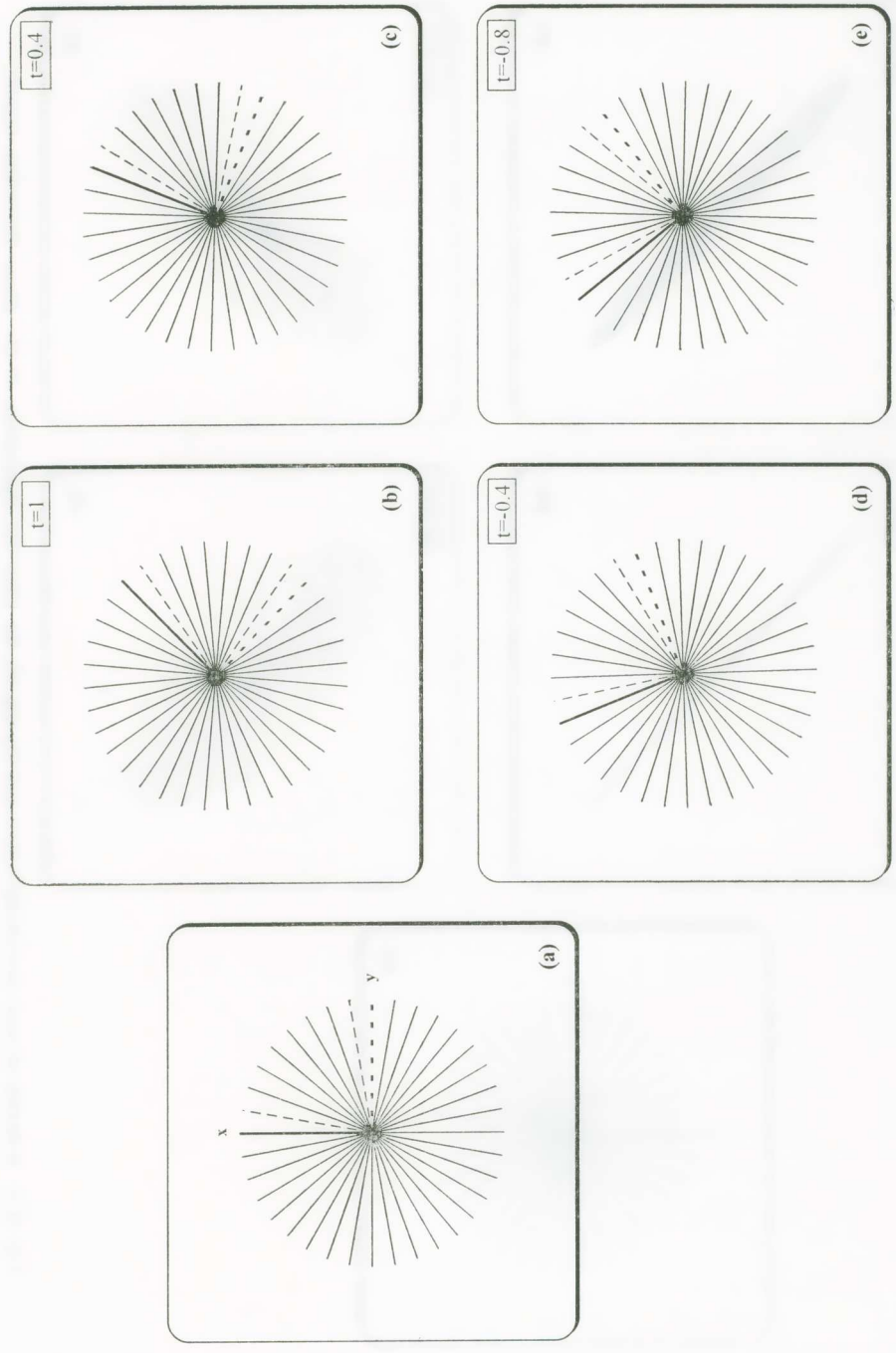


Fig. II.1. A family of unit vectors: **(a)** before and **(b)**, **(c)**, **(d)**, **(e)** after the application of the twist distortion tensor.

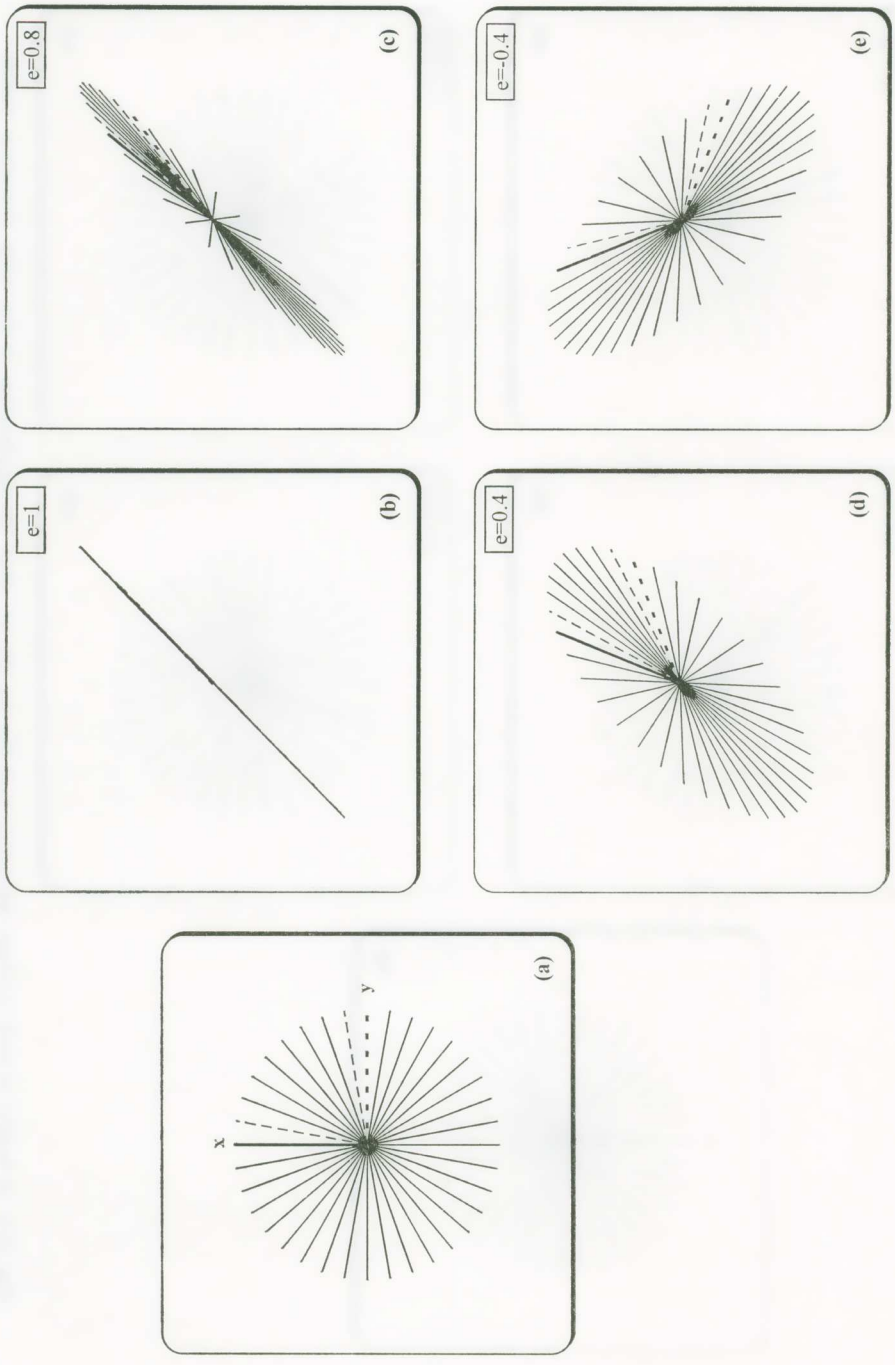


Fig. II.2. A family of unit vectors **(a)** before and **(b), (c), (d), (e)** after the application of the shear distortion tensor.

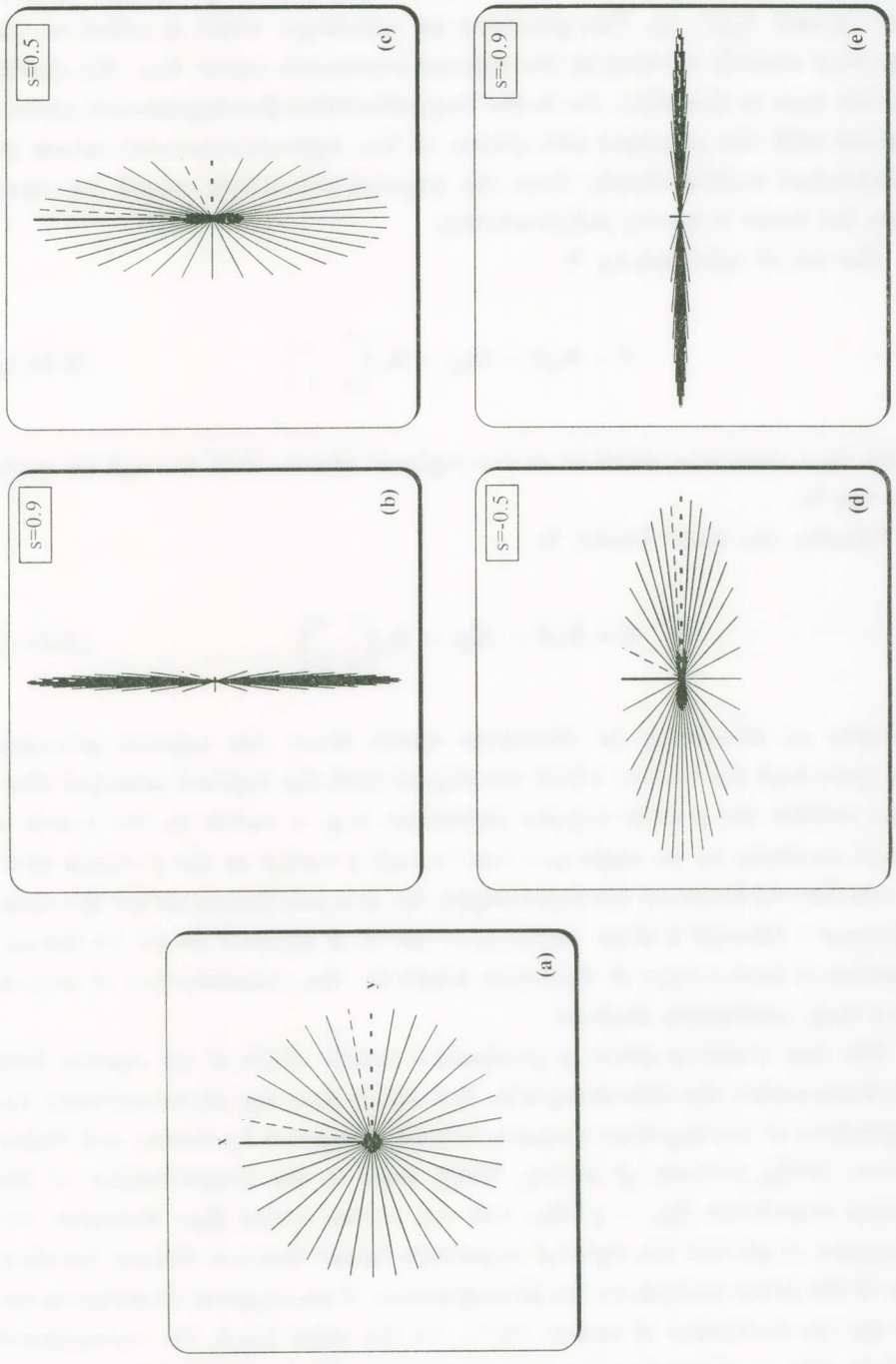


Fig II.3. A family of unit vectors **(a)** before and **(b), (c), (d), (e)** after the application of the splitting distortion tensor.

results to an amplification of the two field components by different factors $N_3(1 + s)$ and $N_3(1 - s)$. This generates an anisotropy which is added to the anisotropy already existing in the regional impedance tensor $\mathbf{Z}_{2D}$. We clarify that this type of distortion due to the local anisotropy (having intrinsic system identical with the principal axis system of the regional structure) cannot be distinguished experimentally from the regional anisotropy except for cases where the latter is known independently.

The act of twist tensor, **T**:

$$\mathbf{T} = N_2(\mathbf{I} + t\boldsymbol{\Sigma}_2) = N_2 \begin{pmatrix} 1 & -t \\ t & 1 \end{pmatrix} \qquad [II.24.b]$$

results to a clockwise rotation of the regional electric field through an angle $\varphi_t = \tan^{-1}t$.

Finally, the shear tensor, **S**:

$$\mathbf{S} = N_1(\mathbf{I} + e\boldsymbol{\Sigma}_1) = N_1 \begin{pmatrix} 1 & e \\ e & 1 \end{pmatrix} \qquad [II.24.c]$$

generates an anisotropy in directions which bisect the regional principal axes. Note that the vectors which are aligned with the regional principal directions exhibit the greater angular deviations (e.g. a vector on the x-axis is rotated clockwise by an angle $\varphi_e = \tan^{-1} e$, and a vector on the y-axis is rotated counter-clockwise by the same angle). So, it is justified to define the *shear parameter* e through a *shear angle*: $\varphi_e = \tan^{-1}e$. A physical model for the explanation of such a type of distortion might be the concentration of current into a long conductive channel.

The real scalar quantity g produces a «*static shift*» of the electric field and characterizes the measuring site. We clarify that the aforementioned decomposition of the impedance tensor, initially proposed by Groom and Bailey *[Groom, 1988], [Groom & Bailey, 1989]*, leads to the determination of the regional impedance $\mathbf{Z}'_{2D} = g\mathbf{A}\mathbf{Z}'_{2D}$ and not of the actual $\mathbf{Z}_{2D}$. However, the absorption of gA into the regional impedance tensor does not destroy the ideal form of the latter and allows the determination of the regional impedances except for the correction of «*static shift*». On the other hand, the conventional analysis fails to determine the correct regional principal impedances, due to

the fact that except g**A** it absorbs also the twist and shear tensors into the regional 2D-tensor, thus dramatically destroying its two-dimensional form, as it is shown later in this paper.

*Uniqueness of the impedance tensor decomposition by Groom and Bailey*

The distortion tensor, **C**, is written analytically:

$$\mathbf{C} = \frac{g}{\sqrt{(1+e^2)(1+t^2)(1+s^2)}} \begin{pmatrix} (1+s)(1-te) & (1-s)(e-t) \\ (1+s)(e+t) & (1-s)(1+te) \end{pmatrix} \quad \text{[II.25.a]}$$

If we consider weak distortions (i.e., t, e and s much smaller than unity), we may ignore 2nd-order terms for the parameters e, s and t, then eq. [II.25.a] becomes:

$$\mathbf{C} = \begin{pmatrix} C_1 & C_2 \\ C_3 & C_4 \end{pmatrix} \approx g \begin{pmatrix} 1+s & e-t \\ e+t & 1-s \end{pmatrix} \quad \text{[II.25.b]}$$

The distortion parameters are easily derived from eq. [II.25.b]:

$$g \approx \frac{C_1 + C_4}{2}, \quad e \approx \frac{C_2 + C_3}{C_1 + C_4}, \quad s \approx \frac{C_1 - C_4}{C_1 + C_4}, \quad t \approx \frac{C_3 - C_2}{C_1 + C_4}$$

In eq. [II.25.a] the normalizing factors are incorporated into g. We consider the set $T$ of all the physically realistic distortion tensors. From this set it is nessecary to exclude the tensors that have the following forms:

$$\mathbf{C} = \begin{pmatrix} C_1 & 0 \\ C_3 & 0 \end{pmatrix}, \quad C = \begin{pmatrix} 0 & C_2 \\ C_3 & 0 \end{pmatrix}, \quad C = \begin{pmatrix} 0 & C_2 \\ 0 & C_4 \end{pmatrix}$$

due to the fact that their effect cannot be attributed to any physical arrangement of earth conductivities. This is evident by studying their effect at the family of unit vectors (see Fig. II.4). The exclusion of these tensors imposes: $s \neq \pm 1$.

Groom and Bailey *[Groom & Bailey, 1989]* define:

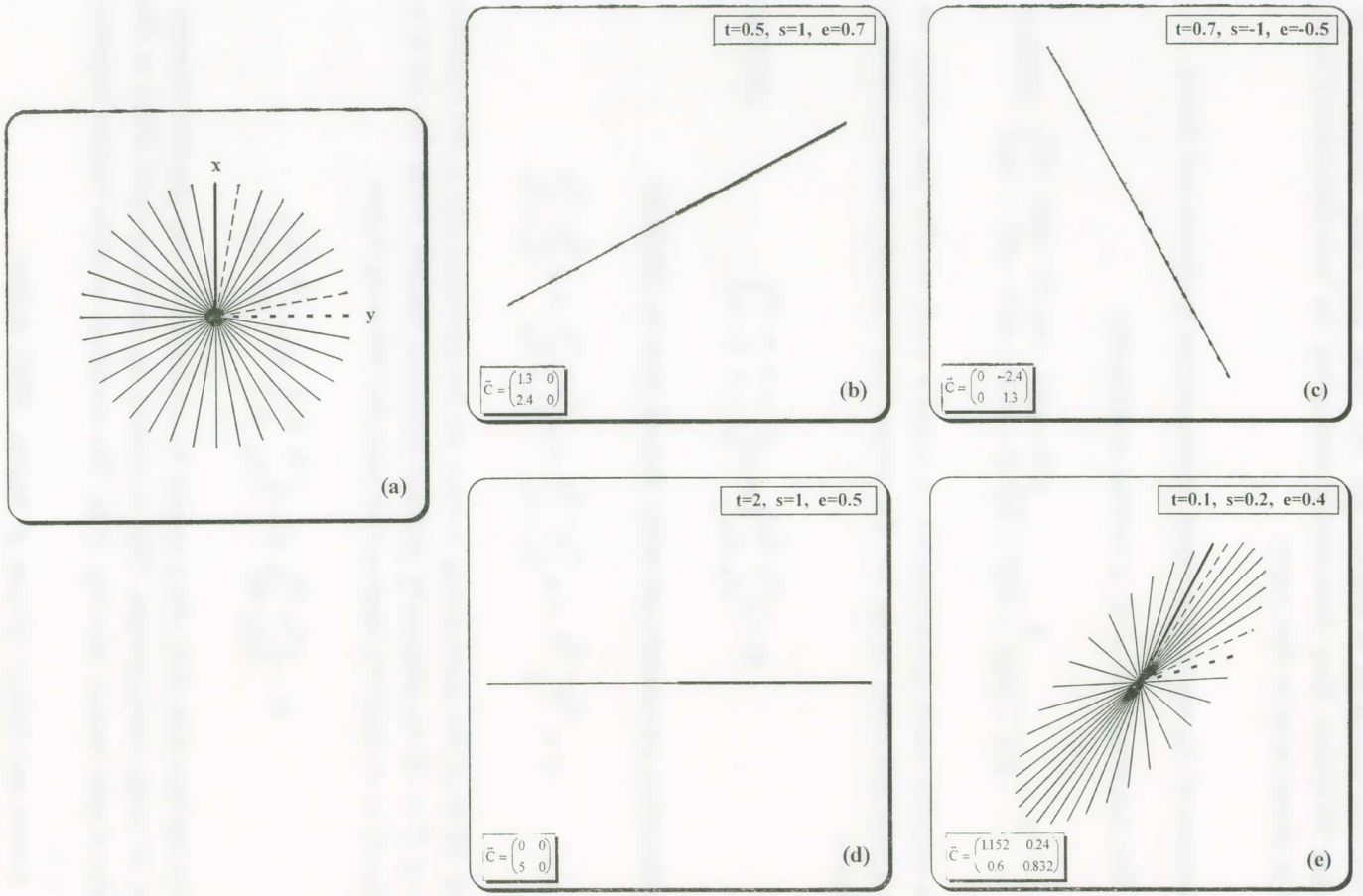


Fig. II.4. A family of unit vectors **(a)** before and **(b), (c), (d)** after the application of physically non-acceptable distortion tensors; **(e)** the application of a physically acceptable distortion tensor.

$$\gamma = \frac{C_2}{C_4} = \frac{e - t}{1 + te}, \text{ if } C_4 \neq 0 \qquad [II.26.a]$$

$$\beta = \frac{C_3}{C_1} = \frac{e + t}{1 - te}, \text{ if } C_1 \neq 0 \qquad [II.26.b]$$

Let us examine some special cases:

- If $\gamma = \beta$ there is a unique solution:

$$t = 0,\ e = \gamma = \beta,\ g = \frac{C_1 + C_4}{2},\ s = \frac{C_1 - C_4}{2g}$$

- If $\gamma = -\beta$, then there is also a unique solution:

$$e = 0,\ t = -\gamma = \beta,\ g = \frac{C_1 + C_4}{2},\ s = \frac{C_1 - C_4}{2g}$$

Fig. II.5 depicts the effects of the distortion tensors which satisfy the restrictions $\gamma = \beta$ or $\gamma = -\beta$.

- If $\gamma \neq \pm\ \beta$ then the distortion parameters e and t can be found by solving the quadratic equations:

$$(\gamma + \beta)e^2 + 2e(1 - \gamma\beta) - (\beta + \gamma) = 0$$
$$(\gamma - \beta)t^2 - 2t(1 + \gamma\beta) - (\gamma - \beta) = 0$$

Each one of the above equations must have two real solutions:

$$t = \frac{(\gamma\beta + 1) \pm \sqrt{(1 + \gamma^2)(1 + \beta^2)}}{\gamma - \beta}$$

$$e = \frac{(\gamma\beta - 1) \pm \sqrt{(1 + \gamma^2)(1 + \beta^2)}}{\gamma + \beta}$$

Groom and Bailey denote $t^+$ the solution with the positive square root for the twist parameter and $t^-$ the alternative solution; an analogous notation can be used for the shear parameter. It is easy to show:

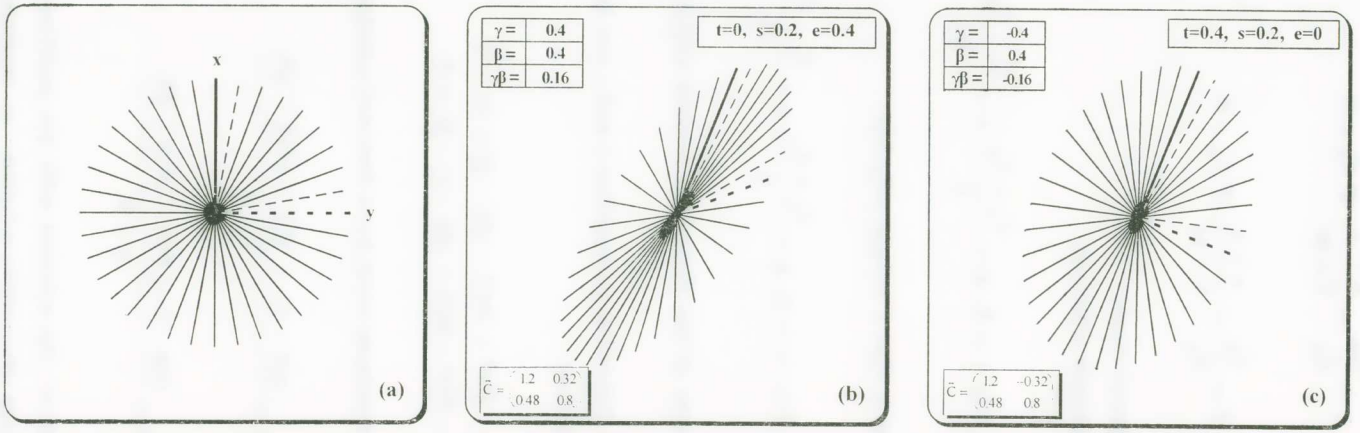


Fig. II.5. A family of unit vectors **(a)** before and **(b)** after the application of a distortion tensor with shear and anisotropy and **(c)** the application of a distortion tensor with twist and anisotropy.

$$t^+ \cdot t^- = -1 \qquad e^+ \cdot e^- = -1 \qquad \text{[II.27]}$$

Thus, there are two sets of solutions for the shear and twist distortion parameters:

$$(e_1,t_1) = (e^+,t^-) \qquad \text{[II.28.a]}$$

$$(e_2,t_2) = (e^-,t^+) \qquad \text{[II.28.b]}$$

Also, note that if $\gamma\beta = -1 \leftrightarrow t = \pm 1$ and if $\gamma\beta = +1 \leftrightarrow e = \pm 1$. Furthermore, if we consider for the distortion parameters the solution set (g, t, e, s) as valid, then the solution set (-gets, $-t^{-1}$, $-e^{-1}$, $s^{-1}$) also holds. This does not imply that it is always possible to discriminate between «*small*» distortion ($|t|, |e| < 1$) and «*large*» distortion ($|t|, |e| > 1$) solution. Only if $0 \leq |\gamma\beta| \leq 1$, then $|t_2| < |t_1|$ and $|e_2| < |e_1|$, so we may distinguish between «*small*» and «*large*» distortion solutions. Generally, when $|\gamma\beta| > 1$, the «*small*» and «*large*» distortion solutions are mixed. The effects of the distortion tensor with all the aforementioned possible configurations are depicted in Fig. II.6.

For the spitting parameter, eq. [II.25.a] gives:

$$\frac{1+s}{1-s} = \left(\frac{1+te}{1-te}\right) \cdot \frac{C_1}{C_4}$$

where $te \neq 1$ and $C_4 \neq 0$. This equation leads to the solutions:

$$s_1 = \frac{(C_1 - C_4) + e_1 t_1 (C_1 + C_4)}{(C_1 + C_4) + e_1 t_1 (C_1 - C_4)} \qquad \text{[II.29.a]}$$

$$s_2 = \frac{1}{s_1} \qquad \text{[II.29.b]}$$

We underline that the condition $|\gamma\beta| < 1$ does not necessarily implies the existence of a «*small*» anisotropy distortion.

The «*static shift*» parameter g is determined by multiplying the distortion tensor **C** with the tensor factor $\mathbf{S^{-1}T^{-1}}$. The inverse of **T** always exists, but the inverse of tensor **S** exists only if $e \neq \pm 1$. If this is the case, then Groom and Bailey proved that the «*static shift*» parameter is given by:

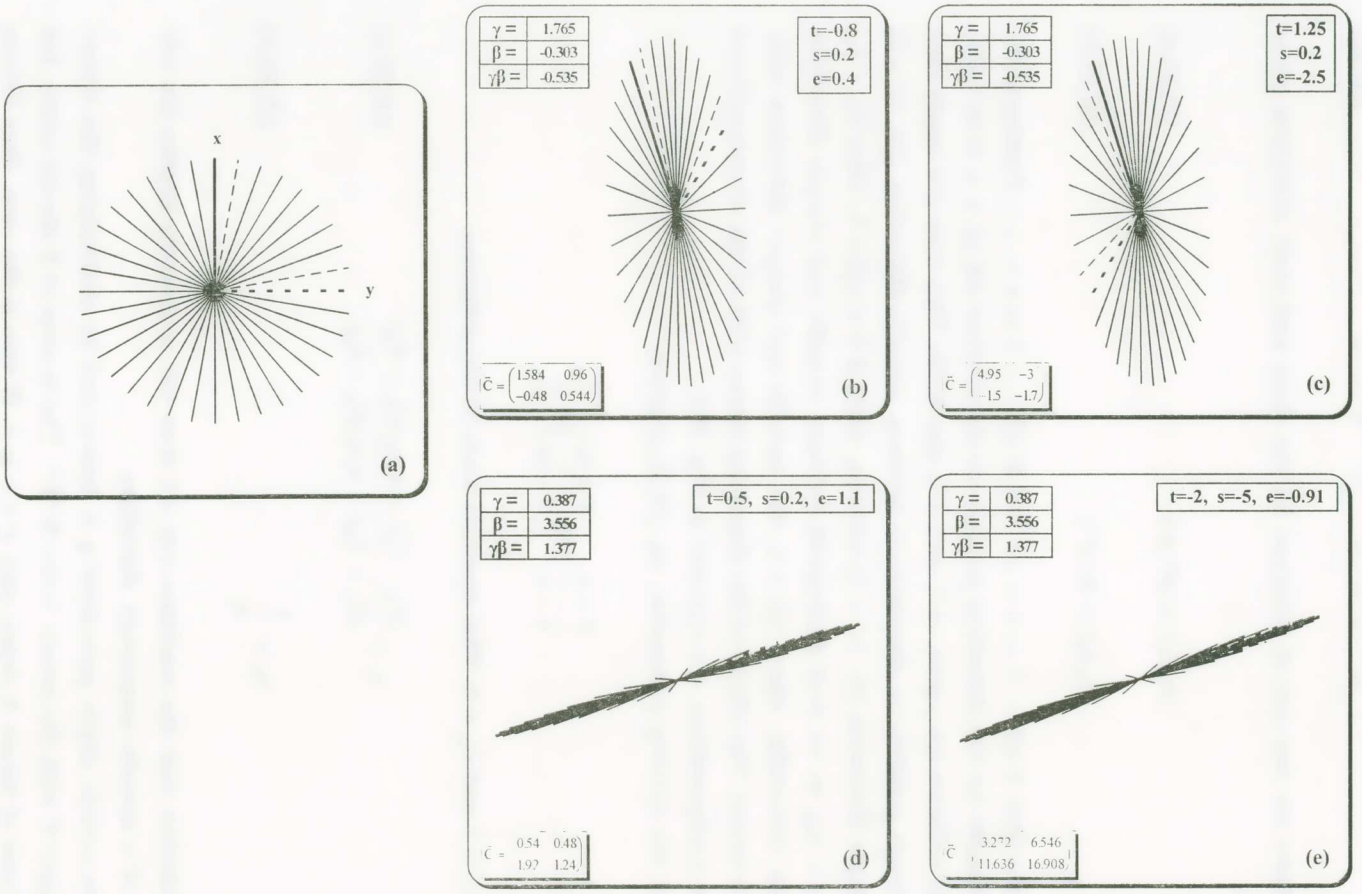


Fig. II.6. A family of unit vectors **(a)** before the application of a distortion tensor; **(b)** after the application of «small» distortion; **(c)** after the application of «large» distortion; **(d)** and **(e)** after the application of «small» twist and «large» shear distortions, and «small» shear and «large» twist distortions respectively.

$$2g_i = \frac{1}{(1-e_i^2)(1+t_i^2)} [C_1(1 + e_i t_i) - C_2(e_i + t_i) - C_3(e_i - t_i) + C_4(1 - t_i e_i)] \quad [II.30.a]$$

where $i = 1, 2$. On the other hand, if $e = \pm 1$, then $t \neq \pm 1$; in such a case we find:

$$g = \frac{C_2}{(s-1)(t \pm 1)} \quad [II.30.b]$$

A final issue to investigate is the order of factorization of the distortion tensor **C**. The tensor **A**, as mentioned above, is absorbed into the regional impedance tensor and hence it does not commute with the others; furthermore the equation $\mathbf{TS} = \mathbf{ST}$ is not generally valid. Thus, we restrict ourselves to two possible factorizations of **C**:

$$\mathbf{C} = g\mathbf{TSA} \text{ or } \mathbf{C} = g\mathbf{STA}$$

Groom and Bailey showed that the latter factorization leads to equations that not always produce a real set of solutions for the distortion parameters and hence it is rejected. Therefore, only one possible order of factorization for the distortion tensor remains:

$$\mathbf{C} = g\mathbf{TSA} \quad [II.31]$$

The above discussion leads to the conclusion that the decomposition of any physically realistic distortion tensor provides a pair of solution sets for the distortion parameters and a selection of one of them can be achieved only after comparisons with physical and geological conditions and restrictions. As a summary, Figs II.7, II.8 and II.9 depict the distorting effect of a semi - static scatterer on the regionally induced electric field for different orders of symmetry of the regional geoelectric structure and for different types of scatterers.

Inserting eq. [II.31] to eq. [II.19.b], the decomposition of the measured impedance tensor is expressed by:

$$\mathbf{Z}_m = \hat{\mathbf{R}} g\mathbf{TSA}\mathbf{Z}_{2D}\hat{\mathbf{R}}^t \quad [II.32.a]$$

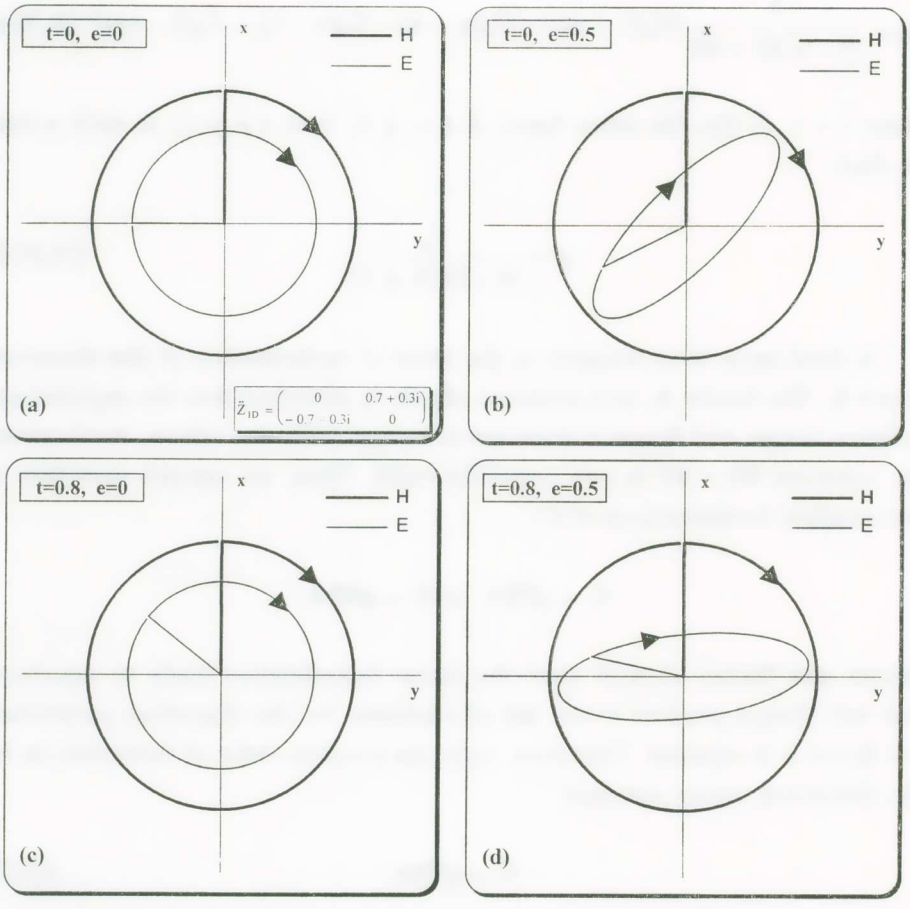


Fig. II.7. The geometrical locus of the electric field vector trace as a result of the rotation of the incident horizontal linearly polarized unitary magnetic field, for **(a)** an ideal 1D-structure; **(b), (c), (d)** a 1D-regional structure with the presence of a local near-surface semi-static scatterer, with different distortion parameters.

Recalling that the matrix g**A** is absorbed into the tensor $\mathbf{Z}_{2D}$ the above equation becomes:

$$\mathbf{Z}_m = \hat{\mathbf{R}}\mathbf{T}\mathbf{S}\mathbf{Z}'_{2D}\hat{\mathbf{R}}^t \qquad \text{[II.32.b]}$$

where:

$$\mathbf{Z}'_{2D} = g\begin{pmatrix} 0 & (1+s)\alpha \\ -(1-s)b & 0 \end{pmatrix} = \begin{pmatrix} 0 & \alpha' \\ -b' & 0 \end{pmatrix} \qquad \text{[II.33]}$$

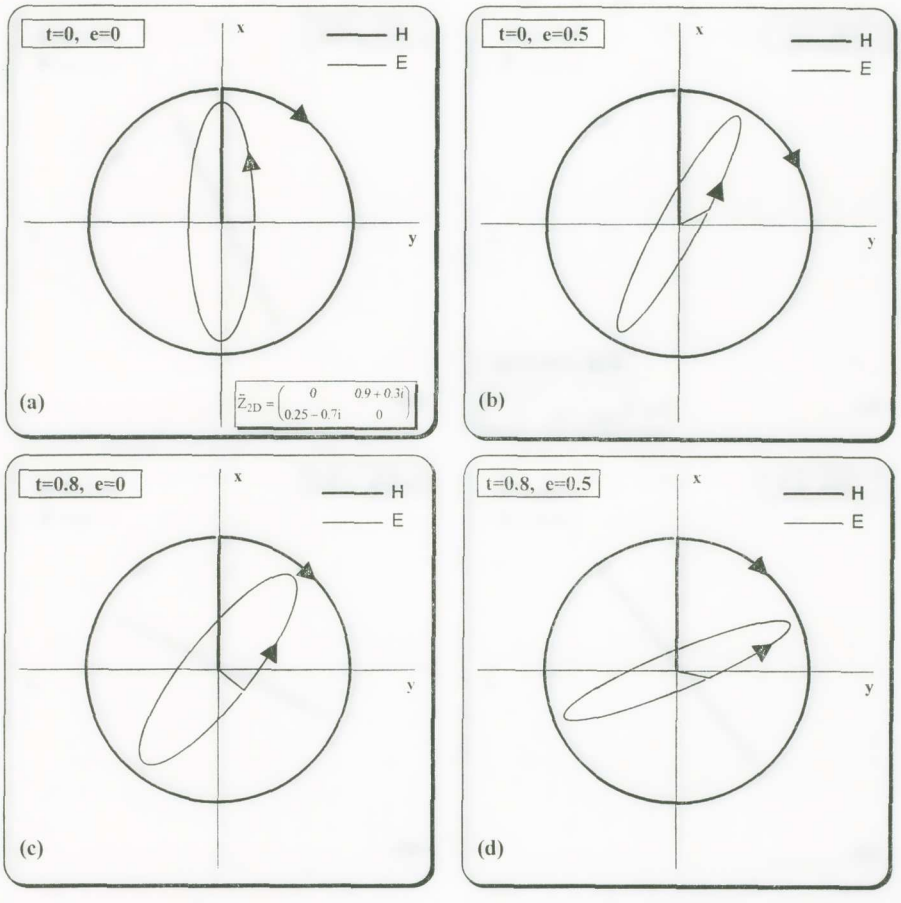


Fig. II.8. The geometrical locus of the electric field vector trace as a result of the rotation of the incident horizontal linearly polarized unitary magnetic field, for **(a)** an ideal 2D-structure; **(b), (c), (d)** a 2D-regional structure, with the presence of a local near-surface semi-static scatterer, with different distortion parameters.

Equation [II.32.b] describes the impedance tensor decomposition suggested by Groom and Bailey *[Groom, 1988], [Groom & Bailey, 1989]*. This decomposition is described through seven real parameters:

- the scaled real and imaginary parts of the major principal impedance $\alpha'$ (or equivalently the major apparent resistivity and phase),
- the scaled real and imaginary parts of the minor principal impedance b′ (or equivalently the minor apparent resistivity and phase),

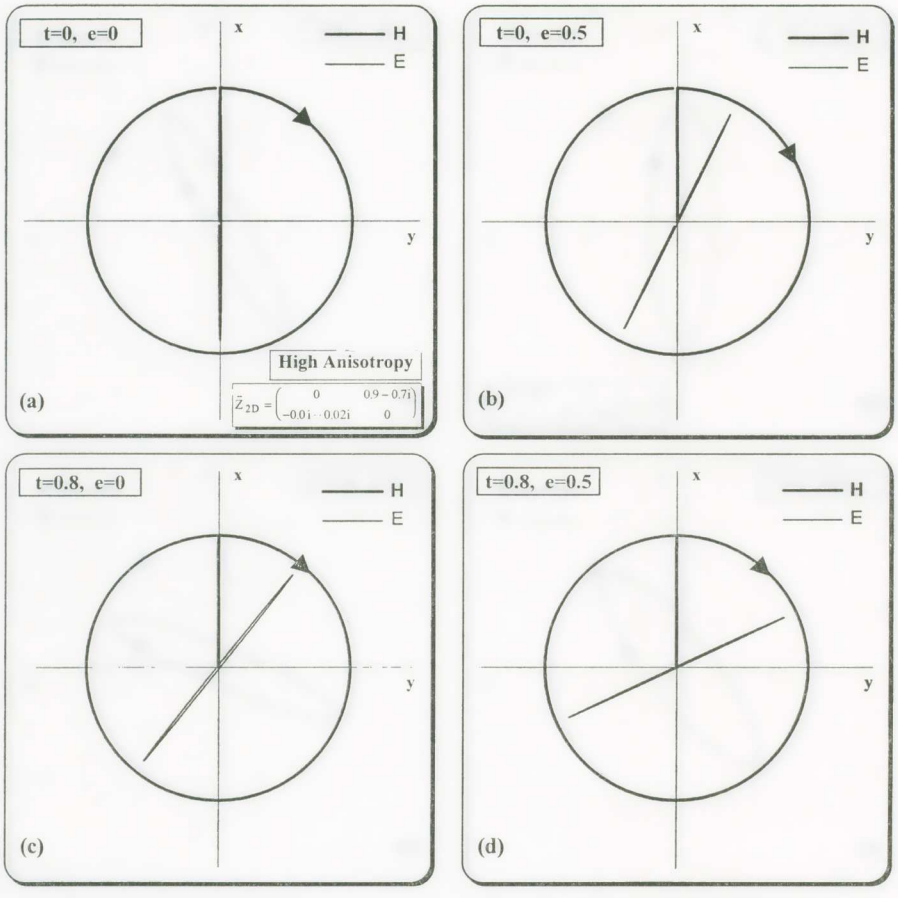


Fig. II.9. The geometrical locus of the electric field vector trace as a result of the rotation of the incident horizontal linearly polarized unitary magnetic field, **(a)** for a 2D-structure with high anisotropy; **(b), (c), (d)** a 2D-regional structure with high anisotropy, but with the presence of a near-surface semi-static scatterer, with different distortion parameters.

- the azimuth angular deviation θ between the principal axis system of the regional structure and the measuring coordinate system,
- the shear parameter e and
- the twist parameter t.

In order to determine the above parameters, the measured impedance tensor is represented:

$$Z_m = \frac{1}{2}\left( \alpha_0^m \mathbf{I} + \alpha_1^m \boldsymbol{\Sigma}_1 + \alpha_2^m \boldsymbol{\Sigma}_2 + \alpha_3^m \boldsymbol{\Sigma}_3 \right) \qquad [II.34]$$

where:

$$\alpha_0^m = Z_{xx} + Z_{yy} \qquad [II.35.a]$$

$$\alpha_1^m = Z_{xy} + Z_{yx} \qquad [II.35.b]$$

$$\alpha_2^m = Z_{yx} - Z_{xy} \qquad [II.35.c]$$

$$\alpha_3^m = Z_{xx} - Z_{yy} \qquad [II.35.d]$$

By inserting eq. [II.34] to eq. [II.32.b], the following non-linear system of complex equations is obtained for the coefficients $\alpha_i$:

$$\alpha_0 = t\sigma + e\delta \qquad [II.36.a]$$

$$\alpha_1 = (\delta - et\sigma)\cos 2\theta - (t\delta + e\sigma)\sin 2\theta \qquad [II.36.b]$$

$$\alpha_2 = -\sigma + et\delta \qquad [II.36.c]$$

$$\alpha_3 = -(t\delta + e\sigma)\cos 2\theta - (\delta - et\sigma)\sin 2\theta \qquad [II.36.d]$$

where:

$$\sigma = \alpha' + b' \text{ and } \delta = \alpha' - b' \qquad [II.37]$$

The above system can be solved analytically for the set of parameters $(\sigma, \delta, e, t, \theta)$ from the experimental data. However, it is evident that multiple solutions exist. By restricting the azimuth angle to be $0 \leq \theta \leq \pi$ we overcome the uncertainty $\theta + \kappa\pi$ of the angle determination. After this restriction four possible solutions still remain, due to two multiplicities. The first is generated from the two equivalent solutions for the set of the distortion tensor parameters that has been previously discussed. The last multiplicity can be described by the argument that if $(\sigma, \delta, e, t, \theta)$ is a solution of the system [II.36.a-d], then the set

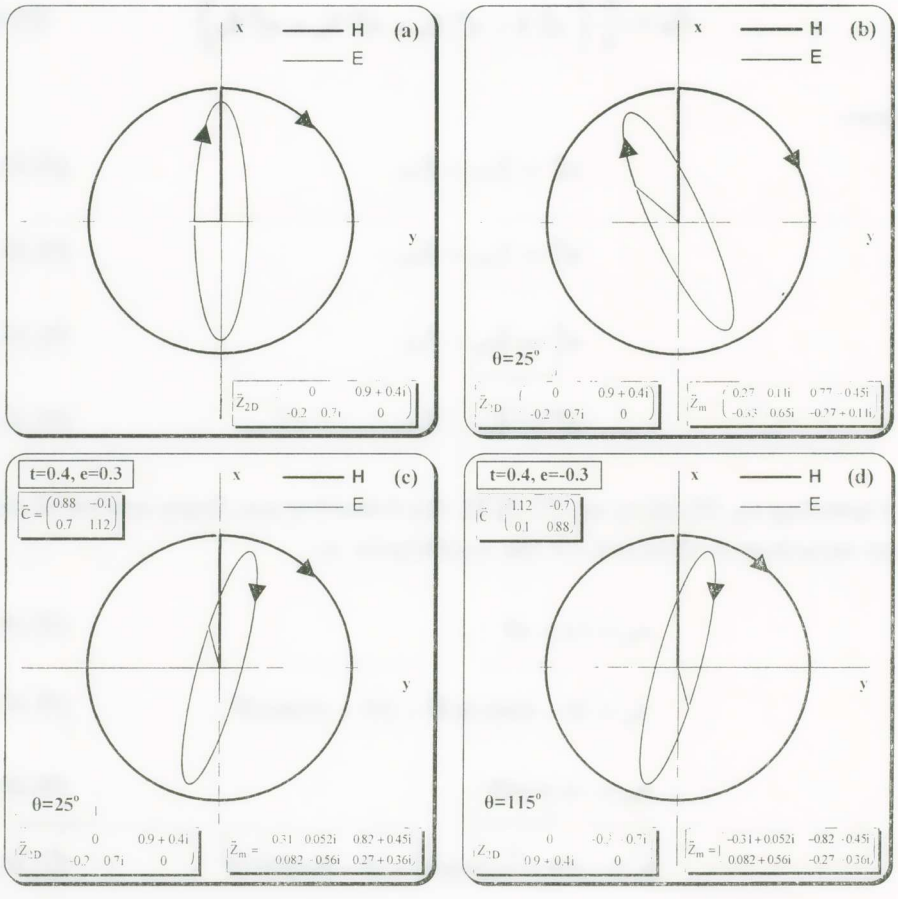


Fig. II.10. The geometrical locus of the electric field vector trace as a result of the rotation of the incident horizontal linearly polarized unitary magnetic field, for **(a)**, **(b)** an ideal 2D - structure, when the measuring and the intrinsic coordinate systems have an angular deviation of $\theta = 0^0$ and $\theta = 25^0$ respectively; **(c)**, **(d)**: a 2D-regional structure with the presence of a local near-surface semi-static scatterer, for the decomposition parameter sets $(\sigma, \delta, e, t, \theta)$ and $(\sigma, -\delta, -e, t, \theta + 90^0)$, respectively.

$\left(-e, t, \sigma, -\delta, \theta + \frac{\pi}{2}\right)$ is also a solution; this is depicted with the example of Fig. II.10. Groom *[Groom, 1988]* has shown that the effect of a twist (t) and a shear (–e) on the electric field in a principal axis system with angular deviation $\theta$ from the measuring system, is the same with that of a twist (t) and a shear (e) on the electric field in a principal axis system with angular deviation

$\theta + \frac{\pi}{2}$ from the measuring system. Also, the sums $\sigma$ of the regional principal impedances are the same and the relevant differences $\delta$ have opposite signs at the two possible solutions. The meaning of the aforementioned arguments is that there is no physical basis to distinguish between the two solutions which are both physically equivalent. The $90^0$ -ambiguity for the angle $\theta$ can be resolved by adopting either the condition $|\alpha'| > |b'|$ or the restriction $\left(0 \leq \theta \leq \frac{\pi}{2}\right)$.

*Comparison between the tensor decomposition by Groom & Bailey and the conventional analysis*

Let us assume that the measured impedance tensor results from a local galvanic distortion of the regionally induced electric field at a large-scale conductivity structure with at most 2D-symmetry and that the magnetic field distortion in negligible.

In the conventional magnetotelluric analysis a measure of the departure from the ideal two-dimensionality of the geoelectric structure is the skew index, *[Swift, 1967]*:

$$|s_1| = \left| -\frac{\alpha_0}{\alpha_2} \right| \qquad \text{[II.38.a]}$$

In the case of the presence of a small-scale surface galvanic scatterer (that distorts the regionally induced electric field), a combination of eqs [II.36.a&c] gives:

$$s = \frac{t\sigma + e\delta}{\sigma - te\delta} \qquad \text{[II.38.b]}$$

It is evident that even if the regional conductivity structure is two-dimensional, the existence of galvanic distortions makes the skew index frequency dependent and non-zero. As an example we consider two marginal cases:

*a)* If the tensor $\mathbf{Z}'_{2D}$ determined by Groom and Bailey decomposition is isotropic, i.e., $\alpha' = b'$ then eq. [II.38.b] provides:

$$s = t = \tan\varphi_t$$

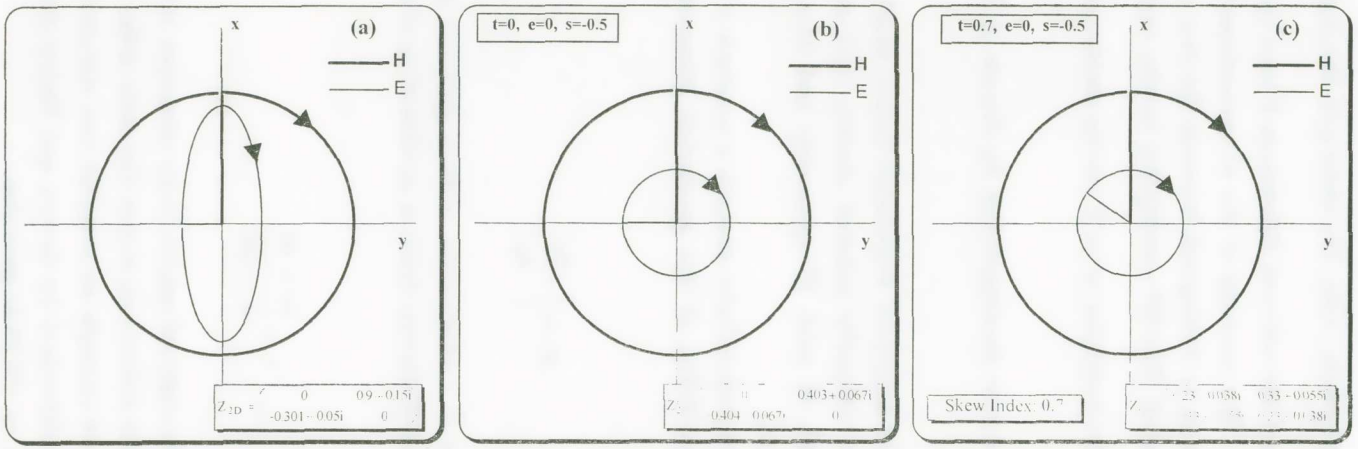


Fig. II.11. The geometrical locus of the electric field vector trace as a result of the rotation of the incident, horizontal linearly polarized unitary magnetic field, for **(a)** an ideal 2D-structure; **(b)** a 2D-regional structure, with the presence of a local near-surface semi-static scatterer, which annuls the regional anisotropy; **(c)** a 2D-regional structure, with the presence of a local near-surface semi-static scatterer, with twist and splitting distorting effects (the splitting distortion annuls the regional anisotropy).

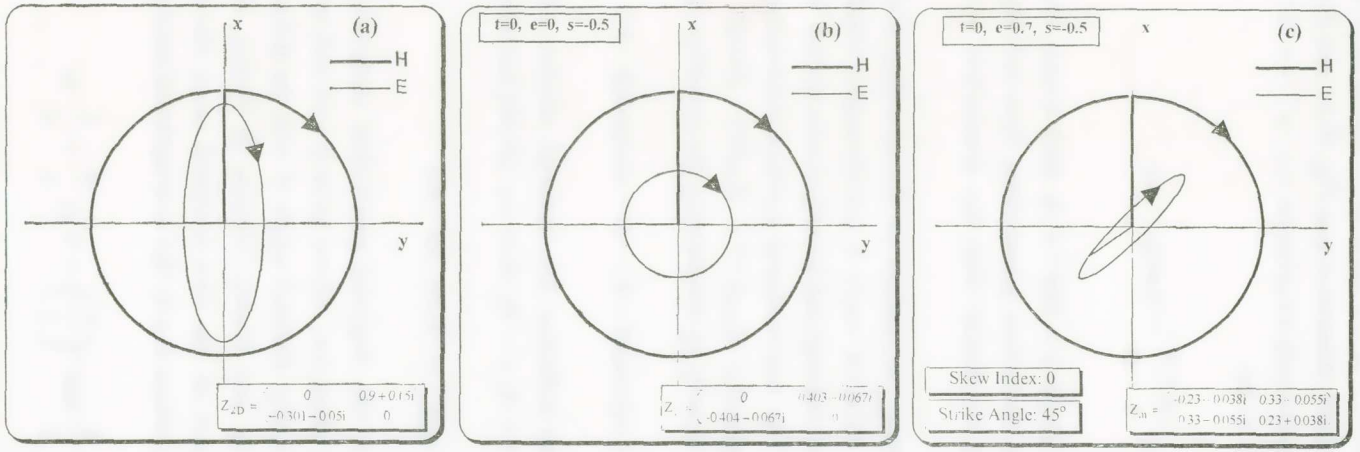


Fig. II.12. The geometrical locus of the electric field vector trace as a result of the rotation of the incident horizontal linearly polarized unitary magnetic field, for **(a)** an ideal 2D-structure; **(b)** for a 2D-regional structure, with the presence of a local nearsurface nearsurface semi-static scatterer, which annuls the regional anisotropy; **(c)** a 2D-regional structure, with the presence of a local near-surface semi-static scatterer, with shear and splitting distortin6 effects (the splitting distortion annuls the regional anisotropy).

Thus, at measuring sites where $t = 0$, the skew index will be zero, irrespectively of the probable existence of shear distortion (see Fig. II.11 and II.12).

*b)* If the tensor $\mathbf{Z}'_{2D}$ is extremely anisotropic, i.e., $|\alpha'| >> |b'|$, then $\delta \approx \sigma$, and the skew index is found to be:

$$s = \frac{t + e}{1 - et} = \tan(\varphi_t + \varphi_e)$$

so, we may define the skew angle $q = \tan^{-1} s$; in such a case, the skew index is determined only from the distortion parameters, thus driving the conventional analysis to the false conclusion that the geoelectric structure has a 3D-symmetry.

One of the most interesting parameters for the modeling of the earth conductivity structure is the azimuth angle $\theta$ (*strike*-angle) which denotes the azimuth angular deviation of the regional principal axis system from the measuring coordinate system. The conventional method determines the strike-angle by minimizing the quantity $|Z_{xx}(\theta')|^2 + |Z_{yy}(\theta')|^2$, *[Swift, 1967]*, *[Sims and Bostick, 1969]*, or equivalently by minimizing the quantity $|\alpha_3(\theta')|^2$, where:

$$\alpha_3(\theta') = -(t\delta + e\sigma)\cos 2(\theta - \theta') - (\delta - et\sigma)\sin 2(\theta - \theta') \qquad [II.39]$$

If the local inhomogeneities influence the induced electric field only with splitting distortion ($s \neq 0$, $t = 0$, $e = 0$), then eq. [II.39] becomes:

$$\alpha_3(\theta') = -\delta \sin 2(\theta - \theta')$$

and the intrinsic system of the regional geoelectric structure is correctly determined. In all the other cases, i.e., where twist ($t \neq 0$) and/or shear ($e \neq 0$) are present, the conventionally derived angle $\theta'$ will be different from the actual strike-angle $\theta$. Groom and Bailey *[Groom & Bailey, 1989]* examine the aforementioned argument at the two marginal cases discussed above:

In the isotropic case *a)* where $\delta \approx 0$, the conventional analysis gives:

$$\theta' = \theta - \frac{1}{2} \tan^{-1}\left(\frac{1}{t}\right) = \theta \pm \frac{\pi}{4} + \frac{1}{2} \varphi_t \qquad [II.40.a]$$

with the assumption that $t \neq 0$ (see Figs II.12 and II.13).

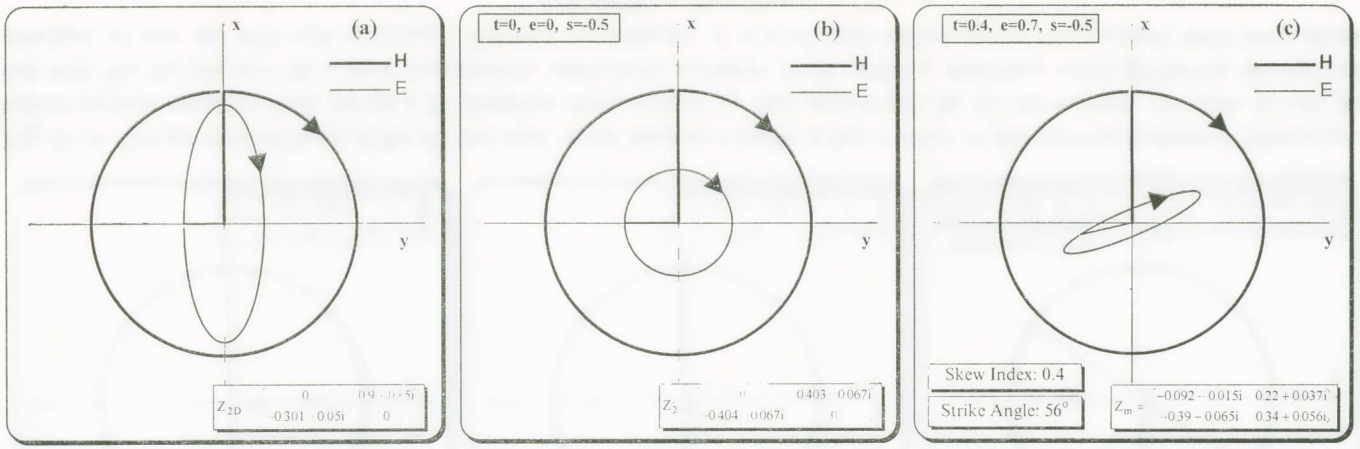


Fig. II.13. The geometrical locus of the electric field vector trace as a result of the rotation of the incident horizontal linearly polarized unitary magnetic field, for **(a)** an ideal 2D-structure; **(b)** a 2D-regional structure, with the presence of a local near-surface semi-static scatterer, which annuls the regional anisotropy **(c)** a 2D-regional structure, with the pre- sence of a local near-surface semi-static scatterer, with twist, shear and splitting distorting effects (the splitting distortion annuls the regional anisotropy).

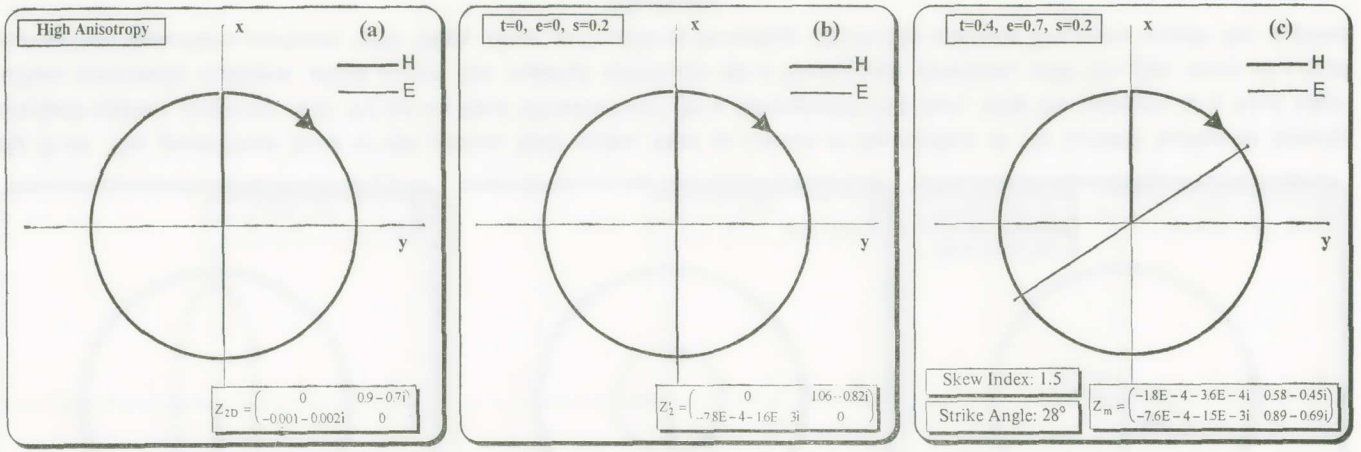


Fig. II.14. The geometrical locus of the electric field vector trace as a result of the rotation of the incident horizontal linearly polarized unitary magnetic field, for **(a)** a 2D-structure characterized by high anisotropy; **(b)** the 2D-regional structure of case **(a)** but with the the presence of a local near-surface semi-static scatterer (with splitting distortion only); **(c)** for the 2D-regional structure of case **(a)** with high anisotropy, but with the presence of a local near-surface semi-static scatterer (with twist, shear and splitting distortions);

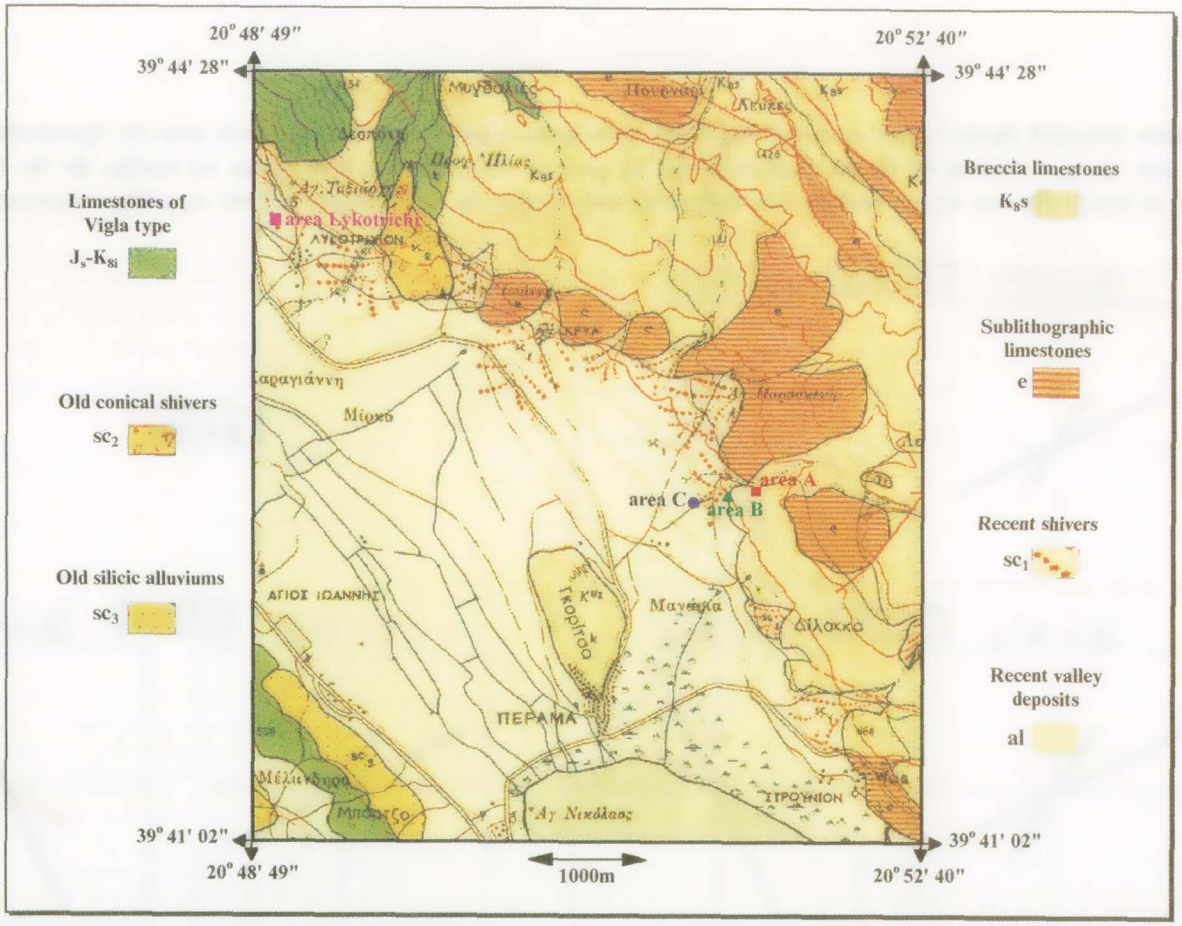


Fig. 2. Geological map of Ioannina region where the measuring sites A, B and C of IOA - station are depicted.

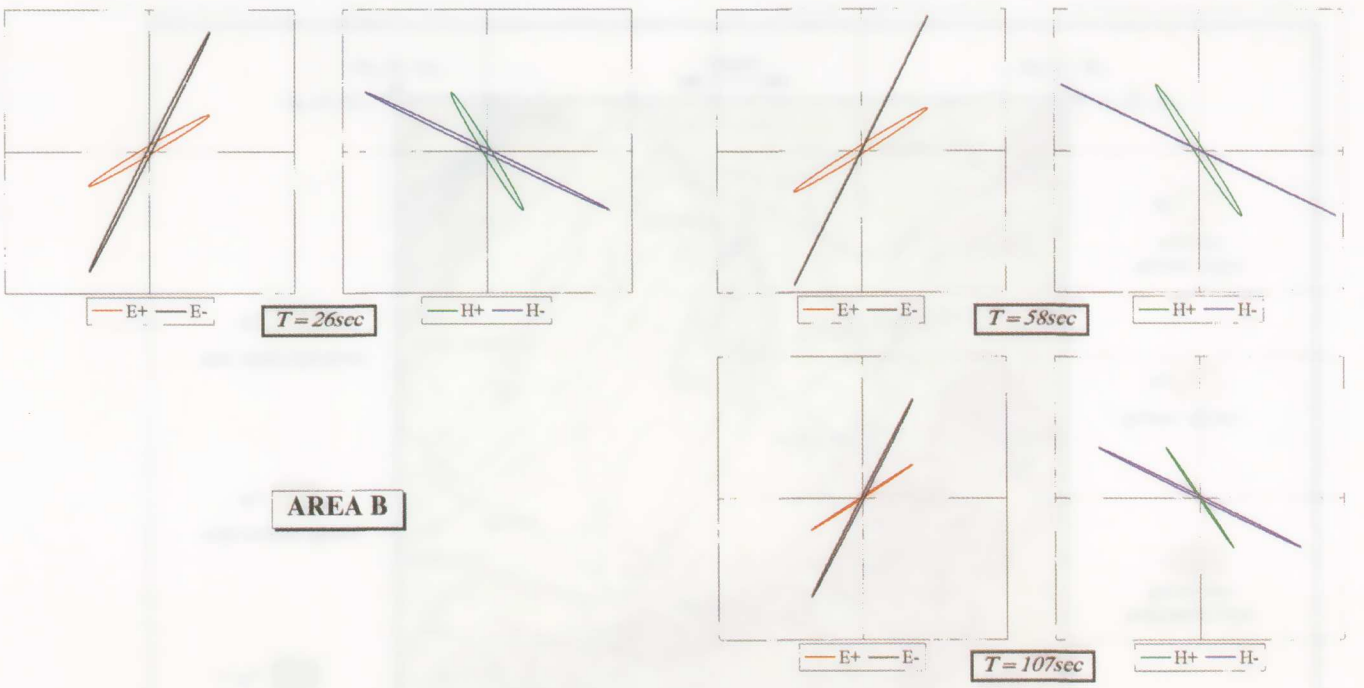


Fig. I.7 **(a)** Polarization ellipses for the two eigenstates of the electric field; **(b)** polarization ellipses for the two eigenstates of the magnetic field; **(c)**, **(d)** ellipses for the E and H polarisation for each of the eigenstates; **(e)**, **(f)**, **(g)**, **(h)** ellipses for E and H polarization respectively, for each one of the eigenstates which result from the superposition of two circularly polarized waves.

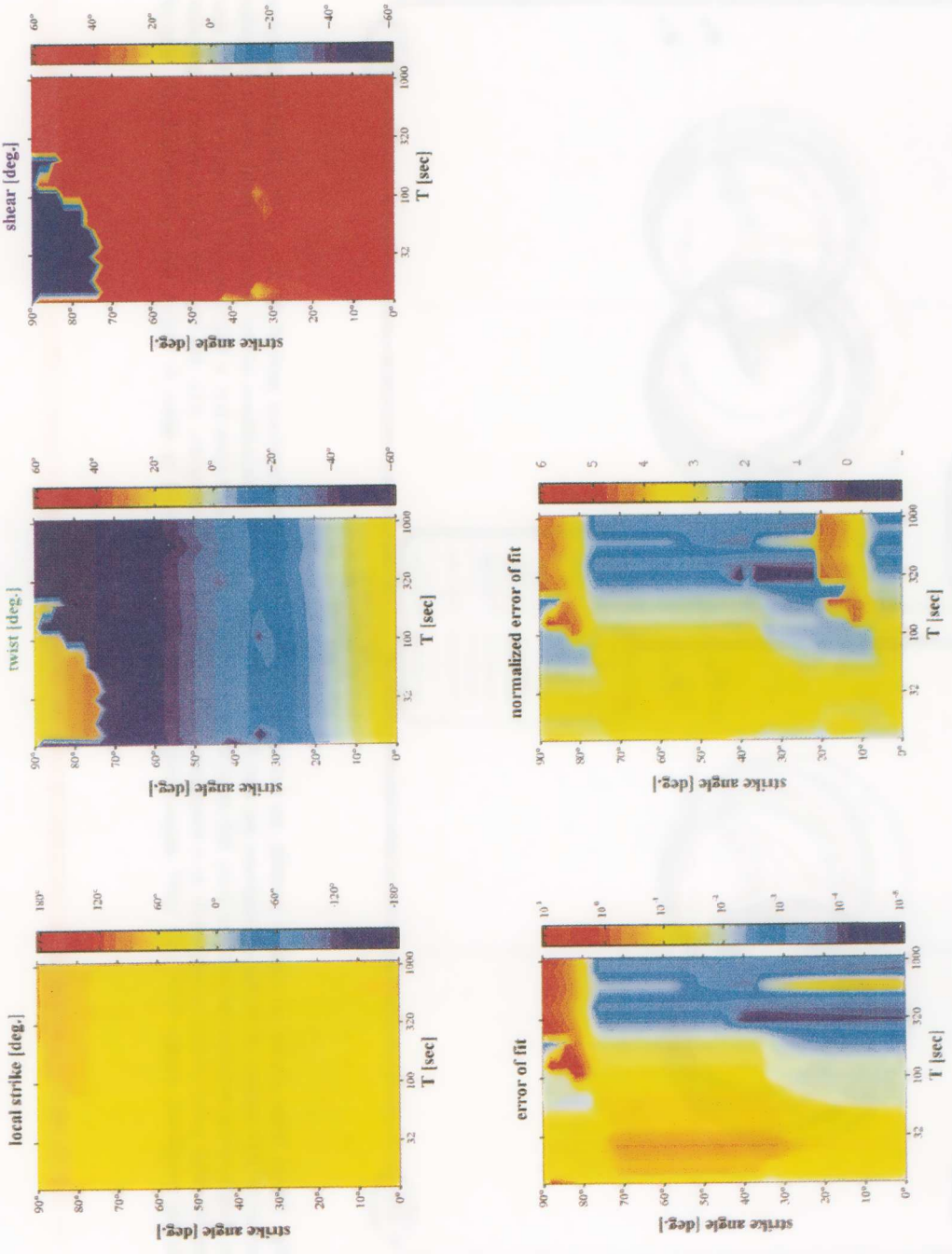


Fig. II.20. The contour plots of the local strike, twist, shear, error of .fit and normalized error of fit versus the period and the rotational angle of the measuring system varying in the range 0°-90°.

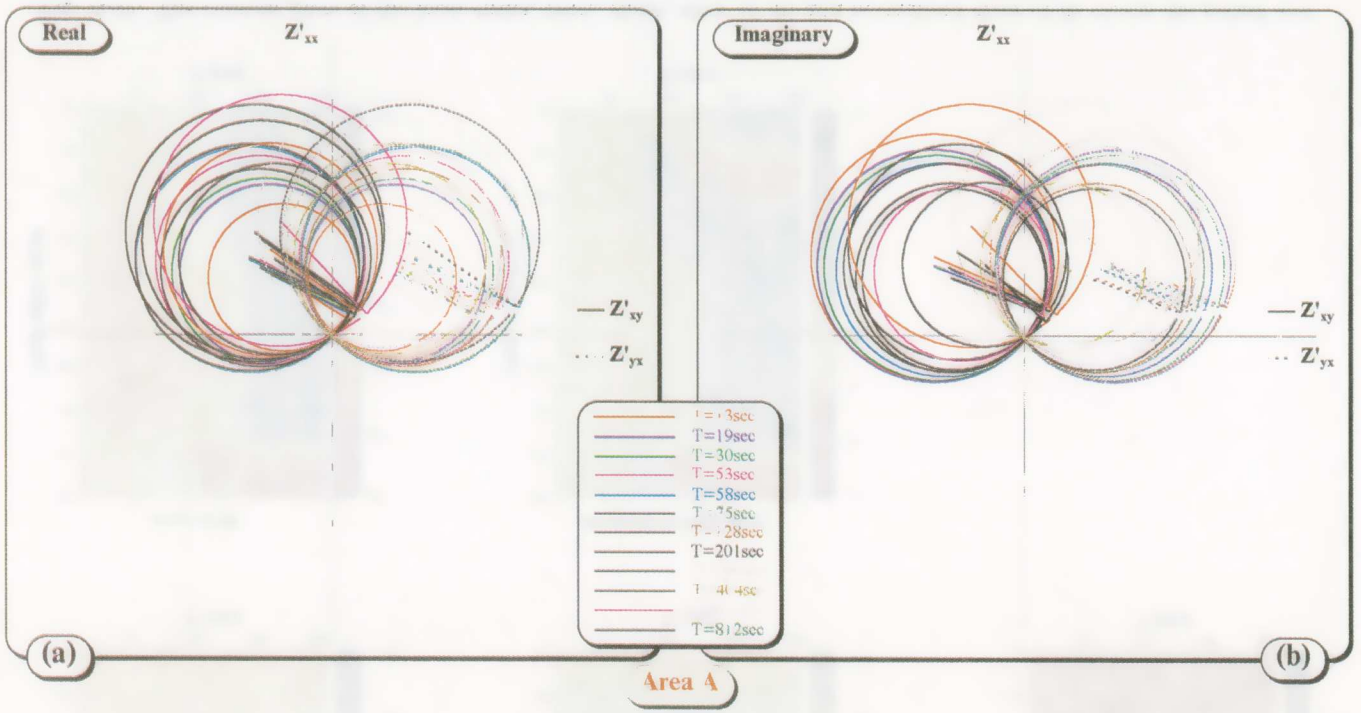


Fig. III.10. Mohr circles at various periods, by taking **(a)** the real and **(b)** the imaginary part of the $Z'_{xx}$ vs $Z'_{xy}$ impedance tensor elements [left swarm of circles at diagrams **(a)** and **(b)**] and of the $Z'_{xx}$vs $Z'_{yx}$ impedance tensor elements [right swarm of circles at diagrams (a) and (b)], determined from MT-data from the site A of Ioannina region [c.f. a line connects the center with the respective first point (which corresponds to a rotational angle equal to$0^0$) of each circle. Also the last two points, which correspond to the rotational angles $179^0$ and $180^0$ respectively, are intentionally omitted in order to depict the counterclockwise way of circle construction].

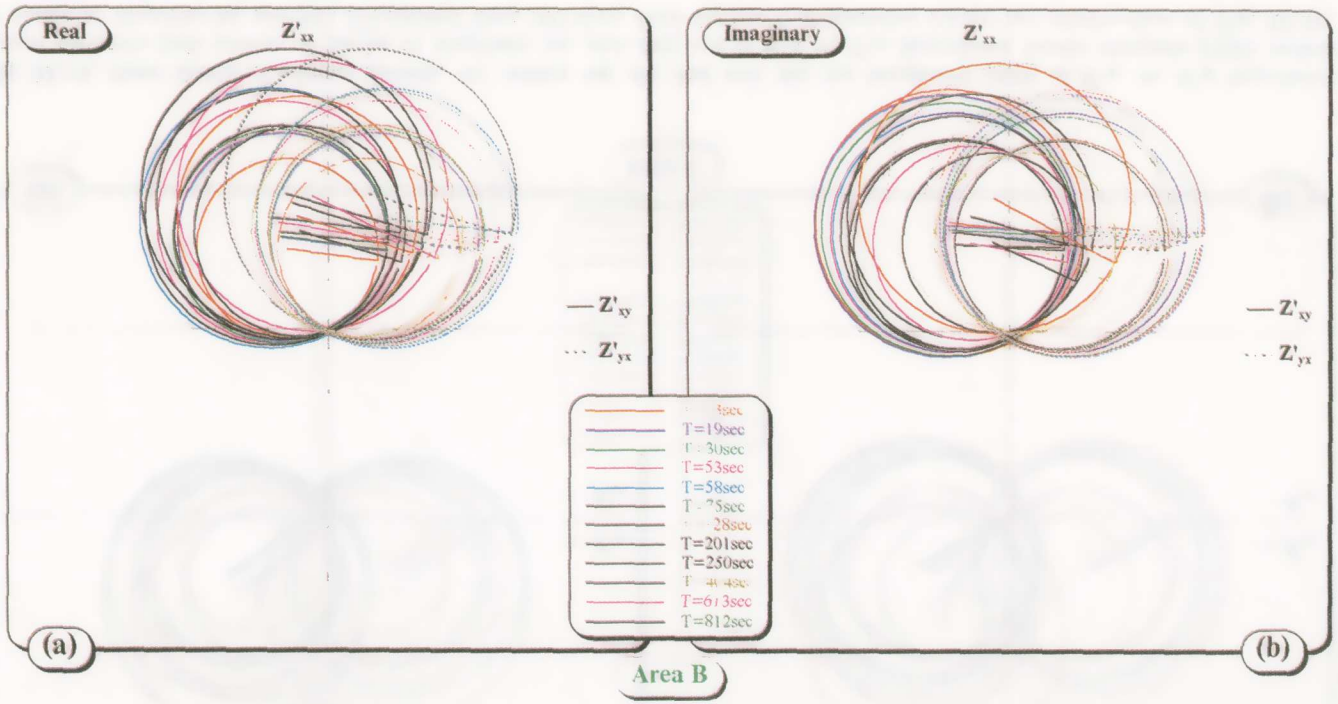


Fig. III.11. Mohr circles at various periods, by taking **(a)** the real and **(b)** the imaginary parts of the $Z'_{xx}$ vs $Z'_{xy}$ impedance tensor elements [left swarm of circles at diagrams (a) and **(b)**] and of the $Z'_{xx}$ vs $Z'_{yx}$ impedance tensor elements [right swarm of circles at diagrams **(a)** and (b)] determined from MT-data from the site B of Ioannina region (see clarification of Fig. III.10).

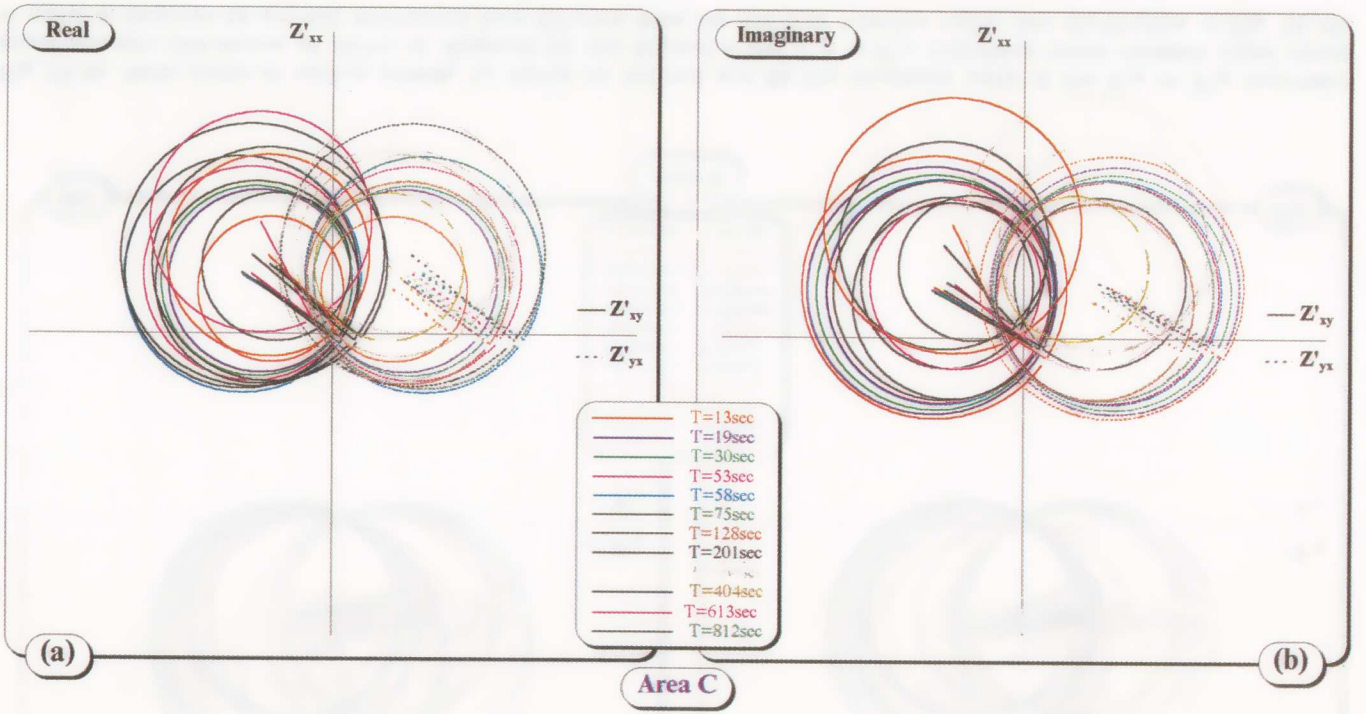


Fig. III.12. Mohr circles at various periods, by taking **(a)** the real and **(b)** the imaginary parts of $Z'_{xx}$ vs $Z'_{xy}$ impedance tensor elements [left swarm of circles at diagrams **(a)** and **(b)**] and of $Z'_{xx}$ vs $Z'_{yx}$ impedance tensor elements [right swarm of circles at diagrams **(a)** and **(b)**], determined from MT-data from the site C of Ioannina region (see clarification of Fig. III.10).

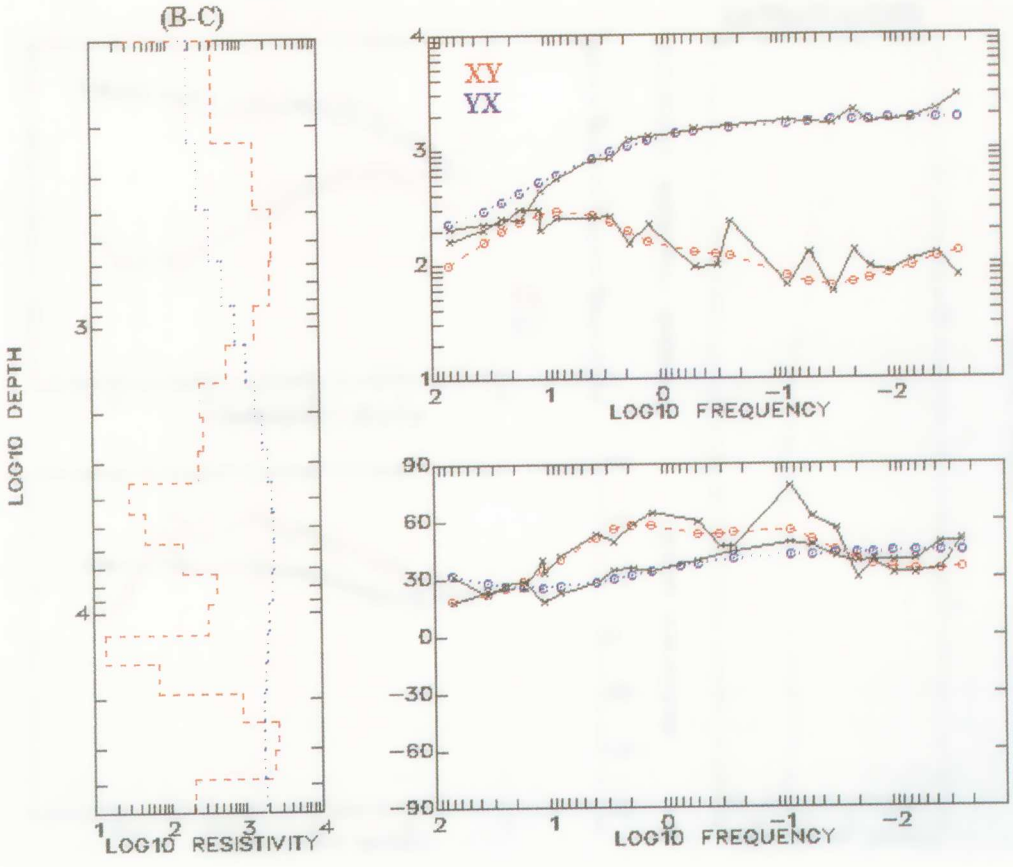


Fig. V.1. 1D-Occam inversion of the site B of Ioannina region.

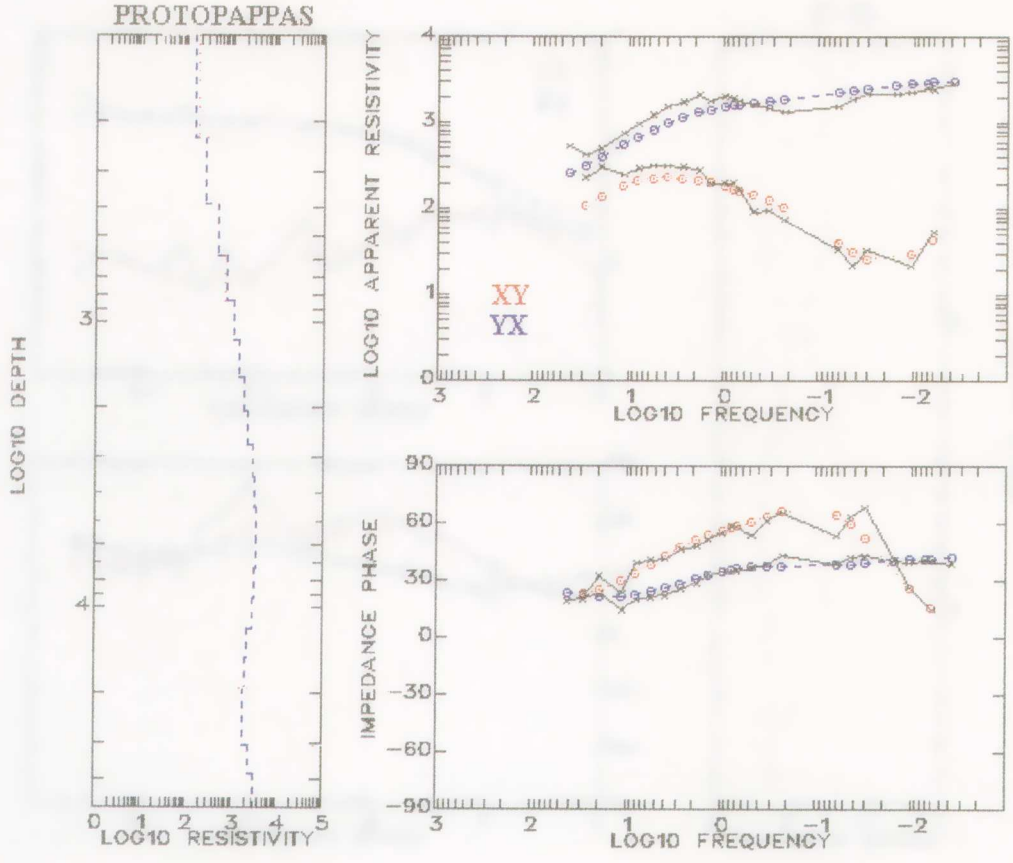


Fig. V.2. 1D-Occam inversion of the Protopappas area.

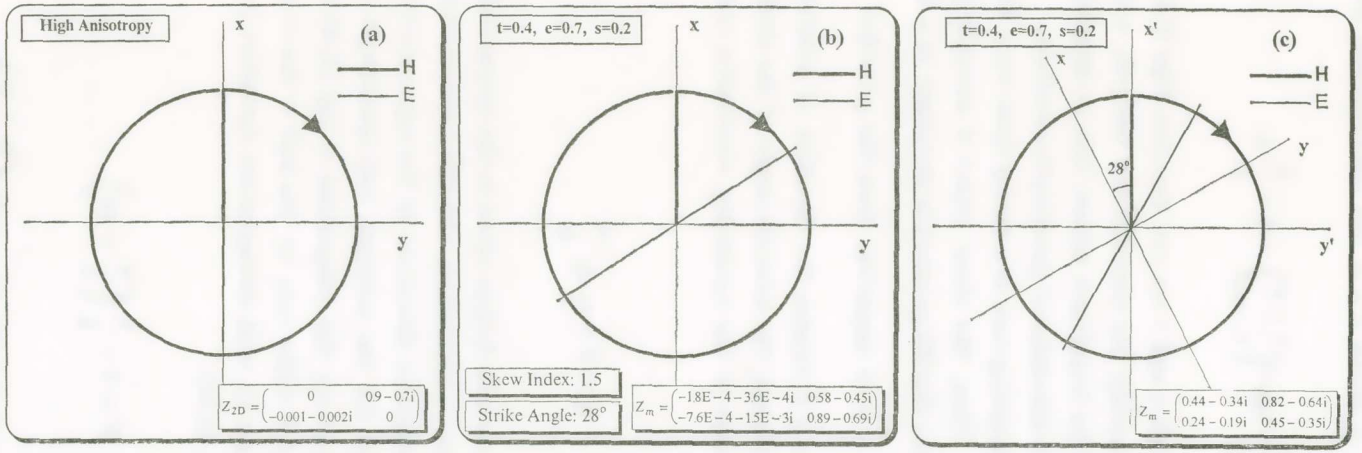


Fig. II.15. The geometrical locus of the electric field vector trace as a result of the rotation of the incident horizontal linearly polarized unitary magnetic field, for **(a)** a 2D-structure characterized by high anisotropy; **(b)** the 2D-regional structure of case **(a)**, but with the presence of a local near surface semi-static scatterer (with twist shear and splitting distortions); **(c)** same case as (b) but the coordinate system is rotated 28° degrees clockwise (i.e., through the strike angle determined by the conventional analysis).

In the anisotropic case *b)* where $\delta \approx \sigma$, the conventional analysis gives:

$$\theta' = \theta + \frac{1}{2} \tan^{-1}\left(\frac{t + e}{1 - et}\right) = \theta + \frac{1}{2} q \qquad [II.40.b]$$

with the assumption that both e and t are not zero (see Figs II.14 and II.15). Thus, they proved that generally the conventional analysis, which does not perform a decomposition of the impedance tensor, fails to determine correctly the principal axes of the two-dimensional geoelectric structure.

We now turn to the interesting case of a strong shear local distortion, i.e., |e| is approximately unity. Then, the shear tensor **S** strongly polarizes the electric field which arises from the 2D-geoelectric structure, at a direction that deviates angle $\frac{\pi}{4}$ (or $-\frac{\pi}{4}$, if e is negative) from the principal axis system. Furthermore, the twist tensor **T** rotates the direction of polarization by the twist angle (Fig. II.16). Therefore, the azimuth angle of the strong local electric field polarization direction at the measuring coordinate system (*local or channelling strike*) is:

$$\theta_l = \theta + \varphi_t \pm \frac{\pi}{4} \qquad [II.41]$$

Let us now compare the parameter $\theta_l$ that refers to the characteristic direction of the electric field strong local polarization with the conventional strike angle $\theta'$ which refers to the characteristic directions of the regional two-dimensional earth conductivity structure for the isotropic and anisotropic cases already discussed. In the isotropic case *a)*, the comparison of eqs [II.40.a] and [II. 41] shows that the angles $\theta_l$ and $\theta'$ differ only by the half of the twist angle (Fig. II.13). In the anisotropic case *b)*, with strong shear distortion ($e \approx 1$), eq. [II. 40.b] becomes (see also Fig. II.16):

$$\theta' = \theta + \frac{1}{2}\left(\frac{\pi}{4} + \varphi_t\right) \qquad [II.42]$$

Thus, the difference between $\theta_l$ and $\theta'$ is the angle $\left(\frac{\varphi_e + \varphi_t}{2}\right)$.

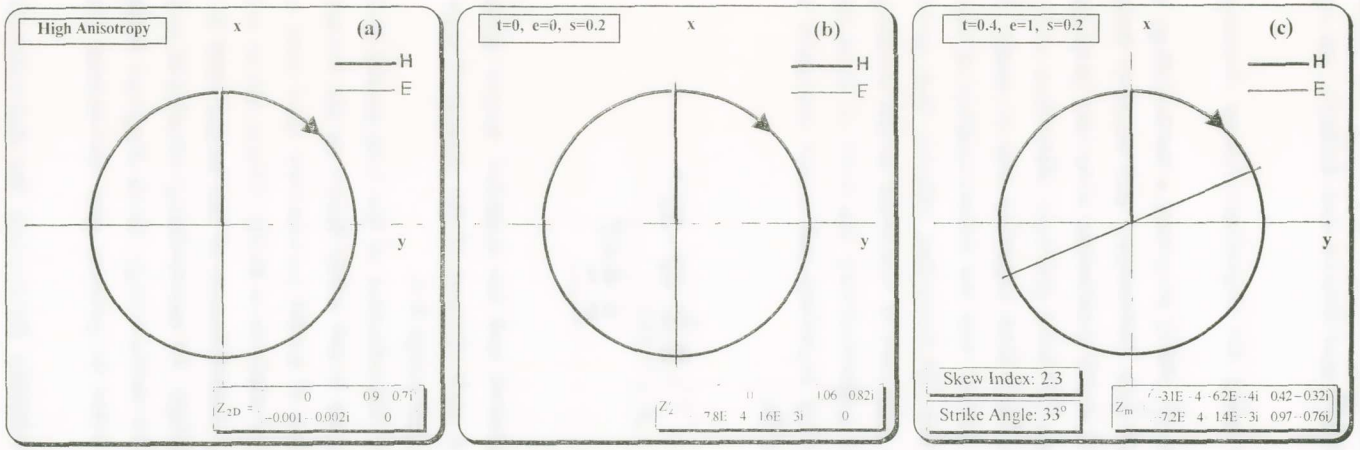


Fig. II.16. The geometrical locus of the electric field vector trace as a result of the rotation of the incident horizontal linearly polarized unitary magnetic field, for **(a)** a 2D-structure characterized by high anisotropy; **(b)** the 2D-regional structure of case **(a)**, but with the presence of a local near-surface semi-static scatterer (with splitting distortion the only); **(c)** the 2D-regional structure of cose **(a)**, but with the presence of a local near-surface semi-static scatterer (with strong shear, twist and splitting distortions).

Smith *[Smith et al., 1995], [Balasis et al., 1997]* has recently shown that the parameterizations of Bahr's and Groom and Bailey's are equivalent.

*II.5. Experimental results using the impedance tensor decomposition*

Groom et al *[Groom et al., 1993]* proposed a methodology in order to deal with three-dimensional galvanic distortions and retrieve information for an underlying two-dimensional earth geoelectric structure [*superposition model: 3D-(local)/2D-(regional)* i.e., 3D-local galvanic distortion over a 2D-regional earth conductivity model]. Their first objective was to assess the dimensionality of the data, while the second was the determination of the structural parameters (after removing the 3D-distortion effects) that provide a physical insight of the actual earth structure of the crust under investigation. At each stage a measure to evaluate quantitatively the error of fit of the model tensor elements to the corresponding experimental tensor elements was calculated. This is the residual error of fit:

$$\varepsilon^2 = \frac{\sum_{i=1}^{2}\sum_{j=1}^{2} \left| Z_{ij}^{th} - Z_{ij}^{m} \right|^2}{\sum_{i=1}^{2}\sum_{j=1}^{2} \sigma_{ij}^{m2}} \qquad \text{[II.43]}$$

where $Z_{ij}^{m}$ and $Z_{ij}^{th}$ the measured and the modeled tensor elements respectively and $\sigma_{ij}^{m}$ the variance of each element of the measured tensor. An acceptable misfit must lie within the range 0-4.

An important aspect of the selection of the best model that fits the MT - data is that its appropriateness is not solely based on the lowest residual error but also on the fewer number of model parameters used over a data set (i.e., a set of frequencies or a set of stations or both). This is the so called, by Groom et al. [*Groom et al., 1993*], «*smoothness*» of the model and it is extensively performed in their methodology by constraining structural and/or distortion parameters of the model. The methodology block diagram is depicted in Fig. II.17 and was followed in order to process and decompose the MT-data of Ioannina region.

This methodology successfully determines the dimensionality of the dominative conductivity structure and also recovers the regional impedance res-

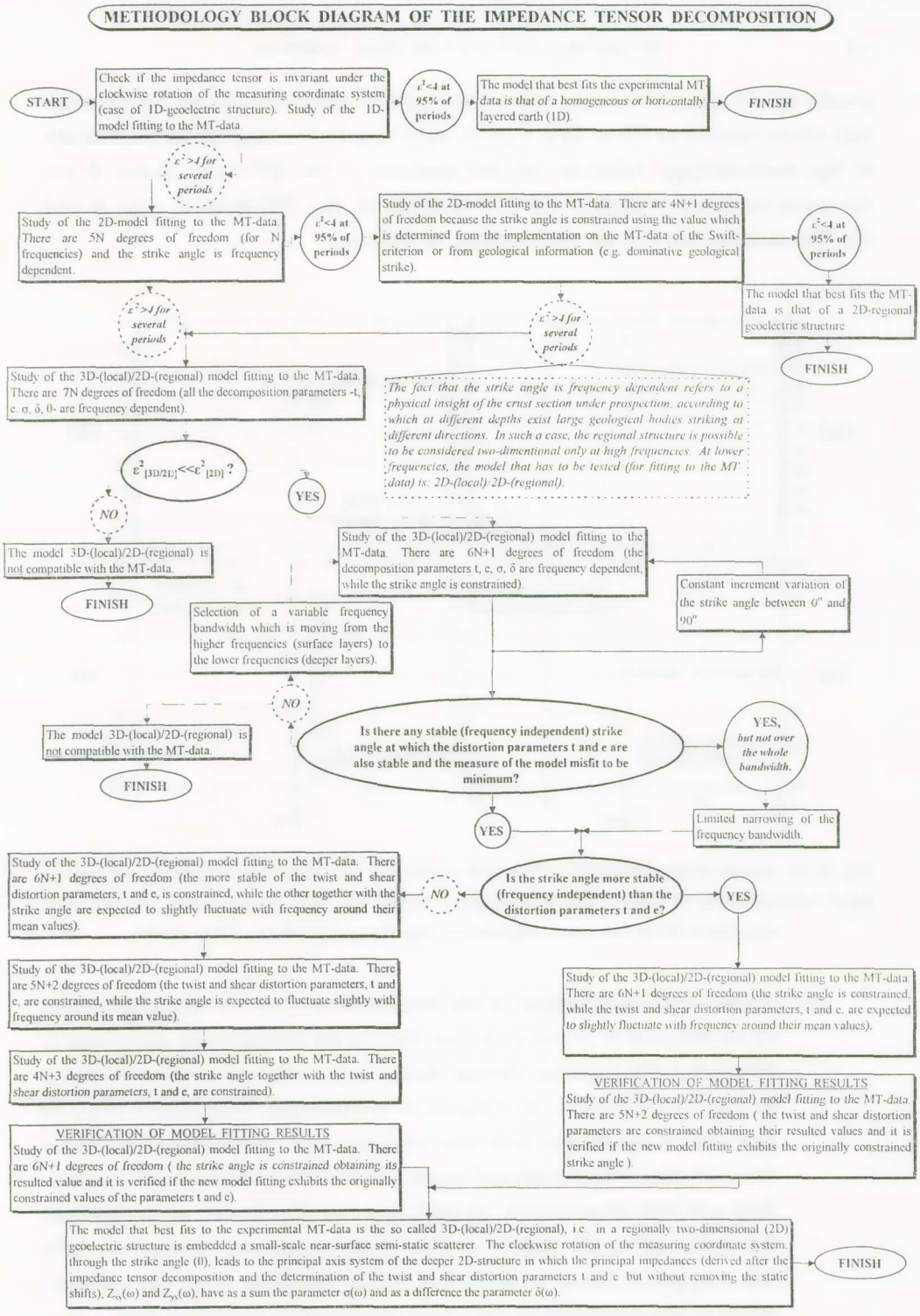


Fig. II.17. The methodology block diagram of the impedance tensor decomposition.

ponses (cf. in case, of course, where the regional structure can be approximately characterized as 1D or 2D). Figs II.18-23 depict the basic steps and results of the methodology followed for the analysis of the MT-data of site B (cf. the same work was repeated for the analysis of the MT-data of sites A and C). The conclusions can be summarized as follows:

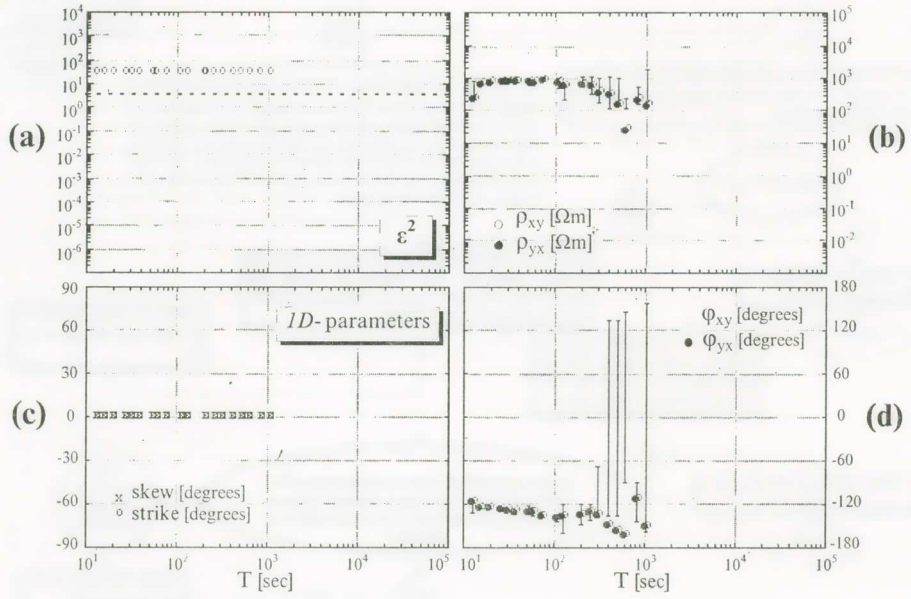


Fig. II.18. Study of the fitting of a 1D-model to the MT data from site B of Ioannina region, **(a)** $\varepsilon^2$ residual error of fitting; **(b), (d)** apparent resistivity and phase of the 1D-structure calculated from the trace impedance; **(c)** the parameters of the model.

(i) A common characteristic of the local near-surface 3D-inhomogeneities at all the sites A, B and C, is that they cause strong shear distortion of the regionally induced electric field; their relevant shear-parameter is close to unity ($|e| \rightarrow 1$). This result is consistent with Bahr's analysis and also in agreement with the experimental polarization diagrams for each site. The directional angle (*local strike*) of this local channelling was also determined, at each site, by the Groom et al method: $\theta_t^A \approx 81^o$, $\theta_t^B \approx 62^o$ and $\theta_t^C \approx 90^o$. These values are compatible with the respective linear polarization angles resulting from the construction of the measured electric field polarization diagrams, $E_{EW} - E_{NS}$,

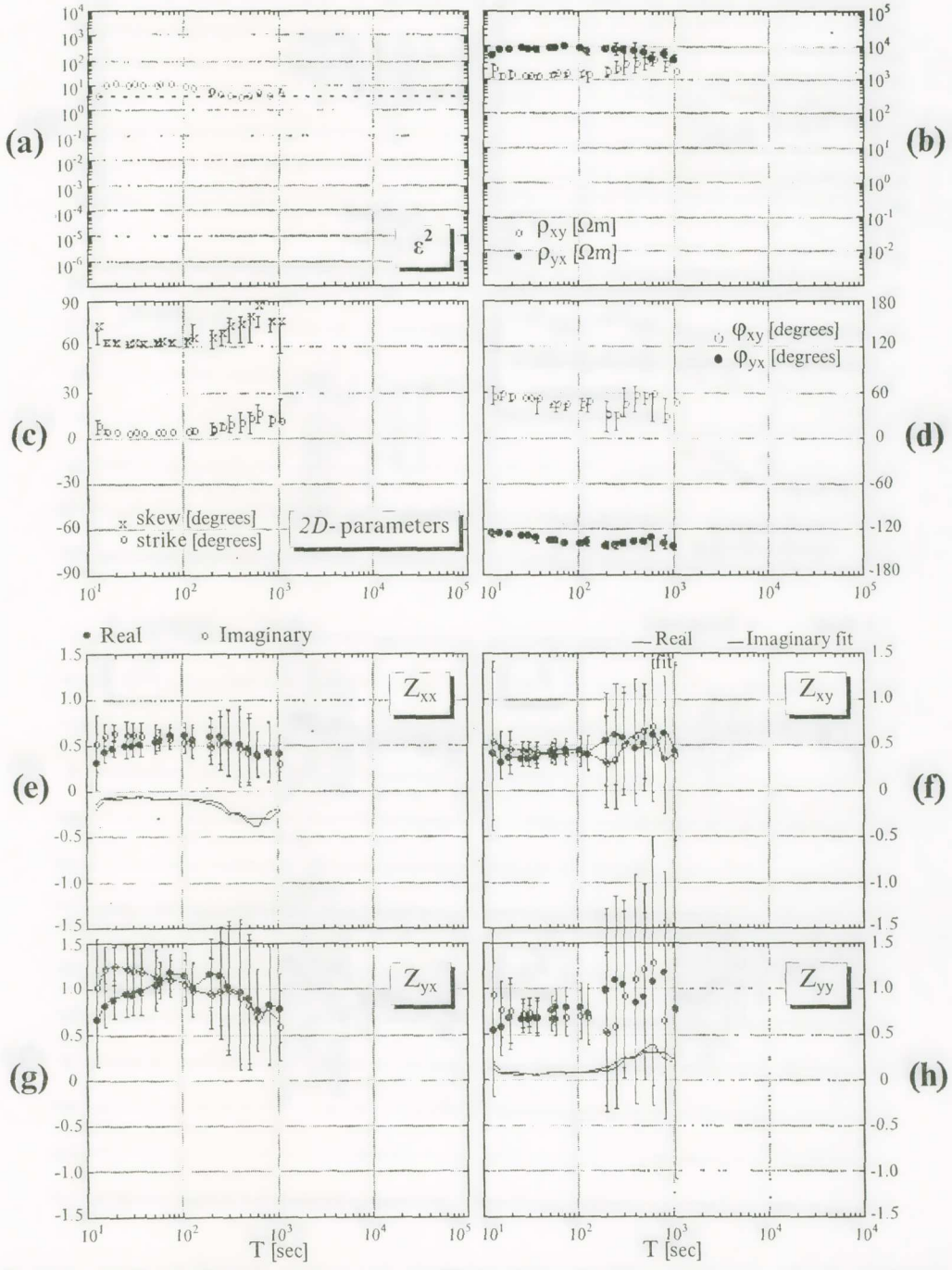


Fig. II.19. Study of the fitting of a 2D-model to the MT-data from site B of Ioannina region; **(a)** $\varepsilon^2$ residual error of fitting; **(b), (d)** apparent resistivities $\rho_{xy}$, $\rho_{yx}$ and the respective phases $\varphi_{xy}$, $\varphi_{yx}$ of the 2D-structure; **(c)** the parameters of the model; **(e)-(h)** fit of the model parametrization to the scaled impedance data.

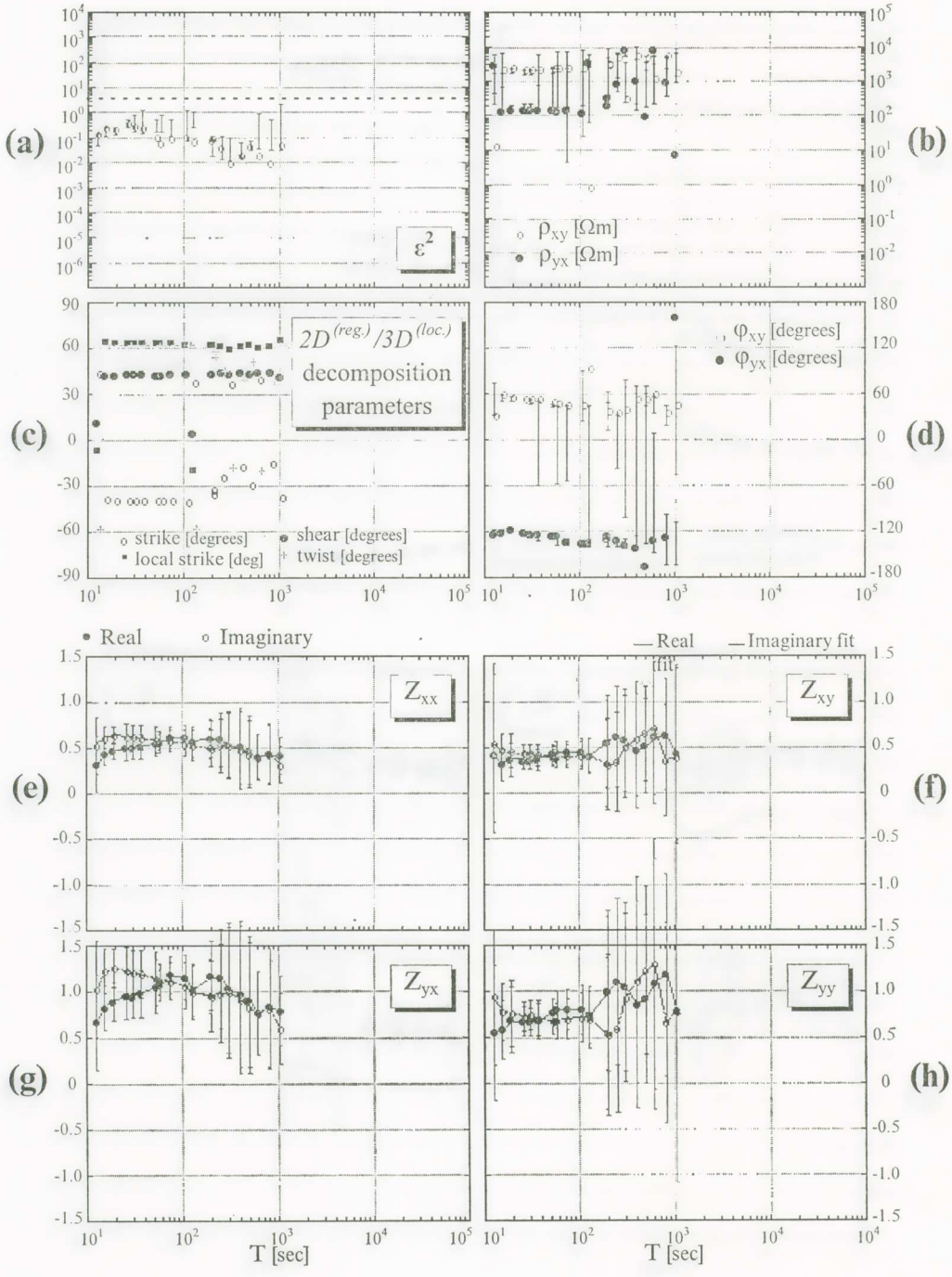


Fig. II.21. Study of the fitting of a 2D-(regional)/3D-(local) model to the MT-data from site B of Ioannina region; **(a)** $\varepsilon^2$ residual error of fitting; **(b), (d)** apparent resistivities $\rho_{xy}$, $\rho_{yx}$ and respective phases $\varphi_{xy}$, $\varphi_{yx}$ of the 2D-basement; **(c)** the unconstrained parameters of the model; **(e)- (h)** fit of the model parameterization to the scaled impedance data.

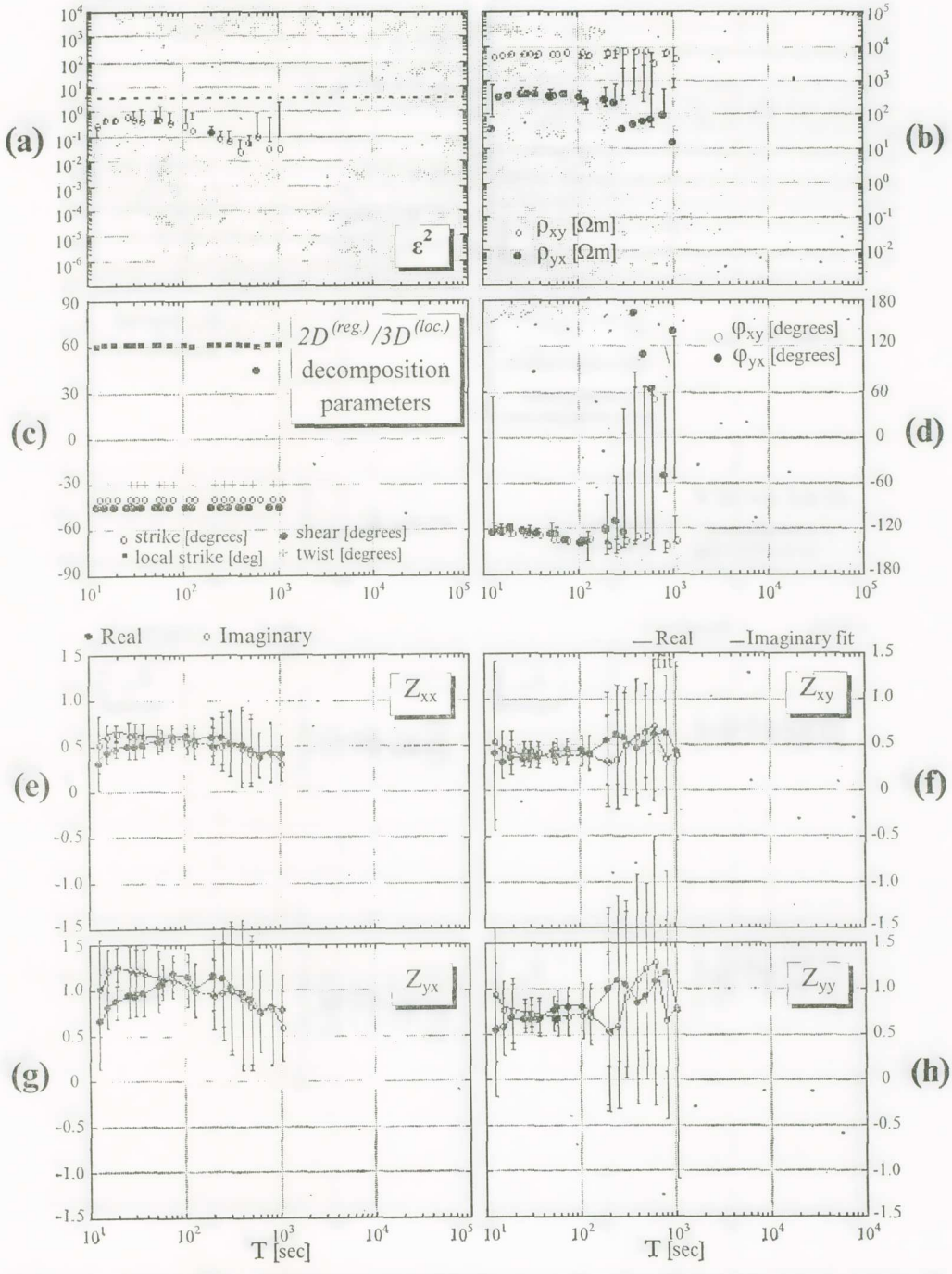


Fig. II.22. Study of the fitting of a 2D-(regional)/3D-(local) model to the MT-data from site B of Ioannina region; **(a)** $\varepsilon^2$ residual error of fitting; **(b), (d)** apparent resistivities $\rho_{xy}$, $\rho_{xy}$ and the respective phases $\varphi_{xy}$, $\varphi_{yx}$ of the 2D-basement; **(c)** the parameters of the model [the strike direction is constrained to $-41^0$]; **(e)-(h)** fit of the model parameterization to the scaled impedance data.

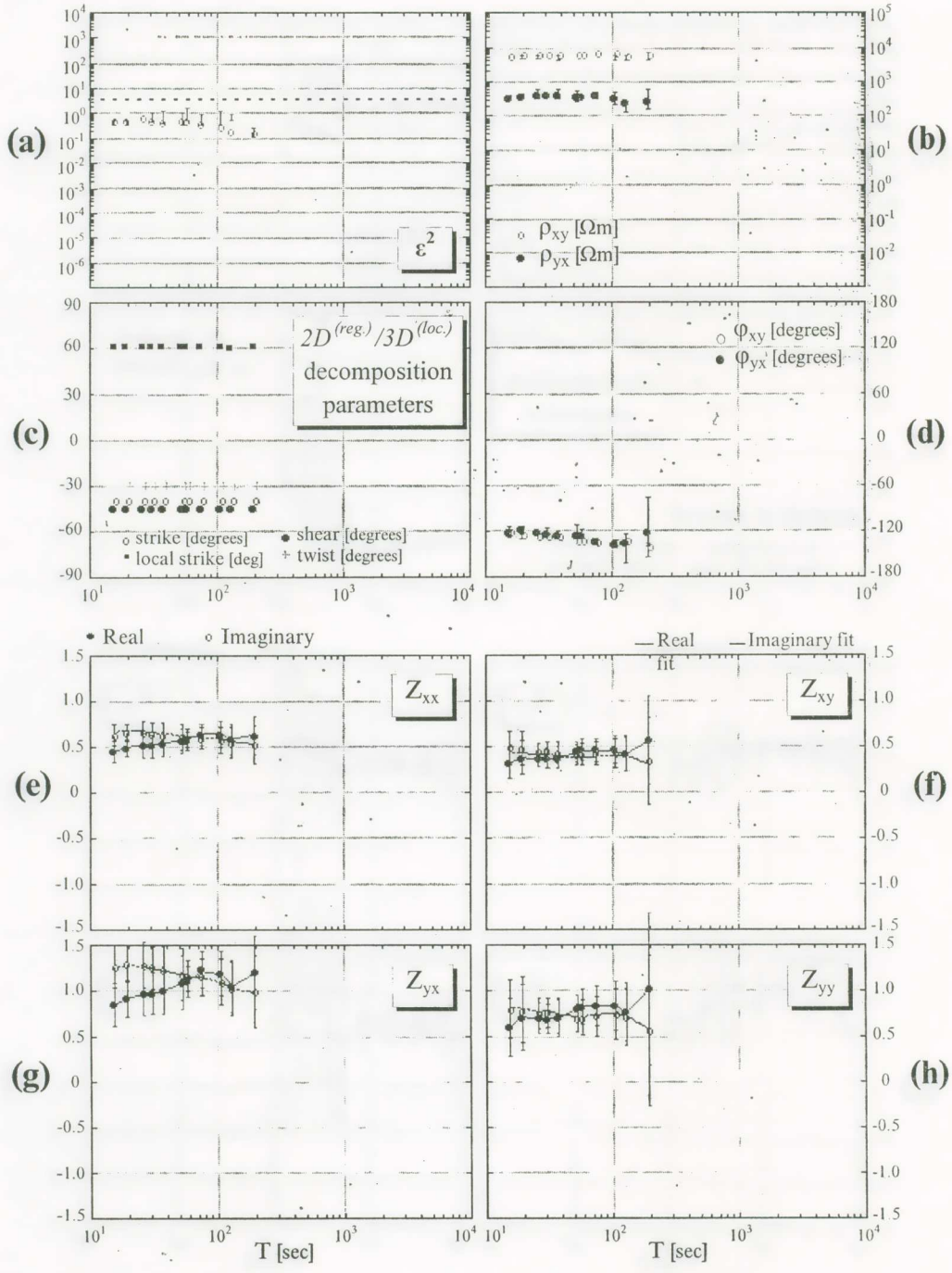


Fig. II.23. Study of the fitting of a 2D-(regional)/3D-(local) model to the MT-data in a restricted period range (15-200 sec) from site B of Ioannina region **(a)** $\varepsilon^2$ residual error of fitting; **(b), (d)** apparent resistivities $\rho_{xy}$, $\rho_{yx}$ and the respective phases $\varphi_{xy}$, $\varphi_{yx}$ of the 2D-basement; **(c)** the parameters of the model [the strike direction is constrained to $-41^0$]; **(e)-(h)** fit of the model parameterization to the scaled impedance data.

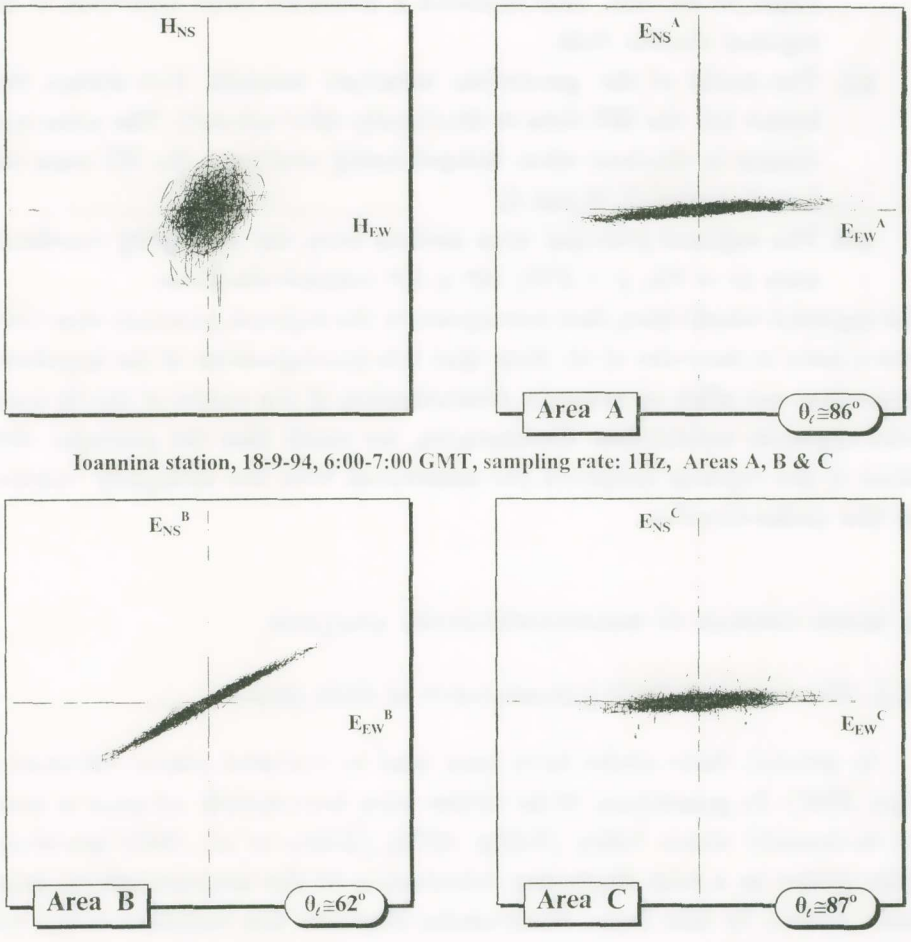


Fig. II.24. Experimental polarization diagrams of the measured electric field at the sites A, B and C of Ioannina region. The local polarization angle (clockwise from NS-direction) of the electric field is depicted. For the sake of comparison, the same diagram for the magnetic field is also given.

at each one of the sites A, B and C respectively (see Fig. II.24); in the same figure we also depict, for the sake of comparison, the polarization diagram of the measured magnetic field, $H_{EW} - H_{NS}$. Figure II. 24 shows that, the electric field at all sites A, B and C, exhibits strong polarization but at different directions (i.e., $\sim$N86°E, $\sim$N62°E and $\sim$N87°E) respectively, which are in agreement with the values mentioned above. The value of the twist-parameter was approximately

found to be –0.6. This indicates a moderate twist distortion of the regional electric field.

(ii) The model of the geoelectric structure beneath IOA-station that better fits the MT-data is *3D-(local)/ 2D-(regional)*. The same conclusion is obtained when independently analyzing the MT-data collected at sites A, B and C.

(iii) The regional principal axes deviate from the measuring coordinate axes ($x \rightarrow$ NS, $y \rightarrow$ EW) $40^o \pm 15^o$ counter-clockwise.

The apparent resistivities, that correspond to the regional principal directions, have a ratio of the order of 10. Note that this decomposition of the impedance tensor does not allow an accurate determination of the values of the 2D-basement apparent resistivities. Furthermore, we recall that the principal directions of the regional induction are determined with the ambiguity concerning the strike-direction.

## III. MOHR CIRCLES IN MAGNETOTELLURIC ANALYSIS

### *III.1. The magnetotelluric representation of Mohr circles*

In general, Mohr circles have been used to represent tensor information *[Nye, 1957]*. In geophysics, Mohr circles have been mainly adopted to study the mechanical stress. Lilley *[Lilley, 1976], [Lilley et al., 1989]* introduced Mohr circles as a tool displaying information of the magnetotelluric impedance tensor. In this form, Mohr circles illustrate the variation of the real and imaginary parts of the element $Z'_{xx}(\theta)$ versus the real and imaginary parts either of the element $Z'_{xy}(\theta)$ or the element $Z'_{yx}(\theta)$, as the horizontal axes of the measuring coordinate system are rotated clockwise through an angle $\theta$, varying $0^o \leqslant \theta \leqslant 180^o$ (the real and imaginary parts are taken separately). By this representation it is possible to extract information from the impedance tensor, in a very convenient way, concerning the dimensionality of the geoelectric structure and the decomposition model parameters that best fit the MT data.

Let us consider the initially selected measurig coordinate system to be: x-axis $\rightarrow$ NS, y-axis $\rightarrow$ EW, at which the experimental MT-data are collected and the impedance tensor, $\mathbf{Z}_m$, is derived. The clockwise rotation of this system through an angle $\theta$ produces a new measuring coordinate system (x',y'). At

this system, the elements $Z'_{ij}(\theta)$ of the impedance tensor $\mathbf{Z}'(\theta)$ are determined from the expansion of the equation:

$$\mathbf{Z}'(\theta) = \hat{R}(\theta)\mathbf{Z}_m\hat{R}^t(\theta) \qquad [III.1]$$

Thus, it is:

$$Z'_{xx} = \frac{(Z_{xx} + Z_{yy})}{2} + \frac{(Z_{xy} + Z_{yx})}{2}\sin(2\theta) + \frac{(Z_{xx} - Z_{yy})}{2}\cos(2\theta) \qquad [III.2.a]$$

$$Z'_{xy} = \frac{(Z_{xy} - Z_{yx})}{2} + \frac{(Z_{xy} + Z_{yx})}{2}\cos(2\theta) - \frac{(Z_{xx} - Z_{yy})}{2}\sin(2\theta) \qquad [III.2.b]$$

$$Z'_{yx} = -\frac{(Z_{xy} - Z_{yx})}{2} + \frac{(Z_{xy} + Z_{yx})}{2}\cos(2\theta) - \frac{(Z_{xx} - Z_{yy})}{2}\sin(2\theta) \qquad [III.2.c]$$

By taking the real parts of the complex quantities $Z_{ij}$, the combination of eqs [III.2.a] and [III.2.b] leads to:

$$(Z'_{x\,x_r}(\theta) - Z_{2_r})^2 + (Z'_{xy_r}(\theta) - Z_{1_r})^2 = \left(\frac{Z_{xy_r} + Z_{yx_r}}{2}\right)^2 + \left(\frac{Z_{xx_r} - Z_{yy_r}}{2}\right)^2 \qquad [III.3]$$

where the rotationally invariant quantities $Z_{1_r}$ and $Z_{2_r}$ are given respectively:

$$Z_{1_r} = \frac{Z_{xy_r} - Z_{yx_r}}{2} \qquad [III.4.a]$$

$$Z_{2_r} = \frac{Z_{xx_r} + Z_{yy_r}}{2} \qquad [III.4.b]$$

Equation [III.3] describes a circle at a diagram of the quantity $Z'_{xx_r}(\theta)$ versus the quantity $Z'_{xy_r}(\theta)$, with the variation of the rotation angle $\theta$ (see Fig. III.1). The circle is characterized by the parameters:

- centre coordinates: $Z'_{xy_r} = Z_{1_r}$, $Z'_{xx_r} = Z_{2_r}$ [III.5.a]
- radius: $R = \frac{1}{2}\left[(Z_{xy_r} + Z_{yx_r})^2 + (Z_{xx_r} - Z_{yy_r})^2\right]^{1/2}$ [III.5.b]

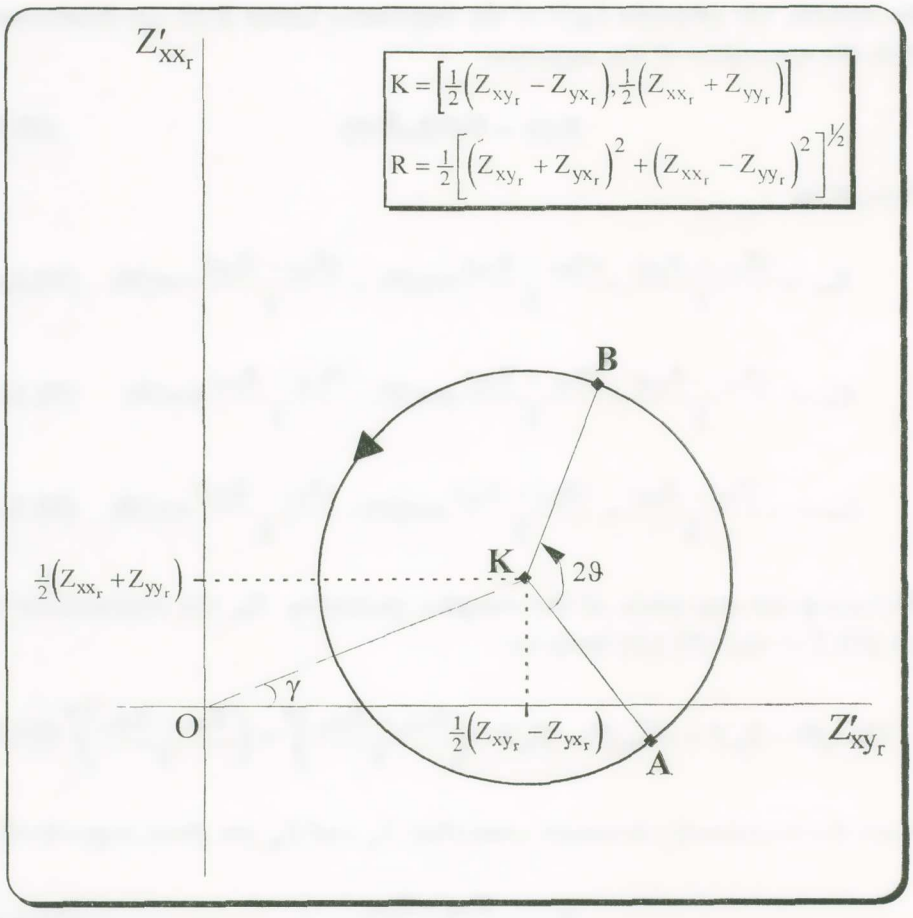


Fig. III.1. Mohr circle for a 3D-structure. Point A corresponds to the measuring coordinate system, while point B to the coordinate system that has an angular deviation θ from the measuring one.

If the point A ($Z_{xy_r}$, $Z_{xx_r}$) of the circle (see Fig. III.1) refers to the initial measuring system, the clockwise rotation of the latter at an angle θ produces a counter-clockwise angular displacement 2θ of A on the circle. The new point B [$Z'_{xy_r}(\theta)$, $Z'_{xx_r}(\theta)$] refers to the new measuring system (x′,y′). The same study is repeated by taking the imaginary parts. These diagrams are the magneto-telluric Mohr circles.

In this paper we also suggest the study of the «*conjugate*»-form of these circles by substituting the element $Z'_{xy_r}(\theta)$ with the element $Z'_{yx_r}(\theta)$ at the construction of the relevant Mohr circles. As it will be shown, additional

important information concerning the earth geoelectric structure can be deduced from such a representation.

*Mohr circle morphology as a result of the geoelectric structure dimensionality*

We study the Mohr circle representation, in cases where the earth conductivity structure has an ideal 1D or 2D-symmetry.

a. *1D-symmetry*

The following restrictions hold:

$$Z'_{xx}(\theta) = Z'_{yy}(\theta) = 0$$
$$Z'_{xy}(\theta) + Z'_{yx}(\theta) = 0$$

By inserting them into eqs [III.5.a-b], we find that the Mohr circle degenerates to a point, i.e., its centre, which lies at the $Z'_{xy_r}$-axis (see Fig. III.2).

b. *2D-symmetry*

The following restrictions hold:

$$Z'_{xx}(\theta) + Z'_{yy}(\theta) = 0$$
$$Z'_{xy}(\theta) + Z'_{yx}(\theta) \neq 0$$

At the principal axis system they become:

$$Z'_{xx}(\theta_0) = Z'_{yy}(\theta_0) = 0$$
$$Z'_{xy}(\theta_0) + Z'_{yx}(\theta_0) \neq 0$$

By substituting them in eqs [III.5.a-b], we reach to the following conclusions:

i) The ordinate of the circle centre, $\frac{Z_{xx_r} + Z_{yy_r}}{2}$, is equal to zero and hence, the centre lies at the $Z'_{xy_r}$-axis. It is evident that the depart of the centre from $Z'_{xy_r}$-axis is a measure of the deviation from the two-dimensionality.

ii) The points where the Mohr circle intersects the $Z'_{xy_r}$-axis are the limits of the quantity $Z'_{xy_r}(\theta)$. The radius is calculated from (see Fig. III.3).:

$$R = \frac{Z'_{xy_r}(\theta)|_{max} - Z'_{xy_r}(\theta)|_{min}}{2} \qquad [III.6]$$

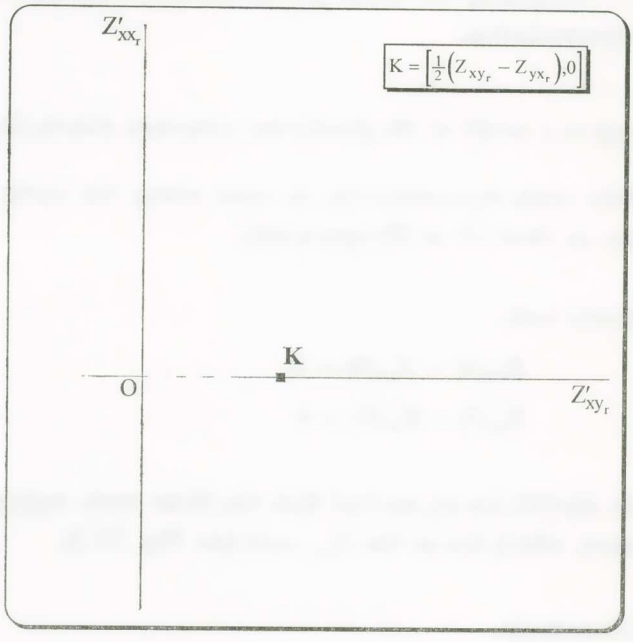


Fig. III.2. Mohr circle for a 1D-structure (the circle degenerates to its centre).

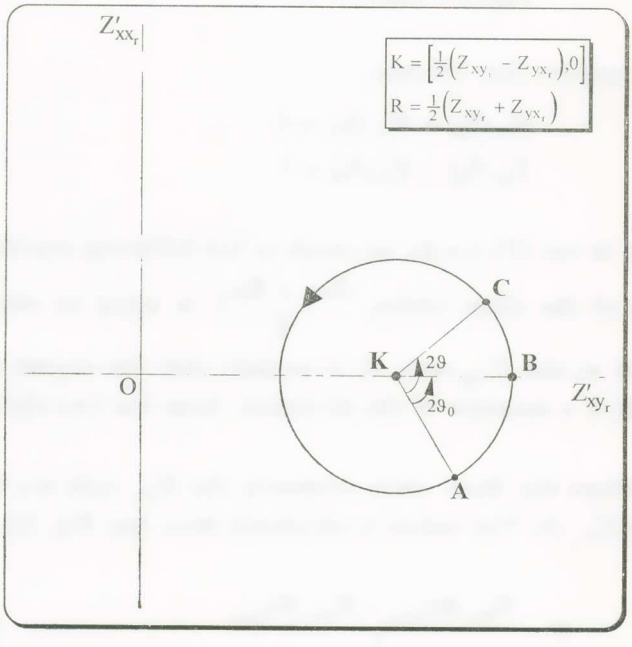


Fig. III.3. Mohr circle for a 2D-structure. Point B which has an angular deviation $2\vartheta_0$ from point A, corresponds to the intrinsic coordinate system, while point C corresponds to the coordinate system that has an angular deviation $\vartheta$ from the measuring one.

In this case the radius of Mohr circle is a measure of the conductivity contrast at the strike and dip directions, i.e., is a measure of the 2D-anisotropy.

iii) The counter-clockwise angular displacements $2\theta_0$ and $(2\theta_0 + \pi)$ respectively, from the circle intersections with the $Z'_{xy_r}$-axis, of the point A $[Z'_{xy_r}(\theta = 0), Z'_{xx_r}(\theta = 0)]$, which refers to the measuring system, actually provide the angles $\theta_0$ and $\theta_0 + \frac{\pi}{2}$ (through which the measuring system (x,y) must be rotated clockwise in order to be aligned with the principal axes, i.e., the strike and dip directions of the 2D-structure).

The morphology of the Mohr circle depicted in Fig. III.1 refers to a geoelectric structure with no specific symmetry (3D). A measure of the three-dimensionality is the angular deviation (hereafter called *skew angle*), $\gamma$, of the centre from the $Z'_{xy_r}$-axis.

*Mohr circle morphology in case of distortion of 1D-geoelectric structure*

In this section we study the effect on Mohr circle morphology of a static shift and of a 3D-distortion of 1D-data; see also *[Lilley, 1993]*. We restrict ourselves only to the real parts of the impedance tensor elements although the same study can be extended for the quadrature parts. In this frame, we consider a model of a homogeneous or horizontally layered earth in which a small-scale surface inhomogeneity (two-dimensional in symmetry) is embedded. This model is referred to as 2D-(local)/1D-(regional). At the intrinsic system of the inhomogeneity the distorted impedance tensor is given by:

$$\mathbf{Z}'(\theta = \theta_l) = \begin{pmatrix} C^l_{xx} & 0 \\ 0 & C^l_{yy} \end{pmatrix} \begin{pmatrix} 0 & z_0 \\ -z_0 & 0 \end{pmatrix} = \begin{pmatrix} 0 & C^l_{xx} z_0 \\ -C^l_{yy} z_0 & 0 \end{pmatrix}$$

The relevant Mohr circle has the parameters:

- centre coordinates: $Z'_{xy_r} = \frac{1}{2}(C^l_{xx} + C^l_{yy})z_0,\ Z'_{xx_r} = 0$ [III.7.a]

- radius: $R = \frac{1}{2}(C^l_{xx} - C^l_{yy})z_0$ [III.7.b]

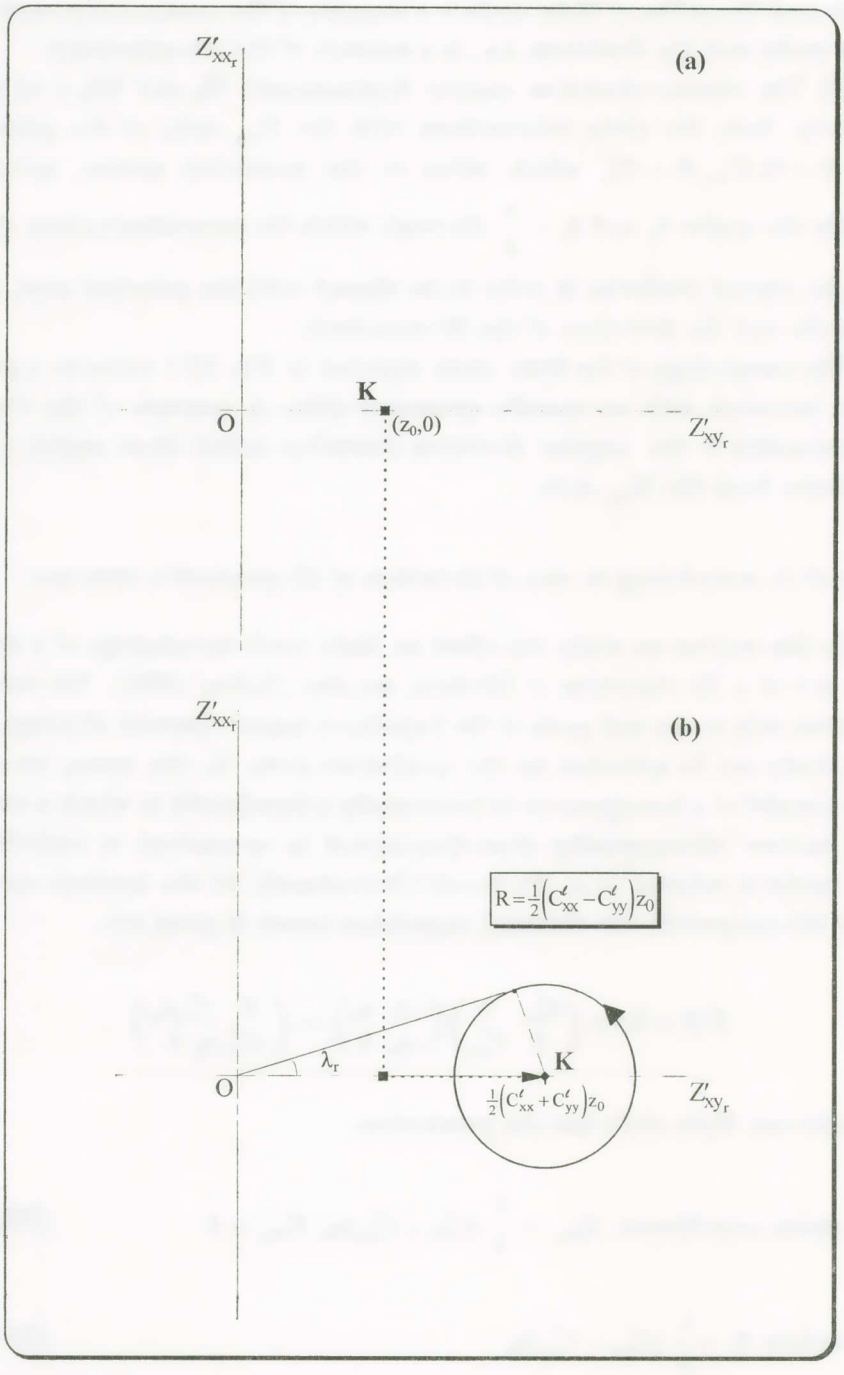


Fig. III.4. Mohr circle for **(a)** a 1D-structure; **(b)** 1D-(regional)/2D-(local).

In the case of 1D-structure, Mohr circle degenerates, as mentioned above, to its centre with coordinates $(z_0, 0)$, [see also Fig. III.4(a)]. Therefore, eqs [III. 7.a&b] reveal the following remark: the act of the static shift causes a horizontal displacement of the centre at the position $\left[\frac{1}{2}(C^l_{xx} + C^l_{yy})z_0, 0\right]$ and furthermore a «circular dilation» of the point-circle to a circle with radius $R = \frac{1}{2}(C^l_{xx} - C^l_{yy})z_0$ [see Fig. III.4(b)]. It is therefore evident that the radius is a measure of the anisotropy of the 2D-scatterer. Lilley, *[Lilley, 1993]*, defined another measure of this anisotropy, termed as anisotropy angle, $\lambda$, which is given by:

$$\lambda = \tan^{-1}\left[\frac{1}{2}\frac{(C^l_{xx} + C^l_{yy})}{\sqrt{C^l_{xx}\, C^l_{yy}}}\right] \qquad \text{[III.8]}$$

and it is independent of the impedance and of frequency. Hence, for all the frequencies Mohr circles (for real and imaginary parts) will lie within an envelope defined by this angle.

Let us suppose now that the embedded inhomogeneity is described by a distortion tensor with no symmetry (3D) which is referred to as 3D-(local)/1D-(regional). In this case the distorted impedance tensor is written as:

$$\mathbf{Z}'(\theta = \theta_l) = \begin{pmatrix} C^l_{xx} & C^l_{xy} \\ C^l_{yx} & C^l_{yy} \end{pmatrix}\begin{pmatrix} 0 & z_0 \\ -z_0 & 0 \end{pmatrix} = \begin{pmatrix} -C^l_{xy}z_0 & C^l_{xx}z_0 \\ -C^l_{yy}z_0 & C^l_{yx}z_0 \end{pmatrix}$$

The corresponding Mohr circle parameters are:

- centre coordinates: $Z'_{xy_r} = \frac{1}{2}(C^l_{xx} + C^l_{yy})z_0, Z'_{xx_r} = \frac{1}{2}(C^l_{yx} - C^l_{xy})z_0$ [III.9.a]

- radius: $R = \frac{1}{2}\left[\sqrt{(C^l_{xx} - C^l_{yy})^2 + (C^l_{xy} + C^l_{yx})^2}\right]z_0$ [III.9.b]

Therefore, the 3D-distortion moves the centre away from the $Z'_{xy_r}$-axis and takes place a «circular dilation» of the point-circle at a new position.

*III.2. Interconnection of the impedance tensor decomposition parameters in the magnetotelluric representation of Mohr circles*

As already discussed in detail, Groom and Bailey *[Groom, 1988], [Groom & Bailey, 1989], [Groom et al., 1993]* suggested a decomposition of the measured impedance tensor when a small-scale near-surface inhomogeneity, with no specific symmetry (3D), is embedded in a two-dimensional regional geoelectric structure. The regional magnetic field is considered to remain unaffected, while the distorting effect on the regionally induced electric field of the semi-static scatterer is described by the tensor product:

$$\mathbf{C} = g\mathbf{TSA}$$

We now proceed to a study of the engagement of the parameters t, e, $\sigma$, $\delta$ and $\theta$ of Groom and Bailey's decomposition in the expressions of the parameters of the magnetotelluric representation of Mohr circles *[Lilley, 1993]*.

At the measuring system the measured impedance tensor is decomposed:

$$\mathbf{Z}_m = \hat{R}\,\mathbf{TSZ}_{2D}\hat{R}^t$$

and the analysis explained in a previous section leads to the non-linear set of complex equations [II.36.a-d] which relate the parameters of the decomposition (t, e, $\sigma$, $\delta$, $\theta$) with the elements $Z_{ij}$ of the measured impedance tensor, $\mathbf{Z}_m$. Lilley *[Lilley, 1993]* introduced the following substitutions:

$$\tan A = t \qquad [III.10.a[$$

$$\tan B = \frac{e\sigma}{\delta} = \frac{\tan E}{\tan D} \qquad [III.10.b]$$

$$\tan C = \frac{e\delta}{\sigma} = \tan E \cdot \tan D \qquad [III.10.c]$$

$$\tan D = \frac{\delta}{\sigma} \qquad [III.10.d]$$

$$\tan E = e \qquad \text{[III.10.e]}$$

Hence, the set of equations [II.36.a-d] is transformed to the set:

$$\alpha_0 = \sigma(\tan A + \tan C) \qquad \text{[III.11.a]}$$

$$\alpha_1 = \delta[(1 - \tan A \cdot \tan B)\cos 2\theta - (\tan A + \tan B)\sin 2\theta] \qquad \text{[III.11.b]}$$

$$\alpha_2 = -\sigma(1 - \tan A \cdot \tan C) \qquad \text{[III.11.c]}$$

$$\alpha_3 = \delta[-(\tan A + \tan B)\cos 2\theta - (1 - \tan A \cdot \tan B)\sin 2\theta] \qquad \text{[III.11.d]}$$

where, the quantities $\alpha_0$, $\alpha_1$, $\alpha_2$, $\alpha_3$ are given from equations [II.35.a-d].
The set of equations [III.11.a-d] can be studied graphically using Mohr circles. We recall that the analysis proceeds separately for the real and imaginary parts.

We now proceed to the formation of an «*atlas*» of different models of the geoelectric structure which belong to the general types 3D-(local)/2D-(regional) or 3D-(local)/1D-(regional) by selecting different sets of the decomposition parameters *[Lilley, 1993]*. For each case we give the morphology of the corresponding Mohr circle together with its characteristic parameters:

- the centre coordinates:

$$\left(\frac{Z_{xy_r} - Z_{yx_r}}{2}, \frac{Z_{xx_r} + Z_{yy_r}}{2}\right) \qquad \text{[III.12.a]}$$

- the circle radius:

$$R = \frac{1}{2}\left[(Z_{xx_r} - Z_{yy_r})^2 + (Z_{xy_r} + Z_{yx_r})^2\right]^{1/2} \qquad \text{[III.12.b]}$$

- the skew angle:

$$\gamma = \tan^{-1}\left(\frac{Z_{xx_r} + Z_{yy_r}}{Z_{xy_r} - Z_{yx_r}}\right) \qquad \text{[III.12.c]}$$

The study is restricted below to the real parts only.

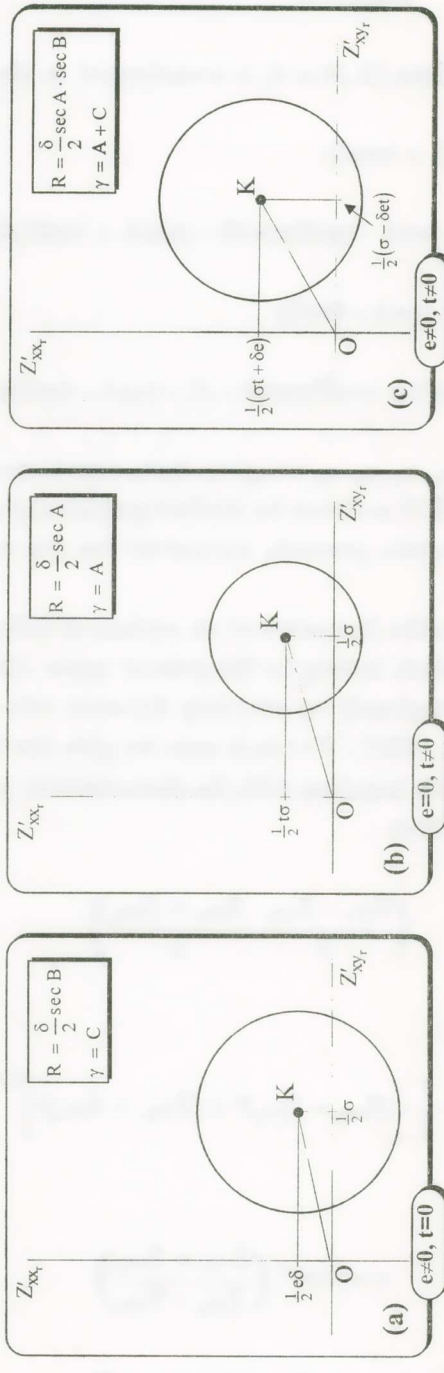


Fig. III.5. Mohr circle for 2D-(regional)/3D-(local) with local distortion: **(a)** shear only; **(b)** twist only; **(c)** twist and shear.

A. Two-dimensional geoelectric structure of the basement

1) Shear distortion only ($e \neq 0$, $t = 0$), [Fig. III.5(a)]

The impedance tensor in the regional principal axis system is given by:

$$\mathbf{Z}' = \mathbf{S}\mathbf{Z}_{2D} = \begin{pmatrix} 1 & e \\ e & 1 \end{pmatrix} \begin{pmatrix} 0 & \alpha \\ -b & 0 \end{pmatrix} = \begin{pmatrix} -eb & \alpha \\ -b & e\alpha \end{pmatrix} \qquad [III.13]$$

The Mohr circle parameters are:

Centre coordinates: $\left(\frac{\sigma}{2}, \frac{e\delta}{2}\right)$

Radius:

$$R = \left[\left(-\frac{e\sigma}{2}\right)^2 + \left(\frac{\delta}{2}\right)^2\right]^{1/2} = \frac{\delta}{2}\left[1 + \left(\frac{e\sigma}{\delta}\right)^2\right]^{1/2} = \frac{\delta}{2}(1 + \tan^2 B)^{1/2} \Rightarrow R = \frac{\delta}{2}\sec B$$

Skew angle: $\tan\gamma = \frac{e\delta}{\sigma} = \tan C \Rightarrow \gamma = C$

2) Twist distortion only ($e = 0$, $t \neq 0$), [Fig. III.5(b)]

The impedance tensor in the regional principal axis system is given by:

$$\mathbf{Z}' = \mathbf{T}\mathbf{Z}_{2D} = \begin{pmatrix} 1 & -t \\ t & 1 \end{pmatrix} \begin{pmatrix} 0 & \alpha \\ -b & 0 \end{pmatrix} = \begin{pmatrix} tb & \alpha \\ -b & t\alpha \end{pmatrix} \qquad [III.14]$$

The Mohr circle parameters are:

Centre coordinates: $\left(\frac{\sigma}{2}, \frac{t\sigma}{2}\right)$

Radius:

$$R = \left[\left(-\frac{t\delta}{2}\right)^2 + \left(\frac{\delta}{2}\right)^2\right]^{1/2} = \frac{\delta}{2}(1 + t^2)^{1/2} = \frac{\delta}{2}(1 + \tan^2 A)^{1/2} \Rightarrow R = \frac{\delta}{2}\sec A$$

Skew angle: $\tan\gamma = \frac{t\sigma}{\sigma} = \tan A \Rightarrow \gamma = A$

3) When shear and twist distortion are present ($e \neq 0$, $t \neq 0$), [Fig. III.5(c)]
The impedance tensor in the regional principal axis system is given by:

$$\mathbf{Z'} = \mathbf{TSZ_{2D}} = \begin{pmatrix} 1 & -t \\ t & 1 \end{pmatrix}\begin{pmatrix} 1 & e \\ e & 1 \end{pmatrix}\begin{pmatrix} 0 & \alpha \\ -b & 0 \end{pmatrix} = \begin{pmatrix} b(t-e) & \alpha(1-te) \\ -b(1+te) & \alpha(t+e) \end{pmatrix} \quad [III.15]$$

The Mohr circle parameters are:

$$\text{Centre coordinates: } \left(\frac{\alpha(1-te)+b(1+te)}{2}, \frac{b(t-e)+\alpha(t+e)}{2}\right) =$$

$$= \left(\frac{\sigma - \delta et}{2}, \frac{\sigma t + \delta e}{2}\right)$$

Radius:

$$R = \left[\left(-\frac{t\delta + e\sigma}{2}\right)^2 + \left(\frac{\delta - te\sigma}{2}\right)^2\right]^{1/2} = \frac{\delta}{2}\left[(1+t^2)\cdot\left(1+\frac{e^2\sigma^2}{\delta^2}\right)\right]^{1/2} \Rightarrow$$

$$\Rightarrow R = \frac{\delta}{2}\sec A \cdot \sec B$$

Skew angle:

$$\tan\gamma = \frac{\sigma t + e\delta}{\sigma - te\delta} = \frac{t + \frac{e\delta}{\sigma}}{1 - t\frac{e\delta}{\sigma}} = \frac{\tan A + \tan C}{1 - \tan A \cdot \tan C} = \tan(A+C) \Rightarrow \gamma = A + C$$

We now study two extreme cases: the weak distortion ($|e|, |t| << 1$) and the strong (2D) distortion ($|e| \to 1$).

4) Weak distortion ($|e|, |t| << 1$)
(4.1) Shear distortion only ($e \neq 0$, $t = 0$), [Fig. III.6(a)]
The impedance tensor in the regional principal axis system is given by:

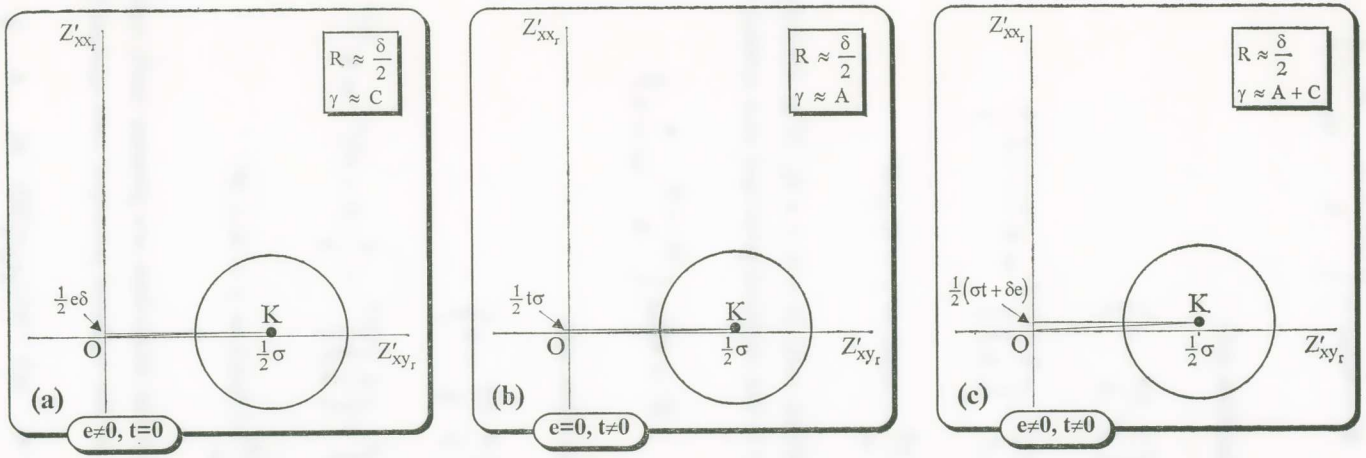


Fig. III.6. Mohr circles for 2D-(regional)/3D-(local) with *weak* local distortion: **(a)** shear only; **(b)** twist only; **(c)** twist and shear.

$$\mathbf{Z}' = \mathbf{SZ}_{2D} = \begin{pmatrix} -eb \to 0 & \alpha \\ -b & e\alpha \to 0 \end{pmatrix}$$

as ($|e| << 1$).
The Mohr circle parameters are:

Centre coordinates: $\left( \frac{\sigma}{2}, \frac{e\delta}{2} \to 0 \right)$

Radius: $R = \left[ \left( -\frac{e\sigma}{2} \right)^2 + \left( \frac{\delta}{2} \right)^2 \right]^{1/2} \Rightarrow R \xrightarrow{|e|<<1} \frac{\delta}{2}$

Skew angle: $\tan\gamma = \frac{e\delta}{\sigma} = \tan C \Rightarrow \gamma = C \simeq 0^0$

(4.2) Twist distortion only ($e = 0$, $t \neq 0$), [Fig. III.6(b)]
The impedance tensor in the regional principal axis system is given:

$$\mathbf{Z}' = \mathbf{TZ}_{2D} \begin{pmatrix} tb \to 0 & \alpha \\ -b & t\alpha \to 0 \end{pmatrix}$$

The Mohr circle parameters are:

Centre coordinates: $\left( \frac{\sigma}{2}, \frac{t\sigma}{2} \to 0 \right)$

Radius: $R = \left[ \left( -\frac{t\delta}{2} \right)^2 + \left( \frac{\delta}{2} \right)^2 \right]^{1/2} = \frac{\delta}{2} (1 + t^2)^{1/2} \Rightarrow R \xrightarrow{|t|<<1} \frac{\delta}{2}$

Skew angle: $\tan\gamma = \frac{t\sigma}{\sigma} = \tan A \Rightarrow \gamma = A \simeq 0^0$

(4.3) When shear and twist distortion are present ($e \neq 0$, $t \neq 0$), [Fig. III.6(c)]
The impedance tensor in the regional principal axis system is given:

$$\mathbf{Z}' = \mathbf{TSZ}_{2D} = \begin{pmatrix} b(t-e) & \alpha(1-te) \\ -b(1+te) & \alpha(t+e) \end{pmatrix} \overset{te \to 0}{\approx} \begin{pmatrix} b(t-e) & \alpha \\ -b & \alpha(t+e) \end{pmatrix}$$

The Mohr circle parameters are:

Centre coordinates: $\left(\frac{\sigma - \delta et}{2} \rightarrow \frac{\sigma}{2}, \frac{\sigma t + \delta e}{2}\right)$

Radius:

$$R = \left[\left(-\frac{t\delta + e\sigma}{2}\right)^2 + \left(\frac{\delta}{2}\right)^2\right]^{1/2} = \frac{\delta}{2}\left[(1 + t^2)\cdot\left(1 + \frac{e^2\sigma^2}{\delta^2}\right)\right]^{1/2} \Rightarrow R \xrightarrow{|e|,|t|<<1} \frac{\delta}{2}$$

Skew angle: $\tan\gamma = \frac{\sigma t + e\delta}{\sigma - te\delta} \overset{te\to 0}{\approx} \frac{\sigma t + e\delta}{\sigma} = t + \frac{e\delta}{\sigma} = \tan A + \tan C$ [III.16.a]

The following relation holds:

$$1 - \tan A \cdot \tan C = 1 - t\frac{e\delta}{\sigma} \overset{te\to 0}{\approx} 1 \qquad \text{[III.16.b]}$$

The combination of eqs [III.16.a and b] provides:

$$\tan\gamma \approx \frac{\tan A + \tan C}{1 - \tan A \cdot \tan C} = \tan(A + C) \Rightarrow \gamma \approx A + C$$

5) Strong (2D) distortion ($|e| \rightarrow 1$)

(5.1) Shear distortion only ($e \neq 0$, $t = 0$), [Fig. III.7(a)]

The impedance tensor in the regional principal axis system is given by:

$$\mathbf{Z}' = \mathbf{S}\mathbf{Z}_{2D} = \begin{pmatrix} -eb & \alpha \\ -b & e\alpha \end{pmatrix} \overset{|e|\to 1}{\approx} \begin{pmatrix} \mp b & \alpha \\ -b & \pm\alpha \end{pmatrix}$$

The Mohr circle parameters are:

Centre coordinates: $\left(\frac{\sigma}{2}, \frac{\pm\delta}{2}\right)$

The distance of the circle centre from the origin of the axes is calculated from:

$$d \approx \left[\left(\frac{\sigma}{2}\right)^2 + \left(\frac{\pm\delta}{2}\right)^2\right]^{1/2} = \frac{\delta}{2}\left(1+\frac{\sigma^2}{\delta^2}\right)^{1/2} = \frac{\delta}{2}(1+\cot^2 D)^{1/2} \Rightarrow d \approx \frac{\delta}{2}\csc D \quad [\text{III.17.a}]$$

Radius:

$$R \approx \left[\left(-\frac{\pm\sigma}{2}\right)^2 + \left(\frac{\delta}{2}\right)^2\right]^{1/2} = \frac{\delta}{2}\left(1+\frac{\sigma^2}{\delta^2}\right)^{1/2} = \frac{\delta}{2}(1+\cot^2 D)^{1/2} \Rightarrow R \approx \frac{\delta}{2}\csc D \quad [\text{III.17.b}]$$

We draw attention to the fact that the equality of eqs [III.17.a and b] implies that the circle passes through the origin of the axes.

Skew angle: $\tan\gamma \approx \dfrac{\pm\delta}{\sigma} = \pm\tan D \Rightarrow \gamma \approx \pm D$

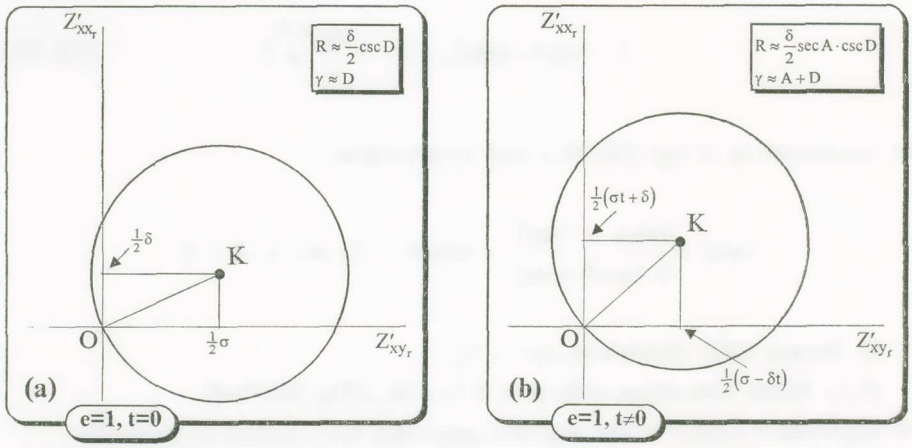


Fig. III.7. Mohr circles for 2D-(regional)/3D-(local) with *strong* shear distortion ($|e| \to 1$): **(a)** without twist; **(b)** with twist.

(5.2) When shear and twist distortion are present ($e \neq 0$, $t \neq 0$), [Fig. III.7(b)]

The impedance tensor in the regional principal axis system is given by:

$$\mathbf{Z}' = \mathbf{TSZ}_{2D} = \begin{pmatrix} b(t-e) & \alpha(1-te) \\ -b(1+te) & \alpha(t+e) \end{pmatrix} \overset{|e|\to 1}{\approx} \begin{pmatrix} b(t\mp 1) & \alpha(1\mp t) \\ -b(1\pm t) & \alpha(t\pm 1) \end{pmatrix}$$

The Mohr circle parameters are:

Centre coordinates: $\left(\frac{\sigma \mp \delta t}{2}, \frac{\sigma t \pm \delta}{2}\right)$

The distance of the circle centre from the origin of the axes is calculated from:

$$d \approx \left[\left(\frac{\sigma \mp \delta t}{2}\right)^2 + \left(\frac{\sigma t \pm \delta}{2}\right)^2\right]^{1/2} = \frac{\delta}{2}\left[(1 + t^2)\cdot\left(1 + \frac{\sigma^2}{\delta^2}\right)\right]^{1/2} =$$
$$= \frac{\delta}{2}\left[(1 + \tan^2 A)\cdot(1 + \cot^2 D)\right]^{1/2} \Rightarrow d \approx \frac{\delta}{2}\,\sec A \,.\, \csc D \qquad \text{[III.18.a]}$$

Radius:

$$R \approx \left[\left(-\frac{\delta t \pm \sigma}{2}\right)^2 + \left(\frac{\delta \mp \sigma t}{2}\right)^2\right]^{1/2} = \frac{\delta}{2}\left[(1 + t^2)\cdot\left(1 + \frac{\sigma^2}{\delta^2}\right)\right]^{1/2}$$
$$= \frac{\delta}{2}\left[(1 + \tan^2 A)\cdot(1 + \cot^2 D)\right]^{1/2} \Rightarrow R \approx \frac{\delta}{2}\,\sec A \cdot \csc D \qquad \text{[III.18.b]}$$

We draw attention to the fact that the equality of eqs [III.18.a and b] implies that the circle passes through the origin of the axes.

Skew angle:

$$\tan\gamma \approx \frac{\sigma t \pm \delta}{\sigma \mp t\delta} = \frac{t \pm \frac{\delta}{\sigma}}{1 \mp t\frac{\delta}{\sigma}} = \frac{\tan A \pm \tan D}{1 \mp \tan A \cdot \tan D} = \tan(A \pm D) \Rightarrow \gamma \approx A \pm D$$

B. Two-dimensional geoelectric structure of the basement with high anisotropy ($|\alpha| >> |b|$)

1) Shear distortion only ($e \neq 0$, $t = 0$), [Fig. III.8(a)]

The impedance tensor at the regional intrinsic coordinate system has the same form as in eq. [III.13] by considering also that: $\sigma \simeq \delta$.

The Mohr circle parameters are:

Centre coordinates: $\left(\frac{\sigma}{2}, \frac{e\delta}{2}\right) \approx \left(\frac{\sigma}{2}, \frac{e\sigma}{2}\right)$

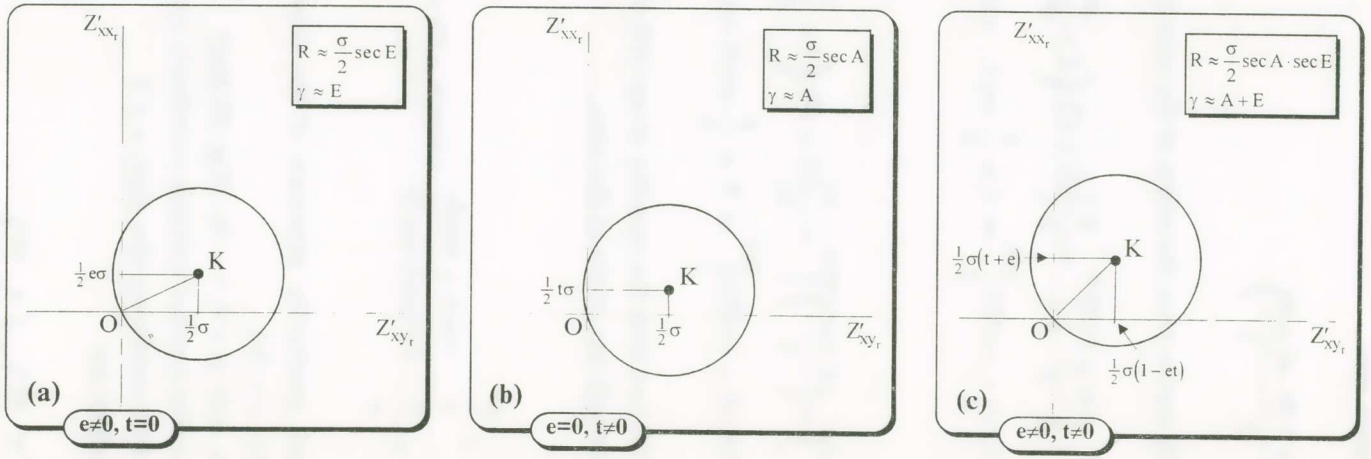


Fig. III.8. Mohr circles for 2D-(regional with high anisotropy)/3D-(local) with local distortion: **(a)** shear only; **(b)** twist only; **(c)** twist and shear.

The distance of the circle centre from the origin of the axes is calculated from:

$$d \approx \left[\left(\frac{\sigma}{2}\right)^2 + \left(\frac{e\sigma}{2}\right)^2\right]^{1/2} = \frac{\sigma}{2}(1 + e^2)^{1/2} \Rightarrow d \approx \frac{\sigma}{2}\,\text{secE} \quad \text{[III.19.a]}$$

Radius:

$$R = \left[\left(-\frac{e\sigma}{2}\right)^2 + \left(\frac{\delta}{2}\right)^2\right]^{1/2} \approx \left[\left(-\frac{e\sigma}{2}\right)^2 + \left(\frac{\sigma}{2}\right)^2\right]^{1/2} = \frac{\sigma}{2}(1 + e^2)^{1/2} \Rightarrow R \approx \frac{\sigma}{2}\,\text{secE} \quad \text{[III.19.b]}$$

Eqs [III.19.a and b] imply that in this case also the circle passes through the origin of the axes.

Skew angle: $\tan\gamma = \frac{e\delta}{\sigma} \approx \frac{e\sigma}{\sigma} = \tan E \Rightarrow \gamma \approx E$

2) Twist distortion only ($e = 0$, $t \neq 0$), [Fig. III.8(b)]

The impedance tensor in the regional intrinsic coordinate system has the same form as in eq. [III.14]. The Mohr circle parameters are:

Centre coordinates: $\left(\frac{\sigma}{2}, \frac{t\sigma}{2}\right)$

The distance of the circle centre from the origin of the axes is calculated:

$$d \approx \left[\left(\frac{\sigma}{2}\right)^2 + \left(\frac{t\sigma}{2}\right)^2\right]^{1/2} = \frac{\sigma}{2}(1 + t^2)^{1/2} \Rightarrow d \approx \frac{\sigma}{2}\,\text{secA} \quad \text{[III.20.a]}$$

Radius:

$$R = \left[\left(-\frac{t\delta}{2}\right)^2 + \left(\frac{\delta}{2}\right)^2\right]^{1/2} \approx \frac{\sigma}{2}(1 + t^2)^{1/2} \Rightarrow R \approx \frac{\sigma}{2}\,\text{secA} \quad \text{[III.20.b]}$$

Eqs [III.20.a and b] are equal, hence the circle passes through the origin of the axes.

Skew angle: $\tan\gamma = \frac{t\sigma}{\sigma} = \tan A \Rightarrow \gamma = A$

3) When shear and twist distortion are present ($e \neq 0$, $t \neq 0$), [Fig. III.8(c)]

The impedance tensor at the regional intrinsic coordinate system has the same form as in eq. [III.15]. The Mohr circle parameters are:

Centre coordinates: $\left(\frac{\sigma - \delta et}{2}, \frac{\sigma t + \delta e}{2}\right) \overset{\sigma \simeq \delta}{\approx} \left(\frac{\sigma(1-et)}{2}, \frac{\sigma(t+e)}{2}\right)$

The distance of the circle centre from the origin of the axes is calculated:

$$d \approx \left\{\left[\frac{\sigma(1-et)}{2}\right]^2 + \left[\frac{\sigma(t+e)}{2}\right]^2\right\}^{1/2} = \frac{\sigma}{2}\left[(1+t^2)(1+e^2)\right]^{1/2} \Rightarrow$$

$$\Rightarrow d \approx \frac{\sigma}{2}\sec A \cdot \sec E \qquad \text{[III.21.a]}$$

Radius:

$$R = \left[\left(-\frac{t\delta + e\sigma}{2}\right)^2 + \left(\frac{\delta - te\sigma}{2}\right)^2\right]^{1/2} = \frac{\delta}{2}\left[(1+t^2)\cdot\left(1+\frac{e^2\sigma^2}{\delta^2}\right)\right]^{1/2} \overset{\sigma \simeq \delta}{\Rightarrow}$$

$$\overset{\sigma \simeq \delta}{\Rightarrow} R \approx \frac{\sigma}{2}\left[(1+t^2)\cdot(1+e^2)\right]^{1/2} \Rightarrow R \approx \frac{\sigma}{2}\sec A \cdot \sec E \qquad \text{[III.21.b]}$$

The equality of eqs [III.21.a and b] implies again that the Mohr circle passes through the origin of the axes.

Skew angle: $\tan\gamma = \frac{\sigma t + e\delta}{\sigma - te\delta} \overset{\sigma \simeq \delta}{\approx} \frac{t+e}{1-te} = \frac{\tan A + \tan E}{1 - \tan A \cdot \tan E} = \tan(A+E) \Rightarrow \gamma \approx A + E$

C. One-dimensional geoelectric structure of the basement ($\alpha = b = z_0$)

The impedance tensor has the simple form: $\mathbf{Z}_{1D} = \begin{pmatrix} 0 & z_0 \\ -z_0 & 0 \end{pmatrix}$

In this case: $\sigma = 2z_0$ and $\delta = 0$.

1) Shear distortion only ($e \neq 0$, $t = 0$), [Fig. III.9(a)]
The impedance tensor becomes:

$$\mathbf{Z}' = \mathbf{S}\mathbf{Z}_{1D} = \begin{pmatrix} 1 & e \\ e & 1 \end{pmatrix}\begin{pmatrix} 0 & z_0 \\ -z_0 & 0 \end{pmatrix} = \begin{pmatrix} -ez_0 & z_0 \\ -z_0 & ez_0 \end{pmatrix}$$

The Mohr circle parameters are:

Centre coordinates: $\left(\frac{\sigma}{2}, 0\right)$

Radius: $R = \left[\left(-\frac{e\sigma}{2}\right)^2 + \left(\frac{\delta}{2}\right)^2\right]^{1/2} = \frac{e\sigma}{2} \Rightarrow R = \frac{\sigma}{2}\tan E$

Skew angle: $\tan\gamma = \frac{e\delta}{\sigma} = 0 \Rightarrow \gamma = 0^o$

2) Twist distortion only ($e = 0$, $t \neq 0$), [Fig. III.9(b)]
The impedance tensor has the form:

$$\mathbf{Z}' = \mathbf{T}\mathbf{Z}_{1D} = \begin{pmatrix} 1 & -t \\ t & 1 \end{pmatrix}\begin{pmatrix} 0 & z_0 \\ -z_0 & 0 \end{pmatrix} = \begin{pmatrix} tz_0 & z_0 \\ -z_0 & tz_0 \end{pmatrix}$$

The Mohr circle parameters are:

Centre coordinates: $\left(\frac{\sigma}{2}, \frac{t\sigma}{2}\right)$

Radius: $R = \left[\left(-\frac{t\delta}{2}\right)^2 + \left(\frac{\delta}{2}\right)^2\right]^{1/2} = \frac{\delta}{2}(1 + t^2)^{1/2} = 0 \Rightarrow R = 0$

which means that the circle degenerates to its centre.

Skew angle: $\tan\gamma = \frac{t\sigma}{\sigma} = \tan A \Rightarrow \gamma = A$

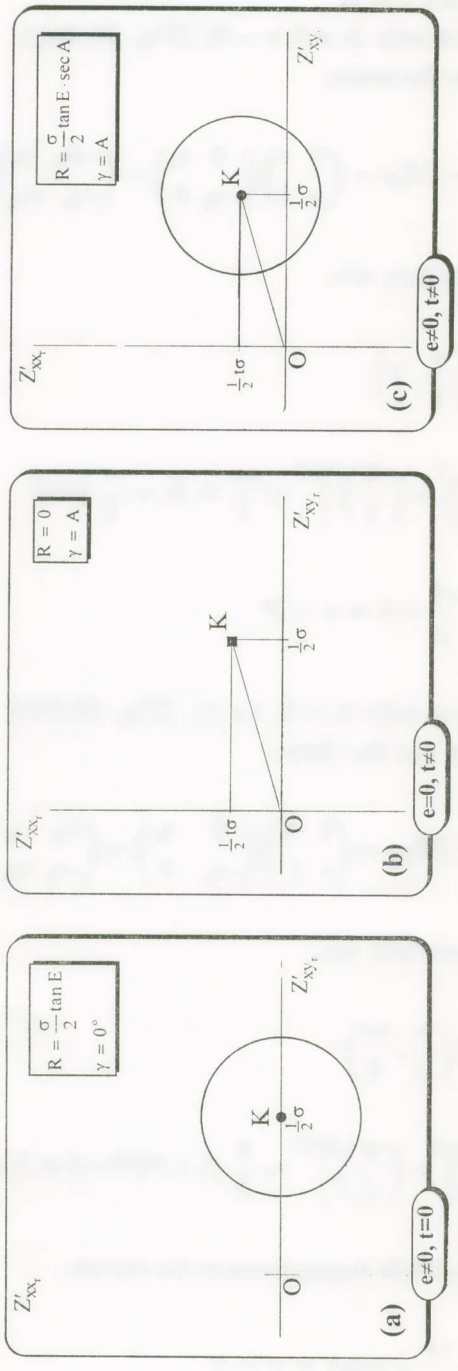


Fig. III.9. Mohr circles for 1D-(regional)/3D-(local) with local distortion: **(a)** shear only; **(b)** twist only; **(c)** twist and shear.

3) When shear and twist distortion are present ($e \neq 0$, $t \neq 0$), [Fig. III.9(c)] The impedance tensor is given by:

$$\mathbf{Z}' = \mathbf{TSZ}_{1D} = \begin{pmatrix} 1 & -t \\ t & 1 \end{pmatrix} \begin{pmatrix} 1 & e \\ e & 1 \end{pmatrix} \begin{pmatrix} 0 & z_0 \\ -z_0 & 0 \end{pmatrix} = \begin{pmatrix} z_0(t-e) & z_0(1-te) \\ -z_0(1+te) & z_0(t+e) \end{pmatrix}$$

The Mohr circle parameters are:

Centre coordinates: $\left( \frac{\sigma - \delta et}{2}, \frac{\sigma t + \delta e}{2} \right) = \left( \frac{\sigma}{2}, \frac{t\sigma}{2} \right)$

Radius:

$$R = \left[ \left( -\frac{t\delta + e\sigma}{2} \right)^2 + \left( \frac{\delta - te\sigma}{2} \right)^2 \right]^{1/2} = \left[ (1+t^2) \cdot (\delta^2 + e^2\sigma^2) \right]^{1/2} \Rightarrow R = \frac{\sigma}{2} \sec A \cdot \tan E$$

Skew angle: $\tan\gamma = \frac{\sigma t}{\sigma} = \tan A \Rightarrow \gamma = A$

*III.3. Experimental analysis using Mohr circles*

Figs III.10-12 depict, for different periods, the Mohr circles, $Z'_{xx}(\theta)$ vs $Z'_{xy}(\theta)$, (solid line circle groups) constructed separately for the real and imaginary parts for the sites A, B and C of Ioannina region. An inspection of these figures shows that, for the frequency band under consideration, all the circles pass approximately through the origin ($Z'_{xy_i} = 0$, $Z'_{xx_i} = 0$), where $i = r, q$ the real and imaginary parts respectively. This *striking* peculiarity indicates that if we rotate clockwise the measuring system by an angle $\theta_l$, i.e., ($x'_{\theta_l}$, $y'_{\theta_l}$), the elements of the first raw of the (rotated) impedance tensor $\mathbf{Z}'(\theta_l) = \hat{\mathrm{R}}(\theta_l)\mathbf{Z}_m\hat{\mathrm{R}}^t(\theta_l)$ become both approximately zero:

$$E'_{x\theta_l} = Z'_{xx}(\theta_l)H'_{x\theta_l} + Z'_{xy}(\theta_l)H'_{x\theta_l} = 0$$

which physically means that irrespectively of the polarization of the incident magnetic field, the electric field is linearly polarized in the direction of $y'_{\theta_l}$-axis. These rotation angles were calculated analytically from the plots (for

the real and imaginary parts) of the Mohr circles at each one of the sites A, B and C, by minimizing the quantity:

$$\sqrt{[Z'_{xx}(\theta)]^2 + [Z'_{xy}(\theta)]^2} \xrightarrow{\theta=\theta_l} \min$$

and are presented versus the period in Fig. III.13. This figure indicates that the local electric field must be strongly linearly polarized in the directions ~N80°E, ~N60°E and ~N90°E at the sites A, B and C respectively; this is a result of the fact that (taking either the real or the imaginary parts) the rotation angles were found to be $\theta_l^A \approx 170^o$, $\theta_l^B \approx 150^o$ and $\theta_l^C \approx 180^o$ for the sites A, B and C respectively (we emphasize that these angles are frequency independent). An independent confirmation results from the construction of the measured electric field polarization diagrams (see Fig. II.24); they show that the electric field at all the sites A, B and C, exhibits strong polarization but in different directions (i.e., ~N86°E, ~N62°E and ~N87°E respectively), which agree with the values mentioned above. We also draw attention to the fact that approximately the same angles have been independently determined (as local channelling directions i.e., ~N81°E, ~N62°E and ~N90°E respectively), from the implementation of Groom and Bailey's decomposition methodology on the experimental data (local strike).

A «*conjugate*» form of the magnetotelluric representation of Mohr circles has been introduced by Makris *[Makris, 1997]*. As the horizontal axes of the measuring coordinate system ($x \rightarrow$ NS, $y \rightarrow$ EW) are rotated clockwise by the angle $\theta$ (where $0^o \leqslant \theta \leqslant 180^o$), the variation of the real (imaginary) part of the impedance tensor element $Z'_{xx}(\theta)$ is plotted versus the element $Z'_{yx}(\theta)$ [instead of representing the variation of the real (imaginary) part of element $Z'_{xx}(\theta)$ versus the element $Z'_{xy}\theta$)]. The corresponding Mohr circles, taking the real and the imaginary parts separately, for the same periods and for each one of the sites A, B and C are also depicted in Figs III.10-12 (dashed-line circle groups). These circles exhibit the same peculiarity, i.e., they also pass through the origin of the axes ($Z'_{yx}$, $Z'_{xx}$), independently of the measuring site, the period and the consideration of either the real or the imaginary parts. This characteristic can be considered as a «*signature*» of the regional geoelectric structure of Ioannina region. It implies that if we rotate clockwise the measuring system by an angle $\theta_r$ ($x'_{\theta_r}$, $y'_{\theta_r}$), the elements of the first column of the (ro-

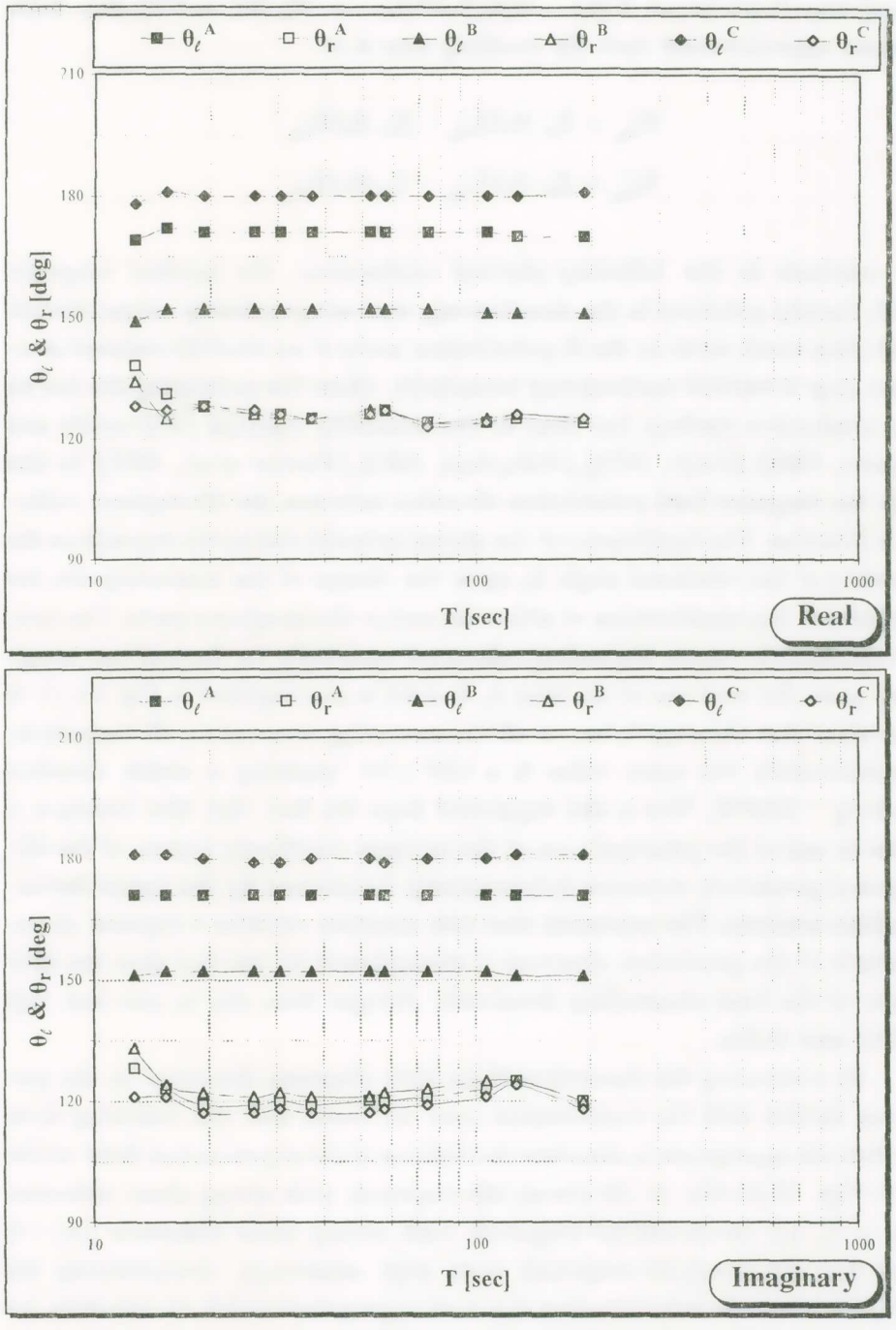


Fig. III.13. The local strike $\theta_l$ and the regional strike $\theta_r$, directions deduced from the Mohr circles constructed using the real and imaginary parts of $Z'_{xy}$ and $Z'_{yx}$ respectively vs $Z'_{xx}$, for various periods for the sites A, B, C of Ioannina region.

tated) impedance tensor $\mathbf{Z}'(\theta_r) = \hat{\mathbf{R}}(\theta_r)\mathbf{Z}_m\hat{\mathbf{R}}^t(\theta_r)$, i.e., $Z'_{xx}(\theta_r)$ and $Z'_{yx}(\theta_r)$, both become approximately zero. By recalling that it is:

$$E'_{x_{\theta_r}} = Z'_{xx}(\theta_r)H'_{x_{\theta_r}} + Z'_{xy}(\theta_r)H'_{y_{\theta_r}}$$

$$E'_{y_{\theta_r}} = Z'_{yx}(\theta_r)H'_{x_{\theta_r}} + Z'_{yy}(\theta_r)H'_{y_{\theta_r}}$$

we conclude to the following physical explanation: the incident magnetic field, linearly polarized in the direction-$x'_{\theta_r}$, does not practically induce electric field; this result refers to the H-polarization mode of an ideal 2D-regional structure (e.g. a vertical conductivity boundary), where the measuring site lies on the conductive medium but close to the resistivity contrast *[d'Erceville and Kunetz, 1962], [Swift, 1971], [Nabighian, 1991], [Fischer et al., 1992]*. In this case the magnetic field polarization direction indicates the 2D-regional strike-axis direction. The significance of the aforementioned statement depends on the stability of the rotational angle, $\theta_r$, upon the change of the measuring site, the period and the consideration of either the real or the imaginary parts. The rotational angle, $\theta_r$, versus the period, calculated separately for the real and imaginary parts, for each one of the sites A, B and C is also depicted in Fig. III.13. It is evident that the angle $\theta_r$ has, at all the measuring sites and for all the periods, approximately the same value $\theta_r \approx 125^o \pm 5^o$, implying a stable direction striking ~N55°W. This is also supported from the fact that this direction is close to one of the principal axes of the intrinsic coordinate system of the 2D-regional geoelectric structure independently determined by the tensor decomposition analysis. The argument that this direction exhibits a regional characteristic of the geoelectric structure is strengthened by the fact that the direction of the local channelling drastically changes from site to site (see Figs III.13 and II.24).

By comparing the theoretical Mohr circle diagrams described in the previous section with the experimental ones, we found that the following three models are appropriate to simulate the features of the experimental Mohr circles (see Figs III.14-16): (i) 3D-(local)/2D-(regional) with strong shear distortion ($|e| \to 1$), (ii) 3D-(local)/1D-(regional) with strong shear distortion ($|e| \to 1$) and (iii) 3D-(local)/2D-(regional) with high anisotropy characterizing the deep structure. In order to select the most appropriate model, we calculate, for each one of these models, the fundamental rotationally invariant parameters of

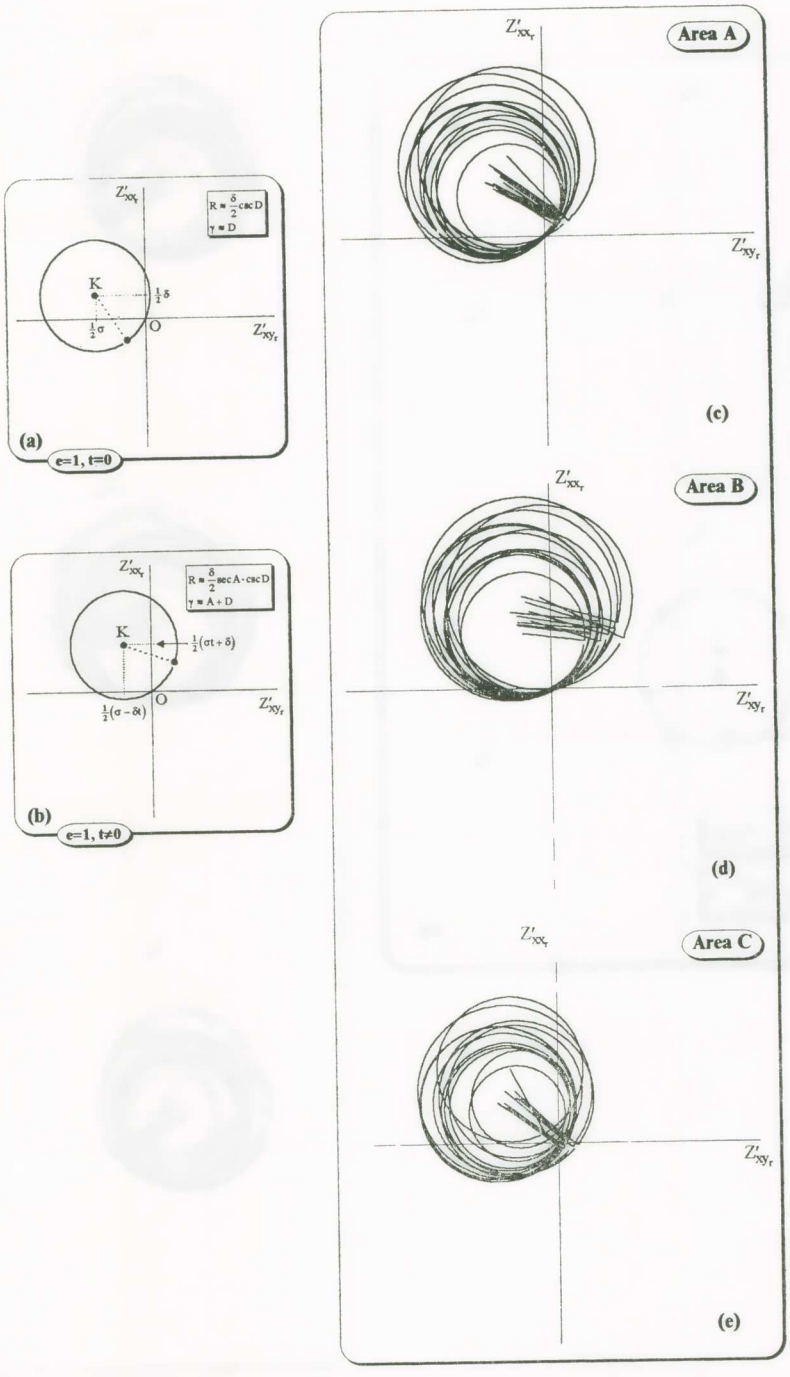


Fig. III.14. Theoretical Mohr circles for 2D-(regional)/3D-(local) with *strong* shear distortion ($|e| \to 1$): **(a)** without twist; **(b)** with twist. Their morphology simulates the experimental Mohr circles **(c)**, **(d)** and **(e)** from areas A, B and C respectively.

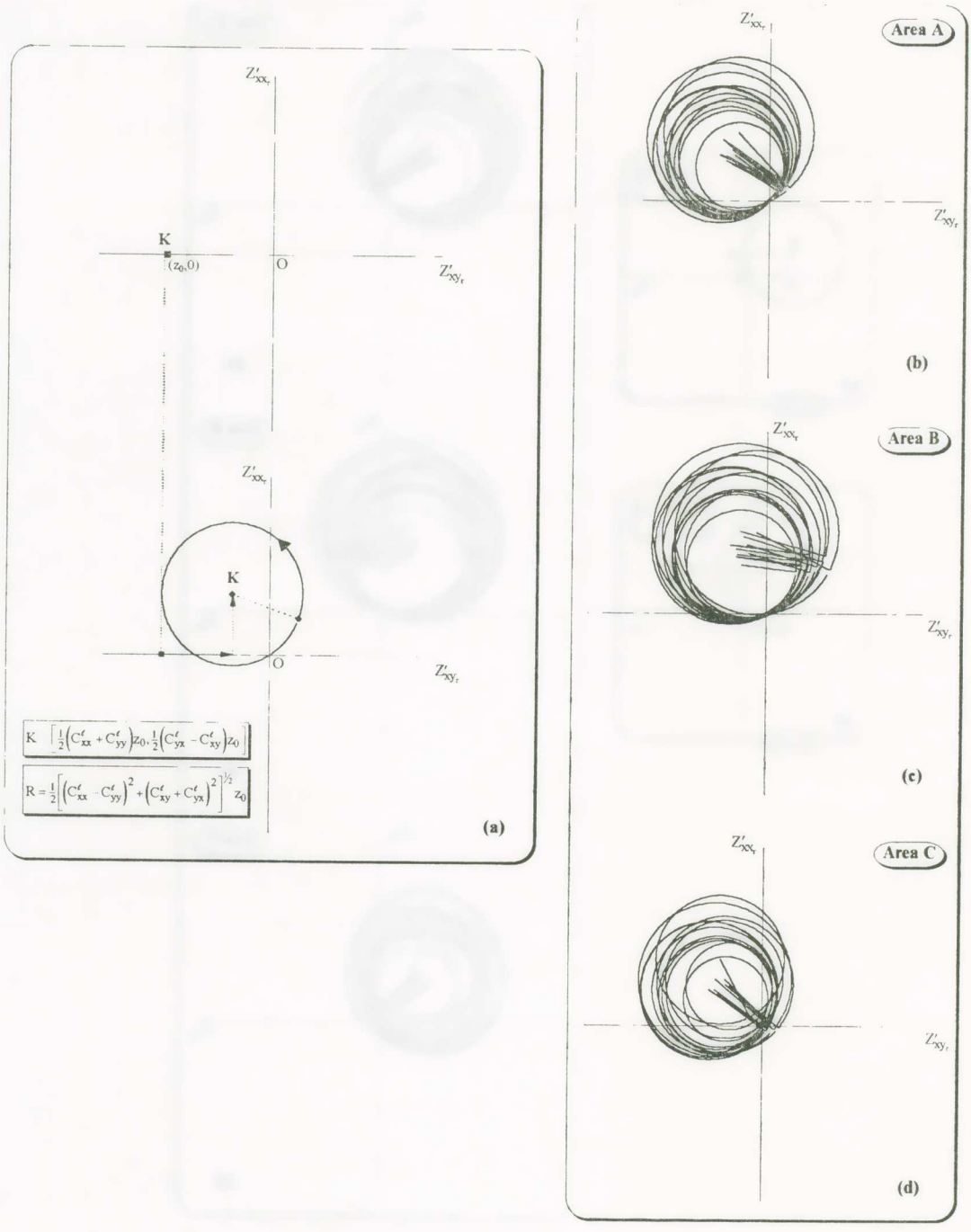


Fig. III.15. **(a)** Theoretical Mohr circle for 1D-(regional)/3D-(local). Its morphology simulates the experimental Mohr circles **(b)**, **(c)** and **(d)** from areas A, B and C respectively.

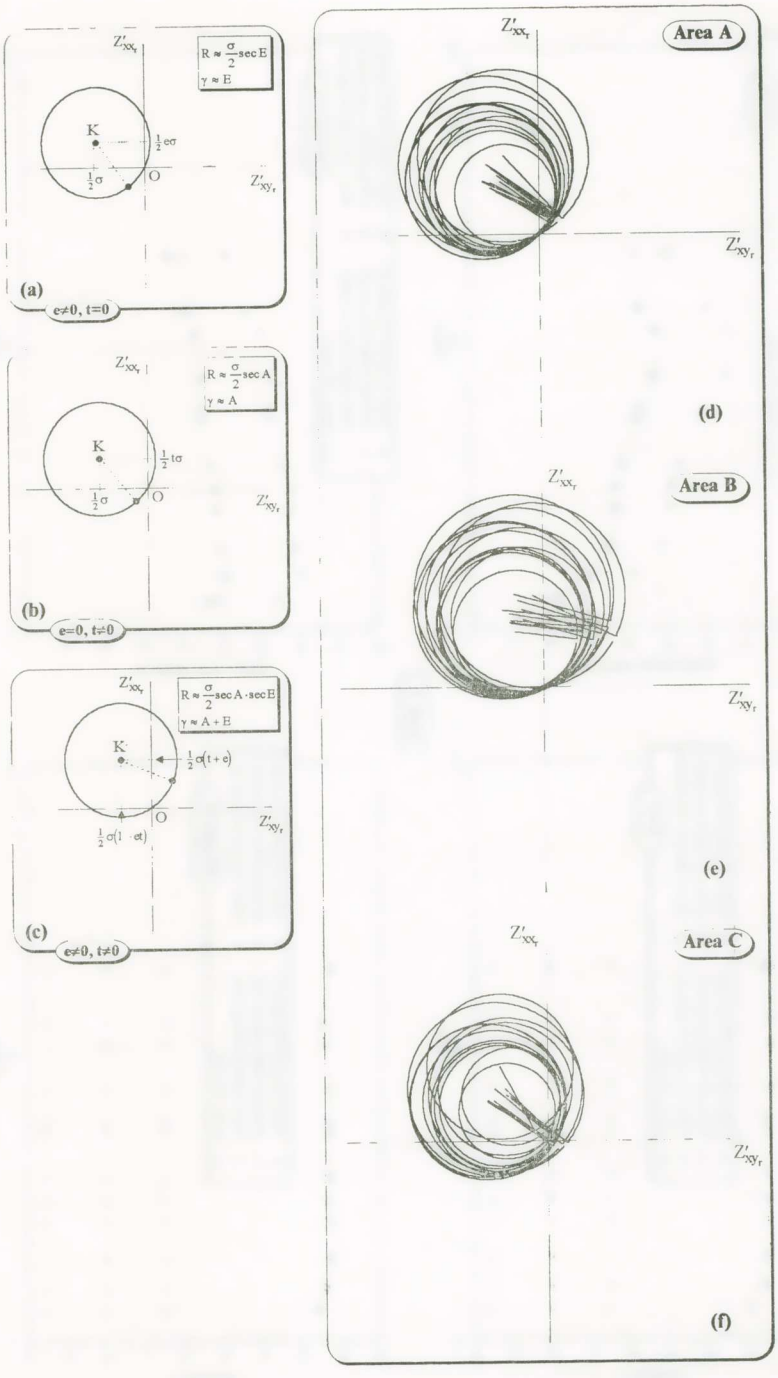


Fig. III.16. Theoretical Mohr circles for 2D-(regional with high anisotropy)/3D-(local) with local distortion: **(a)** shear only; **(b)** twist only; **(c)** shear and twist. Their morphology simulates the experimental Mohr circles **(d), (e)** and **(f)** from areas A, B and C respectively.

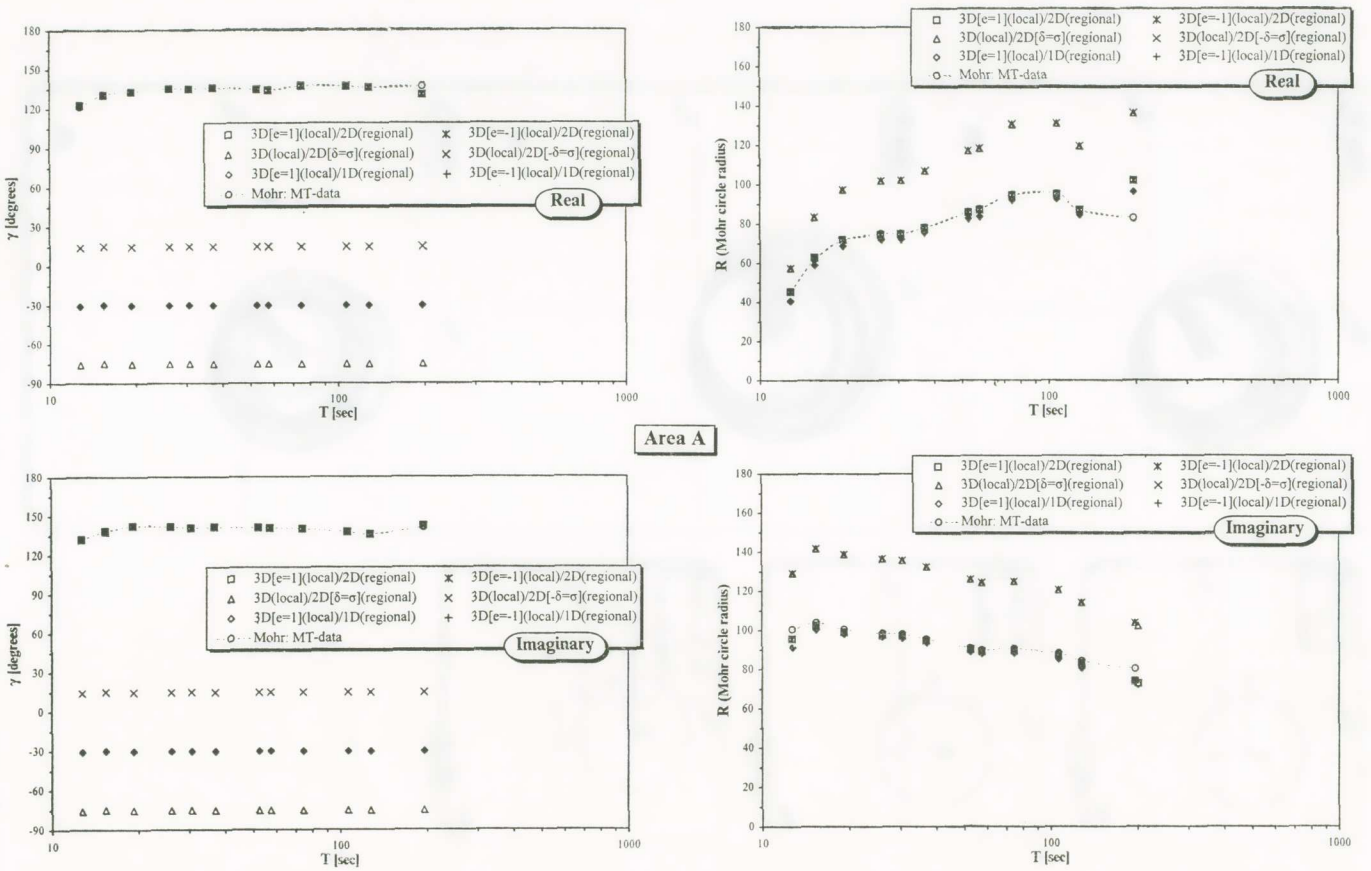


Fig. III.17. The rotationally invariant parameters R (circle radius) and γ (skew angle) of Mohr circles versus the period calculated (separately for the real and imaginary parts) from the MT-data of site A and from geoelectric structure models that best simulate the morphology of the experimental circles.

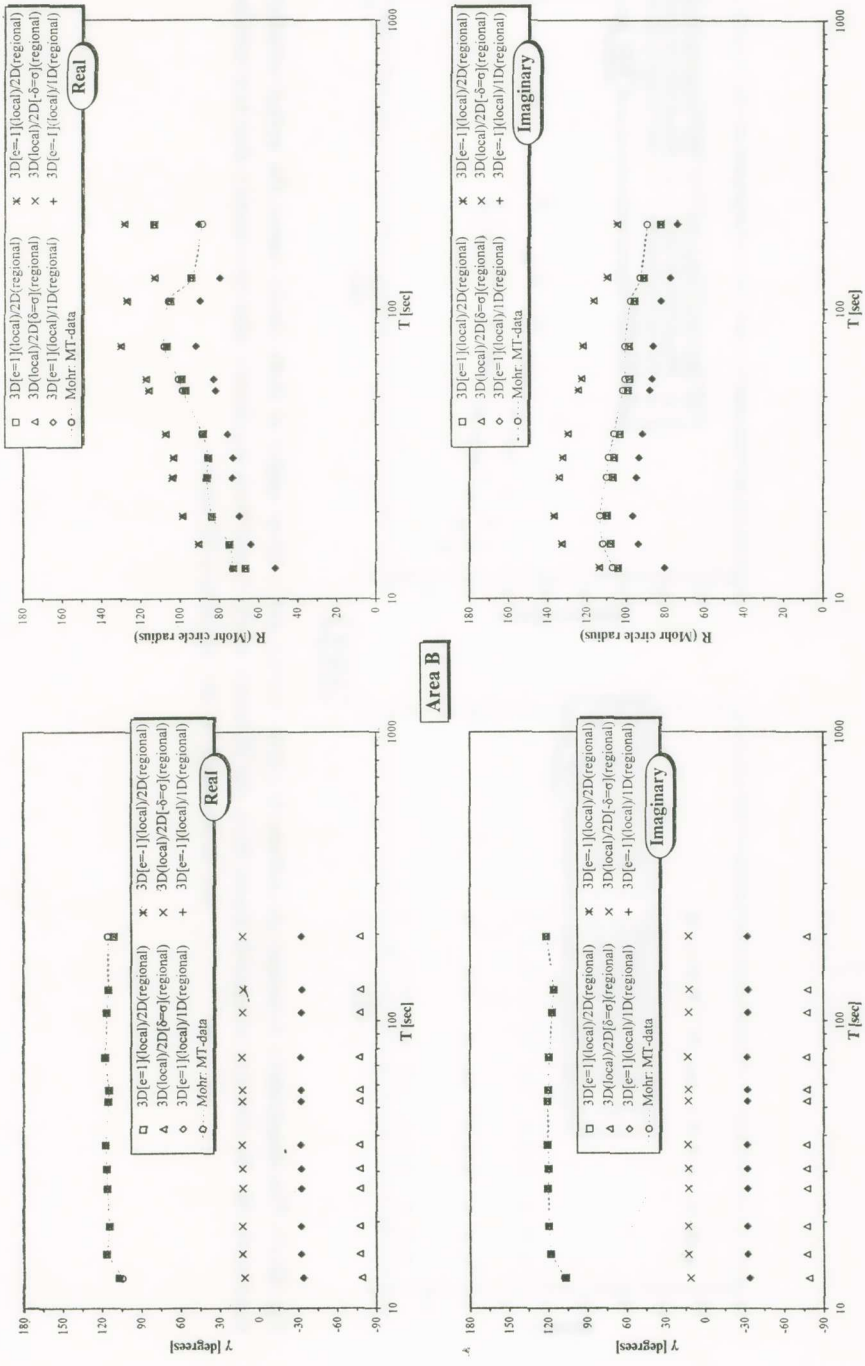


Fig. III.18. The rotationally invariant parameters R (circle radius) and $\gamma$ (skew angle) of Mohr circles versus the period calculated (separately for the real and imaginary parts) from the MT-data of site B and from geoelectric structure models that best simulate the morphology of the experiment circalles.

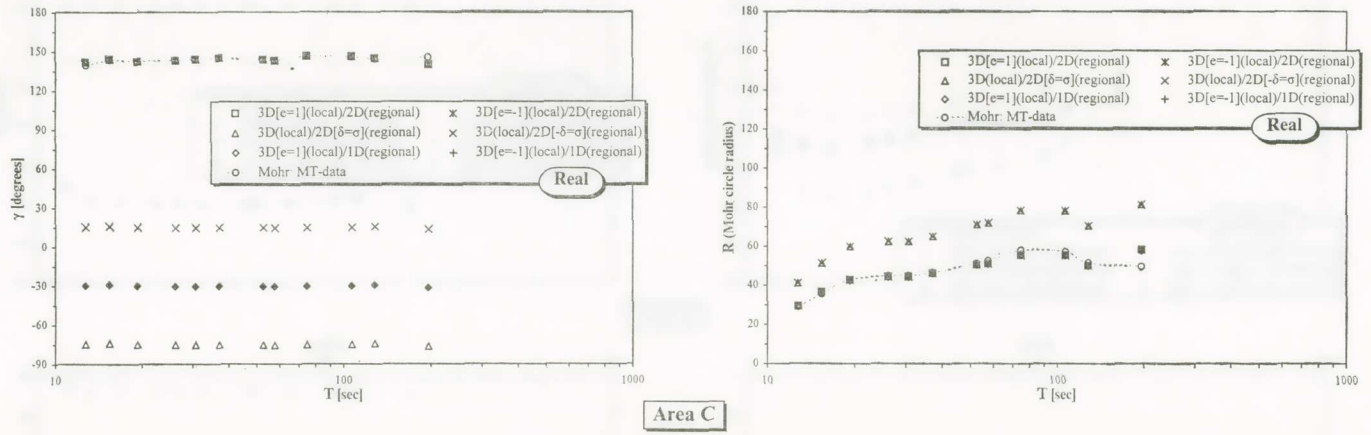


Fig. III.19. The rotationally invariant parameters R (circle radius) and γ (skew angle) of Mohr circles versus the period calculated (separately for the real and imaginary parts) from the MT-data of site C and from geoelectric structure models that best simulate the morphology of the experimental circles.

the corresponding Mohr circle, i.e., the radius, R, and the skew angle, $\gamma$, versus the period (separately for the real and imaginary parts). The theoretical model curves $R_i = R_i(T)$ and $\gamma_i = \gamma_i(T)$ $[i = 1..3]$ are compared with the experimental curves $R = R(T)$ and $\gamma = \gamma(T)$, for the sites A, B and C, in Figs III. 17-19. This comparison reveals that the model which best approximates, at all the measuring sites, the features and the parameter values of the experimental Mohr circles is the 3D-(local)/2D-(regional) with strong shear distortion ($|e| \to 1$). This can be considered as an independent confirmation of the model resulted from the impedance tensor decomposition methodology.

## IV. MAGNETIC PROSPECTION. TIPPER AND INDUCTION ARROWS ANALYSIS

Since we concluded that the regional structure is two-dimensional and we have determined its intrinsic coordinate system, it only remains to distinguish between the dip and strike-directions of the 2D-structure. In order to determine the strike-direction, we elaborate the vertical magnetic field measurements.

It is assumed that $H_z$ -component is linearly related to $H_x$ and $H_y$-components thus the following relation (in the frequency domain) holds *[Jones et al., 1978], [Labson et al., 1985]*:

$$H_z(\omega) = T_x(\omega)H_x(\omega) + T_y(\omega)H_y(\omega)$$

where $T = (T_x, T_y)$ is the transfer function of the vertical magnetic field relative to its horizontal components, termed as *tipper*. Its magnitude is given by:

$$|T| = \sqrt{|T_x|^2 + |T_y|^2}$$

and is a rotationally invariant parameter. This is a measure of the deviation of the structure from the ideal 1D-symmetry. In cases where other scalar parameters have indicated that the structure is two-dimensional, the tipper magnitude will be larger, if the discontinuity of the conductivity across the strike-direction is also larger; furthermore the tipper magnitude increases when the distance from the discontinuity (compared to the skin-depth) becomes smaller.

The determination of the strike-direction of the 2D-structure arises from the fact that the vertical component of the magnetic field is restored in the

case of the E-polarization mode but not in that of H-polarization mode (i.e., it is restored when the horizontal magnetic field lies along the dip-direction).

The dip-direction of the structure corresponds to the angle which satisfies the condition:

$$|H_z(\theta^*)| = \max\ [|H_z(\theta)|]$$

Analytical calculations give for the angle *tipper-dip*:

$$\theta^* = \frac{1}{2}\ \tan^{-1}\left\{\frac{2[\mathrm{Re}(T_x)\mathrm{Re}(T_y) + \mathrm{Im}(T_x)\mathrm{Im}(T_y)]}{|T_x|^2 - |T_y|^2}\right\}$$

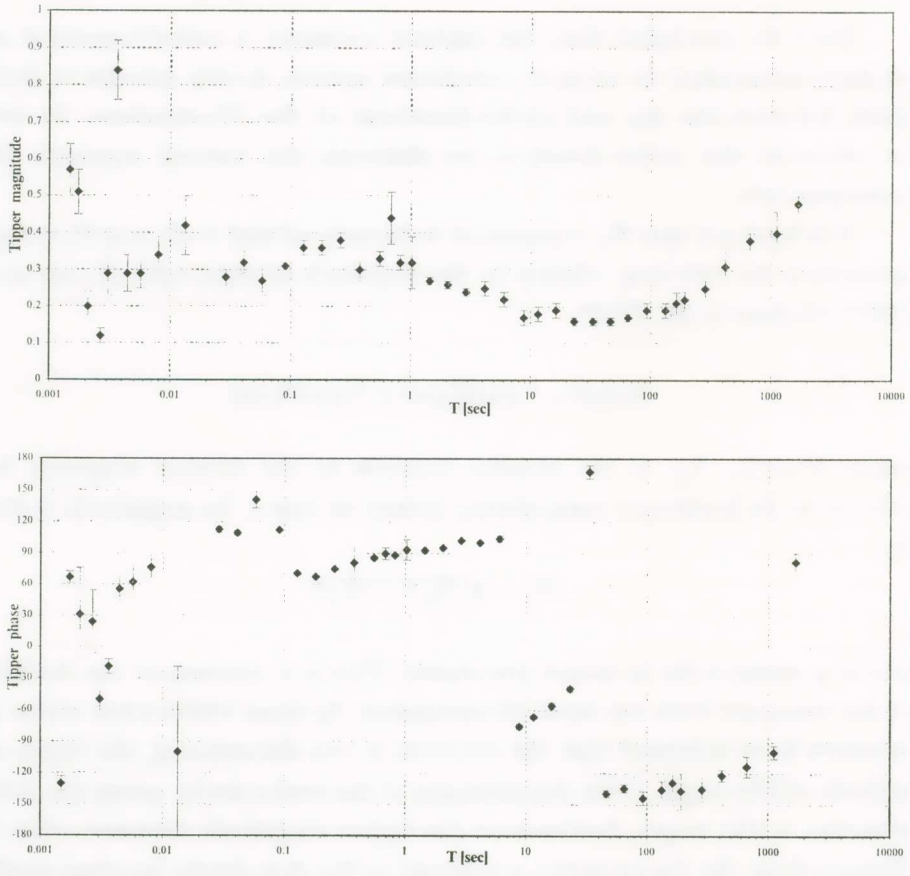


Fig. IV.1. Tipper magnitude and tipper phase versus the period for the site (B-C) of Ioannina region.

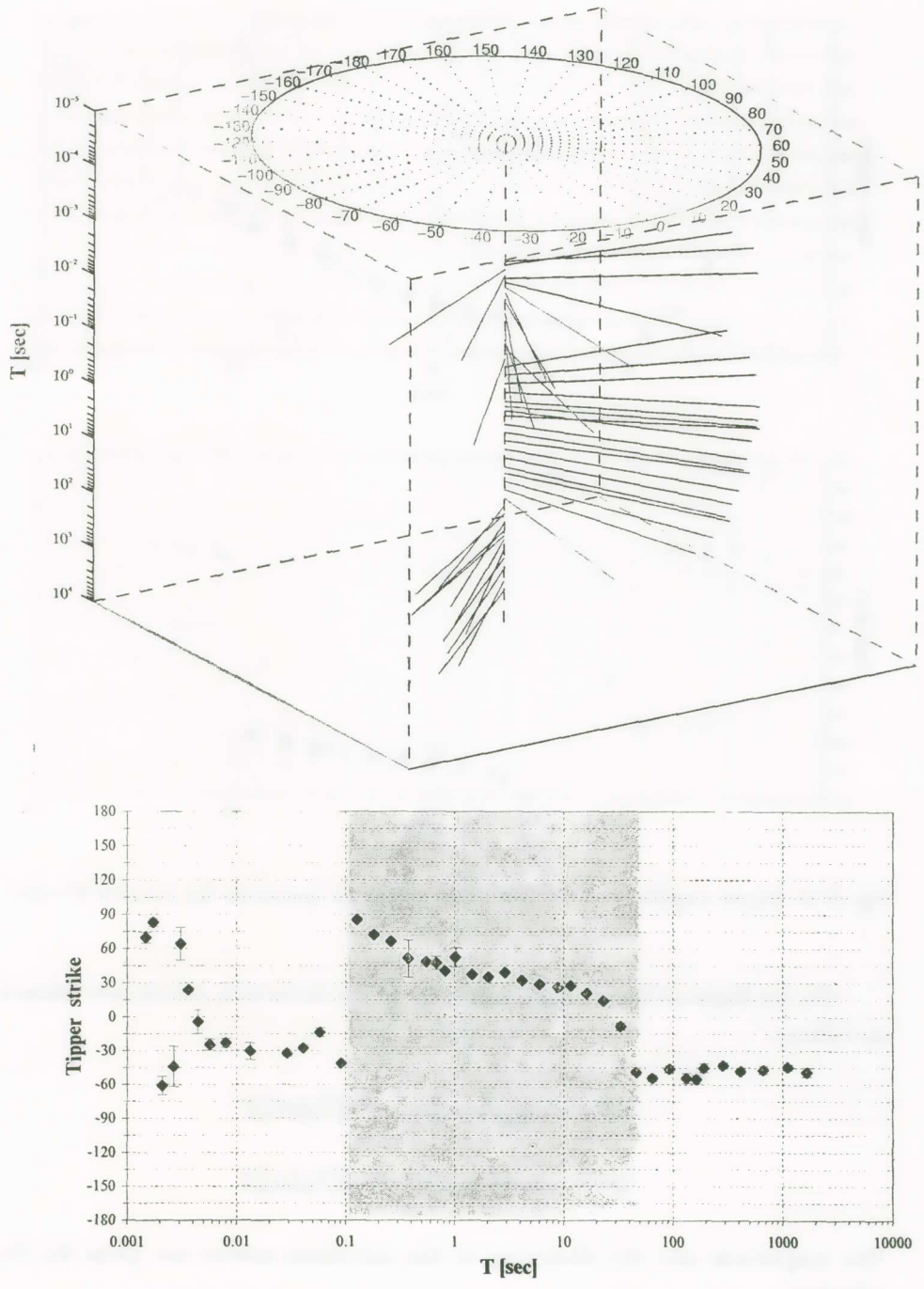


Fig. IV.2. The tipper strike angle versus the period for the site (B-C) of Ioannina region.

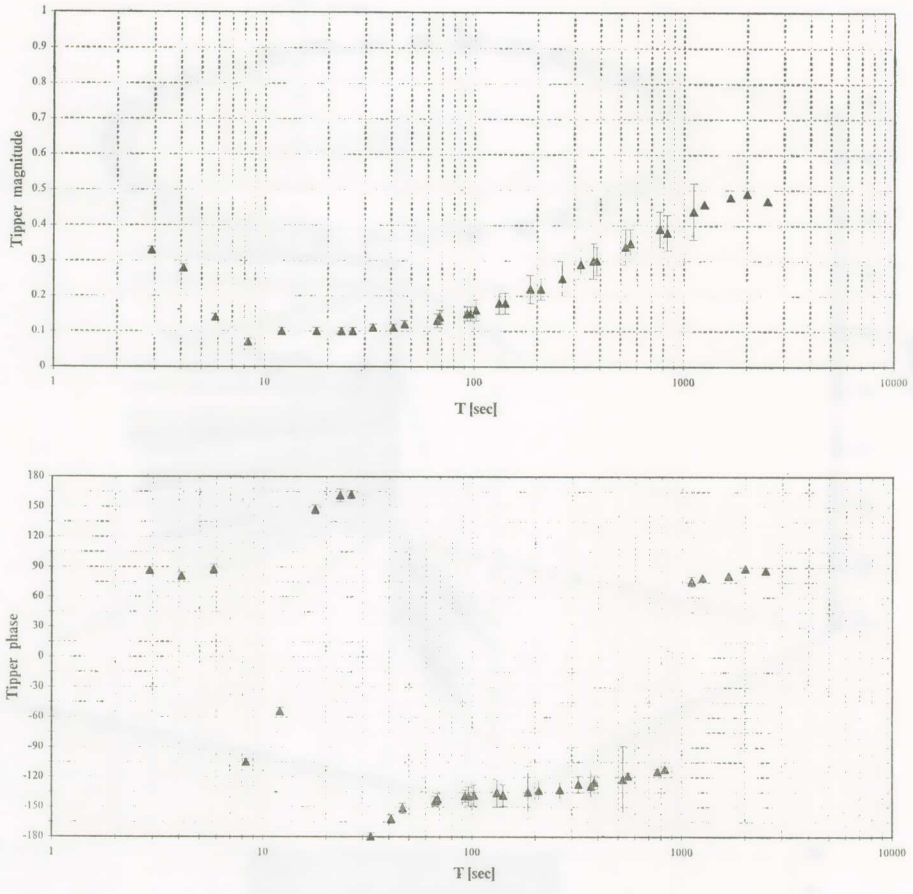


Fig. IV.3. Tipper magnitude and tipper phase versus the period for the Lykotrichi region.

On the basis of the transfer function T, the *induction arrows* are defined as follows:

$$\overline{P}(\omega) = \mathrm{Re}[T_x(\omega)]\,\hat{x} + \mathrm{Re}[T_y(\omega)]\,\hat{y}$$

$$\overline{Q}(\omega) = \mathrm{Im}[T_x(\omega)]\,\hat{x} + \mathrm{Im}[T_y(\omega)]\,\hat{y}$$

The magnitude and the directions of the induction arrows are given by the relations:

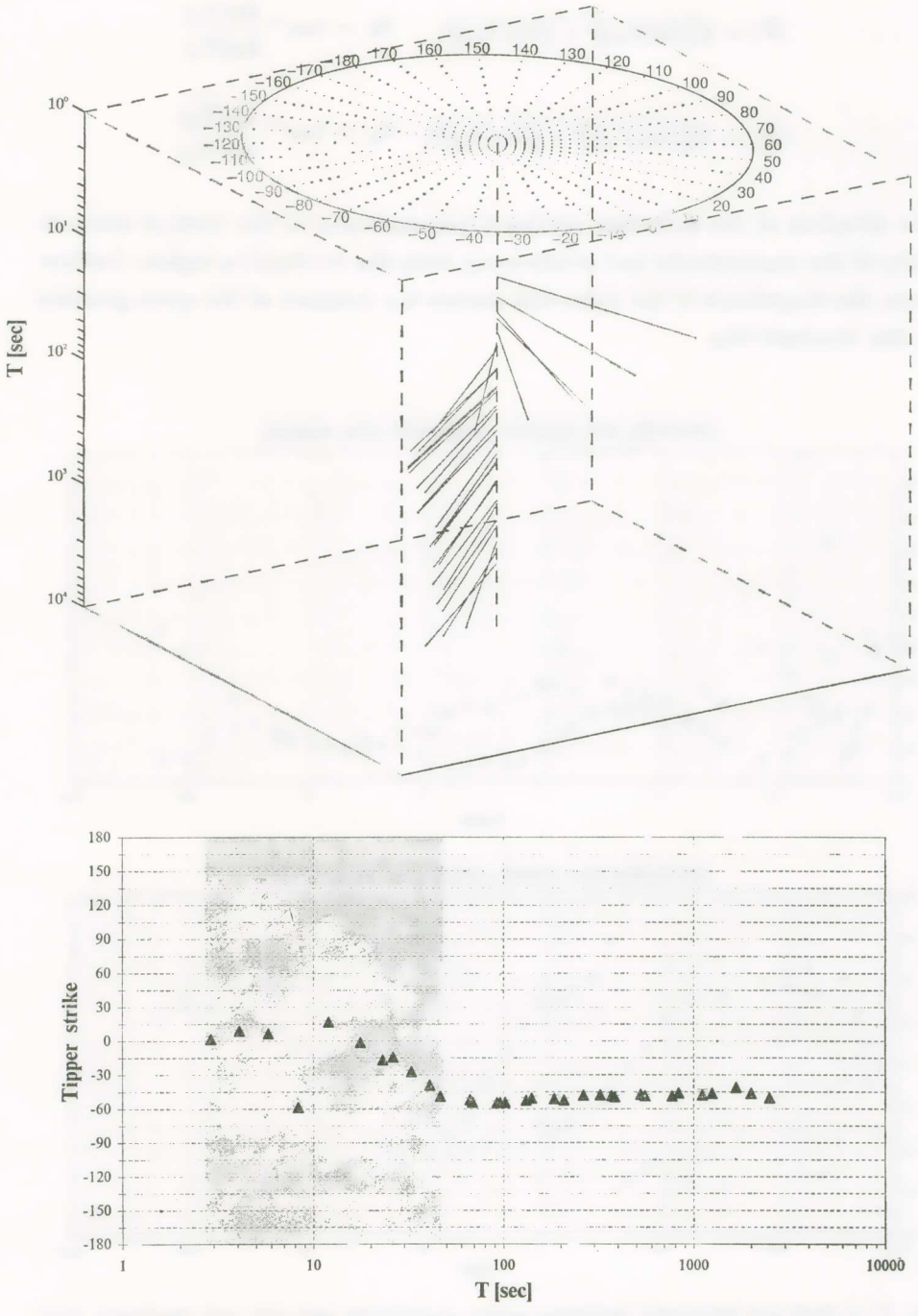


Fug. IV.4. The tipper strike angle versus the period for the Lykotrichi region.

$$|\bar{P}| = \sqrt{[\mathrm{Re}(T_x)]^2 + [\mathrm{Re}(T_y)]^2}, \qquad \theta_{\bar{P}} = \tan^{-1} \frac{\mathrm{Re}(T_y)}{\mathrm{Re}(T_x)}$$

$$|\bar{Q}| = \sqrt{[\mathrm{Im}(T_x)]^2 + [\mathrm{Im}(T_y)]^2}, \qquad \theta_{\bar{Q}} = \tan^{-1} \frac{\mathrm{Im}(T_y)}{\mathrm{Im}(T_x)}$$

The direction of the induction arrows is perpendicular to the vertical discontinuity of the conductivity and points away from the conductive region; furthermore, the magnitude of the induction arrows is a measure of the space gradient of the conductivity.

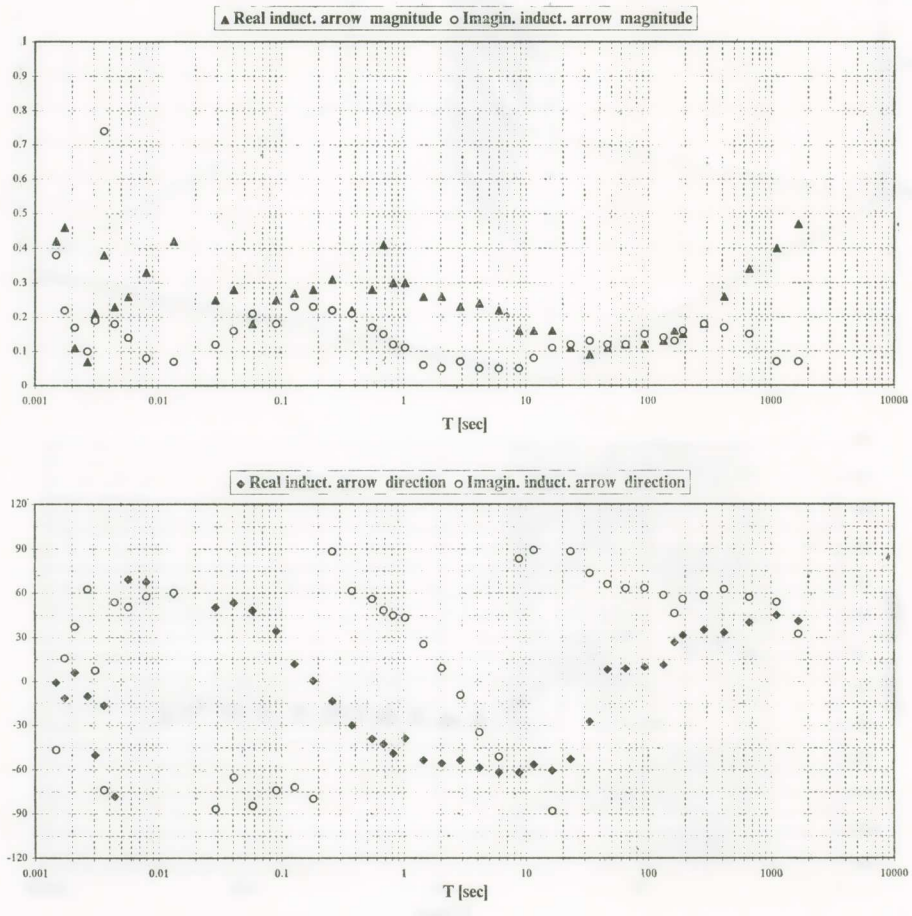


Fig. IV.5. Real and imaginary induction arrow magnitudes and real and imaginary induction arrow directions (dip-directions) for the site (B-C) of Ioannina area.

*IV.1. Experimental analysis of magnetic prospection. Tipper vector and induction arrows*

In Figs IV.1 and IV.2 the tipper magnitude, the tipper phase and the tipper-strike angle versus the period are depicted for the site (B-C) of Ioannina region. In Figs IV.3 and IV.4, the same functions are depicted for Lykotrichi area. EMI's coil magnetometers have been used in order to detect the magnetic field variations. An inspection of these results shows that in the low frequency range, the strike-direction points ~N50°W. The same result is obtained from

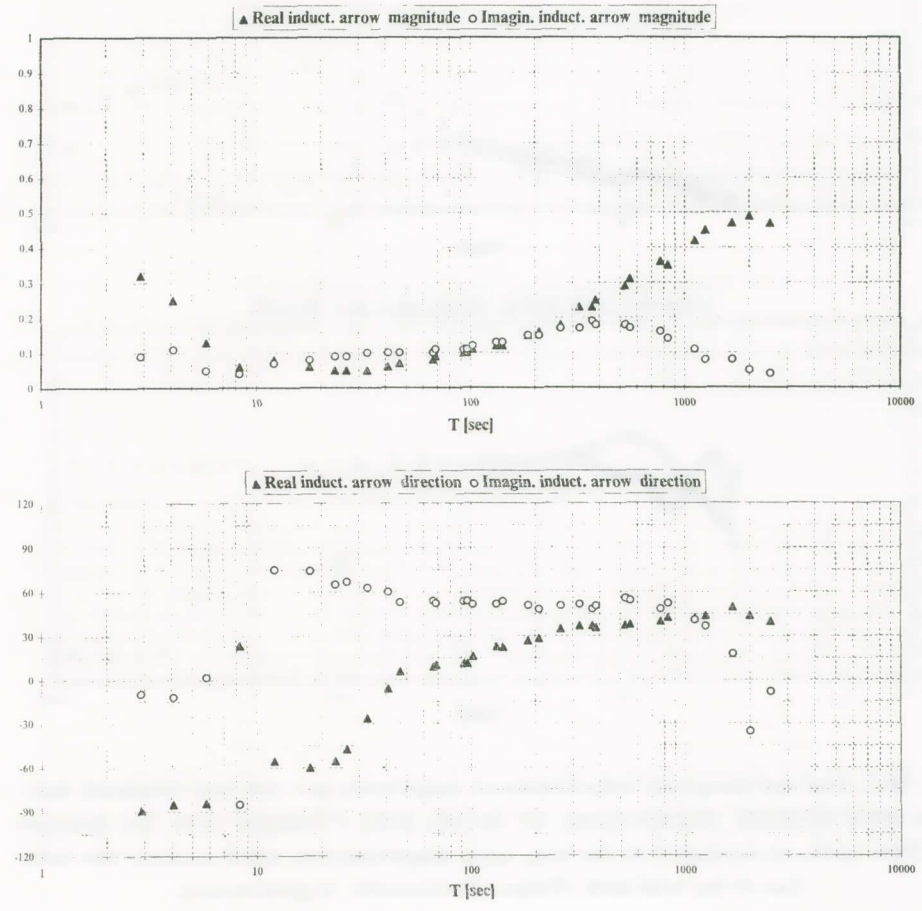


Fig. IV.6. Real and imaginary induction arrow magnitudes and real and imaginary induction arrow directions (dip-directions) for the Lykotrichi area.

the study of the induction arrows (Figs IV.5 and IV.6); the study of the induction arrows was repeated by using magnetometers which measure the variation of the total magnetic field (Torsion Photoelectric Magnetometer) at site (B-C) of Ioannina region (see Fig. IV.7).

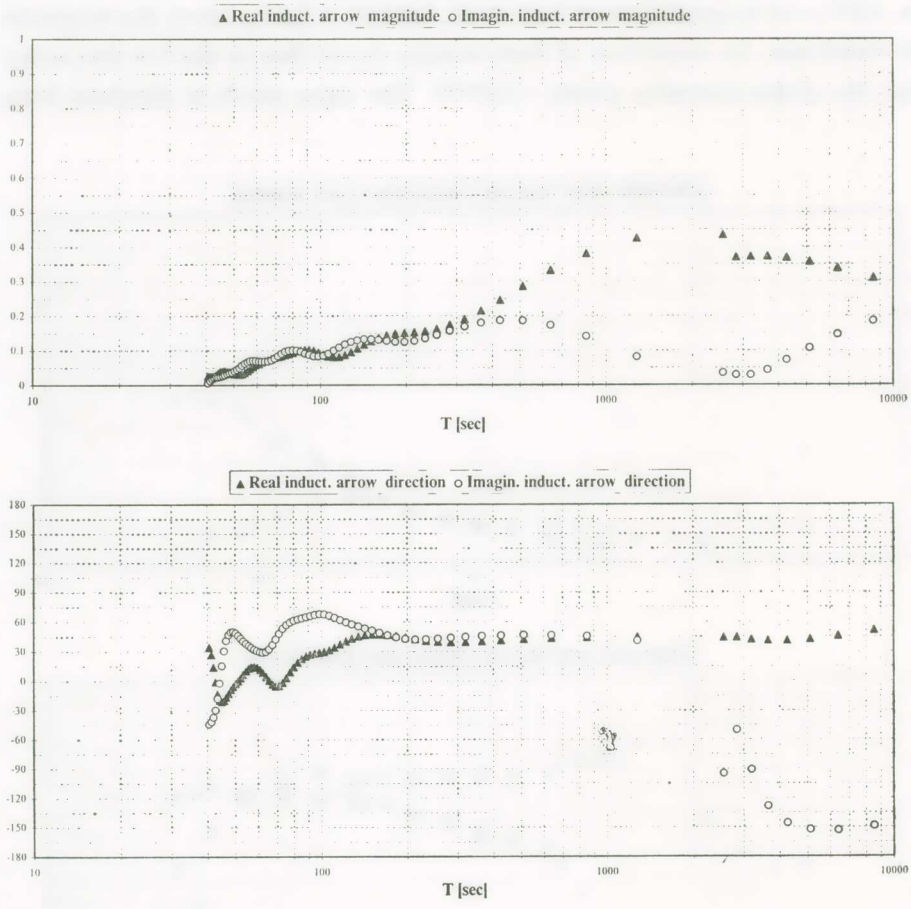


Fig. IV.7. Real and imaginary induction arrow magnitudes and real and imaginary induction arrow directions (dip-directions) for the site (B-C) of Ioannina area. The detection has been made, as mentioned in the text, using magnetometers which measure the variation of the total field (Torsion Photoelectric Magnetometer).

## V. INVERSION OF THE MT-DATA

Although the model found for Ioannina area is 2D-(regional)/3D-(local) we proceeded to an 1D-Occam's inversion of the MT-data from the site (B-C), and from Protopappas area (i.e., ~15Km north-west from Ioannina area). The inspection of the 1D-inversion results (Figs V.1, V.2) indicates the probable existence of a very conductive body, with resistivity of the order of a few Ωm, located at a depth of the order of a few Km and embedded in a more resistive medium with resistivity of the order of a few thousands Ωm. This probably coincides with the results obtained by the magnetic prospection which show the beginning of an anomaly at higher frequencies. As the information concerning the conductive body is very important, especially for the explanation of the «selectivity effect» *[Varotsos et al., 1996a, 1996b]*, a detailed study with a magnetotelluric grid survey of different sites is currently carried out around Ioannina area, the data of which are analysed using 2D-inversion techniques and forward modeling.

## VI. SUMMARY AND CONCLUDING REMARKS

The geoelectric structure of the SES-sensitive area of Ioannina has been studied by means of the MT-method. The study was divided into two basic consecutive stages. The first consists of the conventional MT-analysis which considers the electromagnetic response of the subsurface as unified; in this frame the interpretation of the MT-data [collected at four neighbouring areas A, B, C and (B-C)], after checking the rotational MT-diagrams and the skew and ellipticity indices, resulted to a two-dimensional regional conductivity structure, but with the calculated strike angle $\theta_0$ differing considerably from site to site, thus indicating a more complex structure. Eggers' eigenstate formulation was implemented to the measured impedance tensors from all the sites. The main conclusion of this analysis was that the eigenvectors of the electric field (and of the corresponding magnetic field) are mutually linearly polarized, but they are not perpendicular, thus indicating that the geoelectric structure is not purely two-dimensional.

The experimental facts that (i) the strike-angle differs considerably from site to site and (ii) at each measuring site there is a big difference between the two modes $\rho_{xy}$ and $\rho_{yx}$, led us to assume the existence of a 1D or 2D-regional

structure with the presence of local near-surface 3D-scatterers. Therefore, the MT-study proceeded to the second basic stage at which the measured impedance tensor was decomposed. This was initially made using Bahr's procedure which considers the model of a regional 2D-structure overlaid by 3D-inhomogeneities; the values of the scalar parameters determined by such a procedure, indicated that such a model is appropriate to fit the MT-data from all the sites. Furthermore, Bahr's analysis demonstrated that the local 3D-inhomogeneities produce strong local channelling of the regionally induced currents. This was confirmed experimentally from the measured electric field polarization diagrams which exhibit strong linear electric field polarization with a direction varying drastically from site to site.

The impedance tensor was also decomposed by Groom and Bailey's procedure, which decomposes also the distortion tensor to discrete types of distortion, i.e., twist, shear and splitting distortion. This analysis at all the sites led to the following conclusions: **(i)** the model that best fits the data is 2D-(regional)/3D-(local), in agreement with that derived from Bahr's analysis. **(ii)** The principal axis system of the underlying regional 2D-structure was resolved and found to deviate from the measuring coordinate system ($x \rightarrow$ NS, $y \rightarrow$ EW) by approximately $40^o \pm 15^o$ counterclockwise. The apparent resistivities, that correspond to the regional principal directions, have a ratio of the order of 10. Note that this decomposition of the impedance tensor does not allow an accurate determination of the actual 2D-basement apparent resistivities because the static shifts are not fully removed. **(iii)** The small-scale near-surface 3D-inhomogeneities cause a moderate twist distortion ($t = -0.6$) and a strong shear distortion of the regionally induced electric field ($|e| \rightarrow 1$) [notice that the set of the decomposition parameters is not unique]. The latter is compatible with the strong local channelling inferred by Bahr's analysis and the experimental diagrams of the electric field which depict strong linear polarization; furthermore, the experimental polarization directions of the electric field are in full agreement with the local strike (channelling) directions derived from the implementation of Groom et al's analysis to the MT-data at each site: $\theta_l^A \approx 81^o$, $\theta_l^B \approx 62^o$ and $\theta_l^C \approx 90^o$.

The ambiguity concerning the strike-direction of the 2D-structure and the the non-uniqueness of the decomposition parameter set, resulting from Groom and Bailey's analysis, led us to incorporate to the MT-study the magnetotelluric representation of Mohr circles. The relevant diagrams for all the si-

tes exhibit the same striking peculiarity: the Mohr circles, resulted separately from the real and imaginary parts, pass through the origin ($Z'_{xy}$, $Z'_{xx}$). This fact provided an independent determination of the linear polarization direction of the electric field (local strike) at each one of the measuring sites: ~N80°E for site A, ~N60°E for site B and ~N90°E for site C. These values are in full agreement with those calculated from the experimental polarization diagrams and those derived from the impedance tensor decomposition.

In this paper another «*conjugate*» form of the Mohr circles was introduced, i.e., the plot of the element $Z'_{xx}(\theta)$ versus the element $Z'_{yx}(\theta)$. These plots were constructed for all the measuring sites (A, B and C) and revealed the same striking peculiarity i.e., they also pass through the origin ($Z'_{yx}$, $Z'_{xx}$). This led to the determination of a rotational angle, $\theta_r$, which was found to have the same value at all the sites: $\theta_r \approx 125^o \pm 5^o$. It is justified to assume that the implying direction (~N55°W) can be the strike-direction of the underlying 2D-regional geoelectric structure. This value seems to be compatible with the direction (~N40°W) of one of the principal axes determined by the impedance tensor decomposition and the strike-direction (~N50°W) derived from the magnetic prospection by studying the tipper and the induction arrows.

Furthermore, after introducing the parameter set derived by Groom et al's decomposition into the magnetotelluric representation of Mohr circles, three models which successfully simulate the morphology of the experimentally constructed Mohr circles, were resulted. These are: (a) 2D-(regional)/3D-(local) with strong shear distortion ($|e| \to 1$), (b) 1D-(regional)/3D-(local) with strong shear distortion ($|e| \to 1$) and (c) 2D-(regional)/3D-(local) with the high anisotropy to be referred to the deep structure. By plotting the rotational invariant parameters i.e., the radius R, and the skew angle $\gamma$, of the theoretical and experimental Mohr circles respectively, from all the measuring sites (A, B and C), versus the period, it is concluded that the model which best simulates the properties of the experimentally determined magnetotelluric Mohr circles is the 2D-(regional)/3D-(local) with strong shear distortion ($|e| \to 1$). Although this solution is not unique, this model is the same with the model resulted from Groom et al's analysis.

Finally, the 1D-Occam inversion of the MT-data from the site (B-C) and from the Protopappas area (~15Km north-west from IOA-station) was carried out. It indicates the probable existence of a very conductive body (of the order of a few Ωm) at a depth of the order of a few Km, embedded in a more resi-

stive medium (with resistivity of the order of a few thousands Ωm); a detailed MT-grid survey is currently carried out around Ioannina region and a 2D-inversion (and forward modeling) of the MT-data is performed in order to resolve further the existence of the conductive body.

---

This research was supported by the EC projects EVSV-CTh4-0439 and EPET 388 (coordinator P. Varotsos).

## REFERENCES

Bahr K., 1985, Magnetotellurische Messung des Elektrischen Widerstandes der Erdkruste und des Oberen Mantels in Gebieten mit Localen und Regionalen Leitfahigkeitsanomalien, *Doctoral thesis, Gottingen.*

Bahr K., 1988, Interpretation of the magnetotelluric impedance tensor: regional induction and local telluric distortion, *J. Geophysics vol 62, p 119-127.*

Bahr K., 1991, Geological noise in magnetotelluric data: a classification of distortion types, *Phys. Earth. Planet. Inter., vol 66, 24-38.*

Balasis G., Banks J. R., Whaler K., 1997, Comment on 'Understanding telluric distortion matrices' by J. T. Smith, *Geophys. J. Int., vol. 129, 472-473.*

Berdichevsky M. N., Dmitriev V. I., 1976, Basic principles of interpretation of magnetotelluric curves, *in Geoelectric and Geothermal studies: A. Adam, Ed., Akademini Kiado, 165-221.*

Chave D. A., Torquil J. S., 1994, On electrical and magnetic galvanic distortion tensor decompositions, *J. Geophysical Research, vol. 99, No B3 p 4669-4682.*

Eggers D. E., 1982, An eigenstate formulation of the magnetotelluric impedance tensor, *Geophysics, vol 47, No 8, p 1204-1214.*

d' Erceville I., Kunetz G., 1962, Some observations regarding naturally occuring electromagnetic fields in applied geophysics, *Geophysics, vol 27, p 651.*

Fisher G., Szarka L., Adam A., Weaver J. T., 1992, The magnetotelluric phase over 2-D structures, *Geophys. J. Int., vol 108, p 778-786.*

Groom W. R., Bailey C. R., 1987, A decomposition of the magnetotelluric impedance tensor that is useful in the presence of distortions, *presented at Fifty-seventh Annual Meeting, Society of Exploration Geophysicists, New Orleans.*

Groom W. R., 1988, The effects of inhomogeneities on Magnetotellurics, *Ph. D. thesis, University of Toronto, Research in Applied Geophysics, Geophysics Laboratories, Physics Department, University of Toronto.*

Groom W. R., Bailey C. R., 1989, Decomposition of magnetotelluric impedance tensor in the presence of local three-dimensional galvanic distortion, *J. of Geophysical Research, vol 94, No B2, p 1913-1925.*

Groom W. R., Kurtz D. R., Jones G. A., Boemer E. D., 1993, A quantitative methodology to extract regional magnetotelluric impedances and determine the dimension of the conductivity structure, *Geophys. J. Int., vol 115, p 1095-1118.*

Jones F. W., Vozoff K., 1978, The calculation of magnetotelluric quantities for three-dimensional conductivity inhomogeneities, *Geophysics, vol 43, No 6, p 1167-1175.*

Kaufman A. A., Keller G. V., 1981, The Magnetotelluric Sounding Method, *Elsevier, Amsterdam.*

Keller G. V., Frischknecht F. C., 1986, Electrical methods in geophysical prospecting, *Pergamon.*

Labson V. F., Becker A., Morrison H. F., Conti U., 1985, Geophysical exploration with audio-frequency natural magnetic fields, *Geophysics, vol 50, p 656-664.*

Lilley T., 1976, Diagrams for magnetotelluric data, *Geophysics, vol 41, p 766-770.*

Lilley T., Filloux J. H., Ferguson I. J., Bindoff N. L., Mulhearn P. J., 1989, The Tasman project of seafloor magnetotelluric exploration: Experiment and observations, *Phys. Earth Planet. Int., vol 53, p 405-421.*

Lilley T., 1993, Magnetotelluric analysis using Mohr circles, *Geophysics, vol 58, p 1498-1506.*

Lilley T., 1993, Mohr Circles in Magnetotelluric Interpretation (i) Simple Static Shift (ii) Bahr's Analysis, *J. Geomag. Geoelectr. vol 45, p 833-839.*

Makris J., 1997, Ph.D. thesis, University of Athens, Greece.

Nabighian N. M., 1991, Electromagnetic methods in applied Geophysics, *vol 1 & 2 Society of Exploration Geophysicists.*

Sims W. E., Bostick F. X. Jr., 1969, Methods of magnetotelluric analysis, *Res. Lab. tech. rep. no 58, Univ. of Texas, Austin.*

Smith J. T., 1995, Understanding telluric distortion matrices, *Geophys. J. Int., vol 122, 219-226.*

Spitz S., 1985, The magnetotelluric impedance tensor properties with respect to rotations, *Geophysics, vol 50, No 10, p 1610-1617.*

Swift M. C. Jr., 1967, A magnetotelluric investigation of an electrical conductivity anomaly in the southwestern United States, *Ph.D. thesis, Mass. Inst. of Tech., MA.*

Swift M. C. Jr., 1971, Theoretical magnetotelluric and turam response from two dimensional inhomogeneities, *Geophysics, vol 36, p 38-52.*

Varotsos P., Lazaridou M., Eftaxias K., Antonopoulos G., Makris J., Kopanas J., 1996a, Short term Earthquake Prediction in Greece by Seismic Electric Signals, *A critical review of VAN, World Scientific, p 29-76.*

Varotsos P., Sarlis N., Lazaridou M., Kapiris P., 1996b, A plausible model for the explanation of the selectivity effect of Seismic Electric Signals, *Practica of Athens Academy, vol 71, p 283-351.*

Vozoff K., 1985, Magnetotelluric methods, *Society of Exploration Geophysics.*

Wannamaker P. E., Hohman G. W., San Filippo W. A., 1984a, Electromagnetic modeling of three dimensional bodies in layered earths using integral equations, *Geophysics, vol 49, p 60-74.*

Wannamaker P. E., Hohman G. W., Ward S. H., 1984b, Magnetotelluric responses of three dimensional bodies in layered earths, *Geophysics, vol 49, p 1517-1533.*

Zhang P., Roberts R. G., Pedersen L. B., 1987, Magnetotelluric strike rules, *Geophysics, vol 51, 267-278.*

Zhang P., 1989, Magnetotelluric Study of the Sijan Impact Region: Technics and results, *Uppsala.*